PENNING IONIZATION REACTIONS OF METASTABLE $Ar(^3P_{0,2})$, $Ne(^3P_{0,2})$ and $He(2^3S)$ WITH ORGANIC MOLECULES IN A FLOWING AFTERGLOW APPARATUS

by

MICHAEL THOMAS JONES

B. S., Nebraska Wesleyan University, 1980

A MASTER'S THESIS

submitted in partial fulfillment of the

requirements for the degree

MASTER OF SCIENCE

Department of Chemistry

KANSAS STATE UNIVERSITY

Manhattan, Kansas

1983

Approved by:

Major Professor

TABLE OF CONTENTS

List of Tables iv

List of Figures v

I. Introduction 2

II. Objectives of this Investigation 5

III. Experimental Methods 6

A. General Procedure for Ion Production and Studies of Ion-Molecule Reactions 6

B. Flow Tube 9

C. Ion Sources 10

D. Differentially Pumped Analysis Section 13

E. Calibration 14

F. Materials 17

IV. Model Calculations 19

A. Kinetic Model without Diffusion 19

B. Kinetic Model with Diffusion 21

C. Kinetic Model for the Penning Ionization by He* 25

D. Kinetic Model for the Penning Ionization by Ar* 27

E. Kinetic Model for the Penning Ionization by Ne* 34

F. Kinetics for Cases with Secondary Reactions with Primary Ions 35

V. Experimental Results 38

A. Reference Reactions 38

B. Primary Ions from Penning Ionization of Ar*, Ne*, and He* . 43

C. Secondary Ions from Ion-molecule Reactions with the Neutral Precursor 45

D. Penning Ionization Branching Fractions 48

VI. Discussion 63

A. Penning Ionization 63

B. Branching Fractions 67

C. Fragmentation and Secondary Ion-molecule Reactions 71

1) Diatomic Molecules 71

2) Chlorinated Methanes 71

3) Acetylene 73

4) Other Organic Substrates 74

VII. Conclusions 76

Appendix 1: Operating Instructions 78

Appendix II: Calculations Used in Data Work-up 82

A. Calculations of the Concentration of Reagents Used 82

B. Reactions of He^+ 85

C. Calculation of Rate Constants Needed to Observe Hetero-Ion-Molecule Reactions in the Presence of Homo-Ion-Molecule Reactions 86

D. Emission Data 89

References 95

Acknowledgments 101

List of Tables

Table I. Isotopes of Xe 15

Table II. Free-ion Diffusion Coefficient x Gas Number Density and Diffusion Rate Contents in Helium 26

Table III. Quenching Rate Constants, Diffusion Rate Constants, and Penning Ionization Branching Fractions for NO and CH_3Cl 2B

Table IV. Ion Signal Ratios and Branching Fractions for NO^+ and CH_3Cl^+ 34

Table V. The Penning Ionization Rate Constants and Branching Fractions for $Ar^* + NO \rightarrow Ar + NO^+ + e^-$ 43

Table VI. Parent Ions Produced by Ar* Penning Ionization 46

Table VII. Primary Fragment Ions Produced by Ar* Penning Ionization 47

Table VIII. Parent Ions Produced by He* Penning Ionization 4B

Table IX. Primary Fragment Ions Produced by He* Penning Ionization 49

Table X. Primary Ions Produced by Ne* Penning Ionization 50

Table XI. Secondary Ion-molecule Products Produced in the Penning Ionization Reactions of Ar*, Ne*, and He* 52

Table XII. Branching Fractions for Ar* Penning Ionization 59

Table XIII. Branching Fractions for He* Penning Ionization 61

Table XIV. Branching Fractions for Ne* Penning Ionization 62

Table XV. Relative Populations of NO Ionic States in 5B4.3 Å Photoionization and in $He(2^3S)$ Penning Ionization 66

Table XVI. Ionic States of Parent Ions and their Ionization Potentials 70

List of Figures

Figure 1. Schematic diagram of the flow tube

Figure 2. Schematic wiring diagram for the electron gun

Figure 3. Schematic diagram of the differential pumping system and nose cones

Figure 4. Cold-cathod discharge tube

Figure 5. Slip seal for cold-cathod discharge tube

Figure 6. Isotopic spectra of Xe

Figure 7. Plot of AMU vs. correction factor for mass discrimination of the medium mass range (AMU 1-150) for the quad #250

Figure 8. Plot of AMU vs. correction factor for mass discrimination of the high mass range (AMU 1-500)

Figure 9. Calculated plot of log [Ar*] and $[NO^+]$ vs. time in ms

Figure 10. Calculated plot of log [Ar*] and $[NO^+]$ vs added [NO] for t = 5.7 ms and P_{He} = 0.5 torr

Figure 11. Calculated plot of $[NO^+]$ and $[CH_3Cl^+]$ vs added [NO] and $[CH_3Cl]$ at t = 5.7 ms and P_{He} = 0.5 torr

Figure 12. Calculated plot of log [Ar*] and $[CH_3Cl]$ vs added $[CH_3Cl^+]$ for t = 5.7 ms P_{He} = 0.5 torr

Figure 13. Plot of $N_2^+(B)$ and $N_2(C)$ vs $[N_2]$ from the emission spectra of He* + N_2 and Ar* + N_2

Figure 14. Plot of product ion signals m/z 31, 50, 69, 81, 100, and 131 for the Penning ionization of C_2F_4 by He* vs added C_2F_4

Figure 15. Plot of product ion signals for the Penning ionization of C_2H_2 by Ar* vs added C_2H_2

Figure 16. Plot of product ion signals for the Penning ionization of CH_3Cl by Ar* vs added CH_3Cl

Figure 17. Plot of product ion signals for the Penning ionization of CH_2Cl_2 by Ar* vs added CH_2Cl_2

Figure 18. Plot of total ion signals for NO, CCl_4, $CHCl_3$, CH_2Cl_2 and CH_3Cl for the Penning ionization reactions with Ar*

Figure 19. Plot of total ion signals for NO, C_6F_6, C_2F_4, C_2H_2, and C_6H_6 for the Penning ionization reactions with Ar*

Figure 20. Plot of total ion signals for CO, CCl_4, $CHCl_3$, CH_2Cl_2, and CH_3Cl for the Penning ionization reactions with He*

Figure 21. Plot of total ion signals for CO, NO, N_2, and C_2F_4 for the Penning ionization reactions with He*

Figure 22. Plot of total ion signals for CO, NO, N_2, C_6H_6, CCl_4, CH_2Cl_2, and CH_3Cl for the Penning ionization reaction with Ne*

Figure 23. Schematic potential energy diagram for NO with A*

I. Introduction.

Gas phase ion-molecule reactions are of interest to organic chemists because the intrinsic properties of organic ion-molecule reactions are determined in the absence of the effects of solvation and counter ions. Some gas phase ion-molecule reactions can be expected to behave differently from the same process in solution, since in the latter, the strong effects of solvent molecules on the reacting partners must be overcome, and ion-pairing effects also greatly alter reactivity. However, the results and principles of organic chemistry developed in the condensed phase have served well in understanding most gas phase reactions, and become excellent guides in designing ion-molecule experiments for organic systems.[1]

The first ion-molecule reaction was reported by Dempster in 1916[2] for the reaction of hydrogen molecular ion with hydrogen atoms (eq 1).

$$H_2^+ + H \rightarrow H_3^+ \qquad (1)$$

However, experimental determinations of ion-molecule reaction rate constants were first measured by Tal'roze and Lyubimova[3] in 1952 for the reactions (2) and (3). Shortly thereafter, the results of ion-molecule

$$H_2O^+ + H_2O \rightarrow H_3O^+ + \cdot OH \qquad (2)$$

$$CH_4^+ + CH_4 \rightarrow CH_5^+ + \cdot CH_3 \qquad (3)$$

reactions from other investigators were published.[4-6]

In 1963, Fehsenfeld and Schmeltekoff[7,8] at the U.S. Department of Commerse Research Laboratories at Boulder, Colorado, developed the flowing afterglow (FA) plasma technique to obtain quantitative kinetic data on ion-molecule reactions of interest in atmospheric chemistry. Placing a mass spectrometer at the end of a large diameter flow tube with a fast buffer gas flow, it was possible to detect charged species produced by electron impact methods. Ferguson, et al.,[9] found that ion-molecule

reaction rate constants, product distributions, and other data obtained by the FA technique were in good agreement with results obtained by other methods. These studies established the validity of the results from the FA apparatus, and, presently, FA determined rate constants are considered the "benchmarks" for ion-molecule reactions.

The advantages of the flowing afterglow technique include:

a) ionic species are generally in their ground electronic and vibrational states due to multiple collisions between the ion and the buffer gas prior to reaching the downstream inlet port where the gaseous neutral molecules are added. Thus, the interactions between the ion and the neutral molecules occur at thermal energies with Maxwell-Boltzmann energy distributions;

b) a great variety of both ionic and neutral reactants can be studied and multistep synthesis of ions is possible;

c) ion sources are readily varied from "cool" (thermal electron attachment for generating negative ions" to "hot" methods (microwave discharge and EI);

d) accurate kinetic measurements can be readily made since time is given by (length of the flow tube)/(average transport velocity of the ions);

e) identification of neutral products is possible in some cases (emission spectroscopy or physical isolation);[10]

f) heating or cooling the flow tube gives temperature dependence of reactions rates;

g) reactions of ions with unstable neutrals (e.g. O, H, N, and O_3) are possible.[11]

In the flowing afterglow, as with the use of most conventional ion sources, the studies of positive organic ions have been hindered by for-

mation of a mixture of ions from secondary fragmentations. To reduce the amount of fragmentation, we have investigated the use of a cold-cathode discharge developed to provide a source of rare gas metastable atoms as the active agents to produce positive ions by Penning ionization of neutrals. In many cases Penning ionization provided an efficient method of producing specific organic cations, often without fragmentation. The electronically excited states of the rare gases produced by the cold-cathode discharge source and studied are the $^3P_{0,2}$ metastable states of Ar and Ne, and the 2^3S metastable state of He.

It has generally been accepted that quenching of the metastable states of the rare gases by reagents with ionization potentials below that of the excitation energy of the metastable atom give chemi-ionization as the major quenching channel;[13-17] there are exceptions, i.e. Ar* + Cl_2.[18,19] Chemi-ionization is subdivided according to the processes shown in eqs (h)-(l). The term Penning ionization has been used to describe

(h)	Penning ionization	$A^* + BC \rightarrow A + BC^+ + e^-$
(i)	Rearrangement ionization	$A^* + BC \rightarrow AB^+ + C + e^-$
(j)	Associative ionization	$A^* + BC \rightarrow ABC^+ + e^-$
(k)	Dissociative ionization	$A^* + BC \rightarrow A + B^+ + C + e^-$
(l)	Ion pair formation	$A^* + BC \rightarrow A + B^+ + C^-$

both the simple ionization of the molecule (h) and the associative ionization (j), while other exit channels may be the consequence of Penning ionization, i.e. $BC^+ \rightarrow B^+ + C$. These reactions can be observed with the FA apparatus equipped with a mass spectrometer and their quenching rate constants and product branching fractions, measured and, in some cases, the diffusion coefficients of ions can be determined.[20]

The cold-cathode discharge not only produces metastable atoms which give simple fragment mass spectra for ion molecule studies, but can be

used for other applications, e.g. the use of helium metastable atoms for direct product emission studies[21] and laser-induced excitation (LIE) spectroscopic studies of cations formed by Penning ionization of neutrals.[22]

II. Objectives of this Investigation.

The objectives of this investigation were to (1) establish a method of producing rare gas metastable atoms in the FA, (2) determine quantitatively the branching fractions for Penning ionization reactions of Ar, Ne, and He metastable atoms, and (3) provide evidence that Penning ionization is a useful source for the purpose of selectively generating organic ions.

III. Experimental Methods.

A. General Procedure for Ion Production and Studies of Ion-Molecule Reactions.

The chemistry in the FA apparatus is carried out in a flow tube (Figure 1), which consists of a region to prepare the ion of interest followed by a region in which to examine the interactions of that ion with neutral substrates. Other major components of the FA are a fast pumping system and a quadrupole mass spectrometer to monitor the ion composition of the flow. Helium, which is used as the flow or buffer gas, is introduced (ca. 200 STP cm^3 s^{-1}) into the upstream end (a, Figure 1) of the 1.5 m-long stainless steel flow tube, and the pressure (P_{He}) and flow velocity ($\bar{v}$) are maintained by a Roots blower/mechanical pump system. Our standard operating conditions are P_{He} = 0.5 torr and $\bar{v}$ = 80 m s^{-1}, and variable between P_{He} = 0.3 to 2.0 torr and $\bar{v}$ = 35 to 80 m s^{-1}.

Positive ions are produced by electron impact or chemi-ionization methods by adding small flows (< 1 STP cm^3 s^{-1}) of neutral gasses (e or f in Figure 1) to the buffer gas and allowed to flow past either of two ionization sources, the electron gun (c), or cold-cathode discharge (d) in (Figure 1). The vibrationally excited ions are cooled to their ground state by collisions with the buffer gas in the next 25 cm of the flow tube prior to reaching the inlet port for the neutral reactant (f, Figure 1). If the reagent is added at f the ion-molecule reaction commences at that point.

The flow is maintained by the Roots blower/mechanical pump system and sampled through orifices ($\sim$ 1 mm) in two molybdenum nose cones (h, Figure 1), which separate the three compartments shown in Figure 2. The ions passing through the nose cones are focused by a series of ion lenses into the quadrupole mass spectrometer where they are mass analyzed and counted. The entire mass spectrum of the ions can be monitored as a

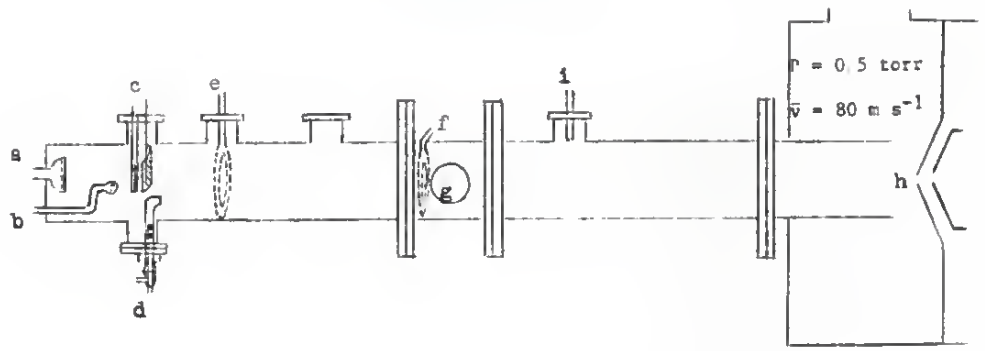

Figure 1. Schematic diagram of the flow tube; (a) coarse frit for buffer gas inlet, (b) shower head ion substrate inlet, (c) electron gun, (d) cold-cathode discharge, (e) ion production inlet, (f) ion-molecule neutral reagent port, (g) quartz view window, (h) nose cones, and (i) pressure transducer. The annular reagent inlets, (e) and (f), have holes on the inside surface which direct the gas flow toward the center of the tube. The distance from (e) and (f) to the first nose cone (h) is 98 and 73 cm, respectively. The distance from (c) and (d) to (h) is 124 cm.

Figure 2. Schematic wiring diagram for the electron gun circuit. The negative high voltage power supply is run at -100 to -150 V. The DC power supply is operated at 4-5 amps using the ThO_2 coated Ir filament, and at 1-2 amps with the Rh filament.

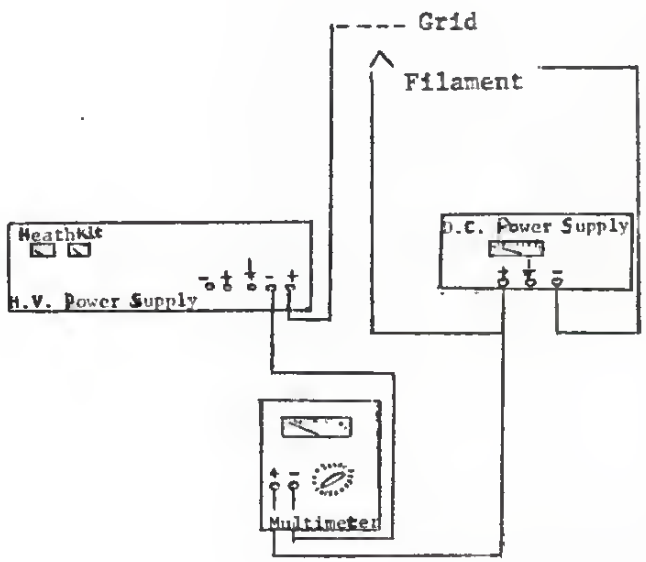

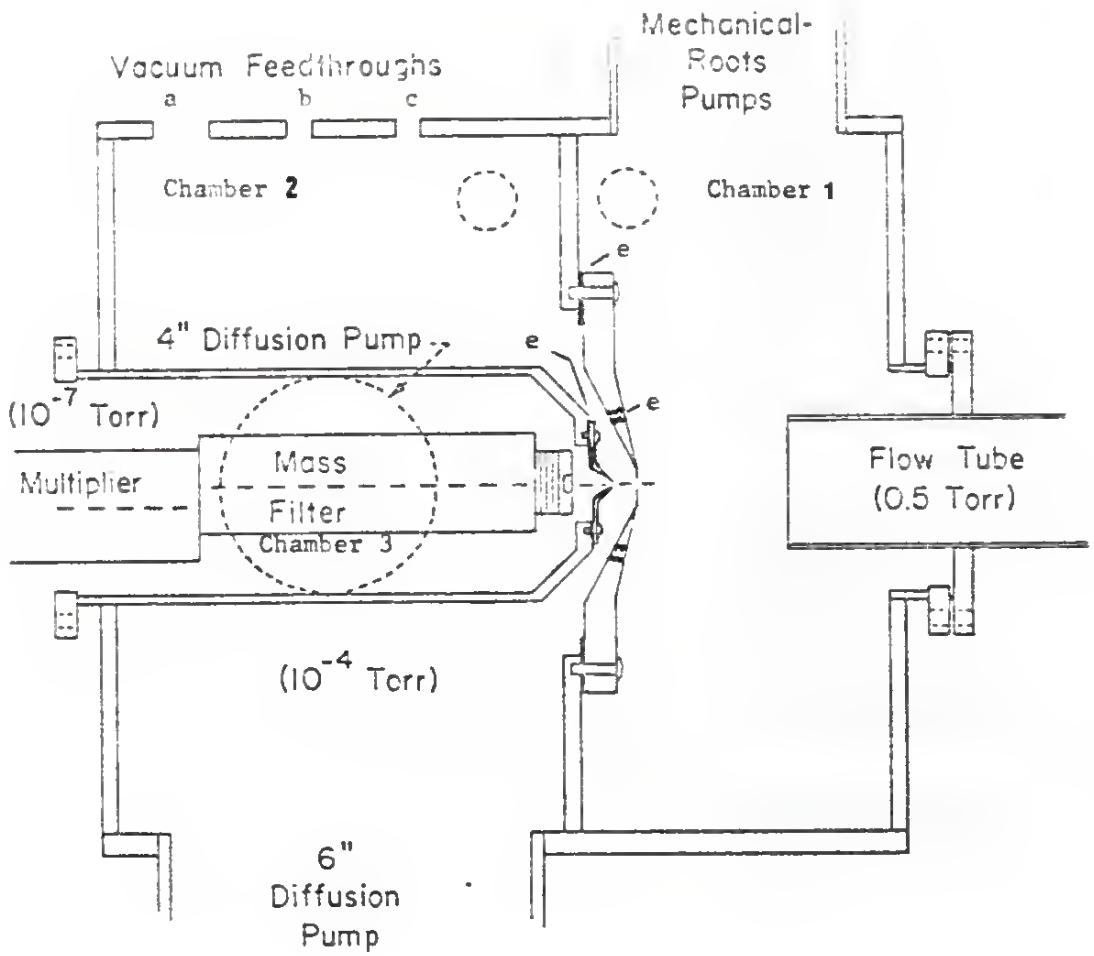

Figure 3. Schematic diagram of the differential pumping system and nose cones. The housing is made of stainless steel, while the nose cones are molybdenum and electrically isolated with teflon spacers (e). The vacuum feedthroughs are (a) electrical connections to the nose cones, (b) for injection of gas samples directly into the mass spectrometer chamber, and (c) for the TC gauge to measure pressure, and (d) is a by-pass port from chamber 1 to chamber 2.

function of concentration changes of the added neutral reagent.

Rate constants for the bimolecular ion-molecule reactions are determined under pseudo-first-order conditions with the added neutral reactant gas concentration in large excess over that of the ion concentration in the flow. In a typical experiment, the concentration of the desired ion is $\sim 10^{8}$ cm^{-3} while the smallest concentration of the added neutral reactant is $\sim 10^{10}$ molecules cm^{-3} in a flow containing $\sim 10^{16}$ atoms cm^{-3} of helium. The ion-molecule reaction distance, which is related to the reaction time, is held constant while the neutral concentration added to the flow is varied. Separate ion intensity measurements are recorded for each neutral reactant concentration and a plot of log $[Ion^{\pm}]$ vs neutral concentration [Q] is constructed. The slope of that plot then yields the bimolecular rate constant using eq (4), where r is the radius of the flow

$$k(cm^{3}\ molecule^{-1}\ s^{-1}) = \frac{d(\log[Ion^{\pm}])}{d[Q](molecule\ cm^{-3})} \times \frac{F_{He}(atm\ cm^{3}s^{-1}) \times 2.78 \times 10^{3}(torr\ atm^{-1})}{P_{He}(torr) \times r^{2}(cm^{2}) \times D(cm)} \qquad (4)$$

tube and D is the distance from the neutral inlet to the first sampling nose cone. The ionic products of the ion-molecule reaction are also monitored during the course of these kinetic experiments. The operational procedures for the FA system can be found in Appendix I.

B. Flow Tube

The flow tube is a 7.15 cm ID by 123.8 cm long stainless steel pipe (supplier: Esco Products, Inc.) as shown in Figure 1(g) was placed just after the injection port for neutral reagents (f, in Figure 1). This port allows observation and measurement of light emission from excited products of the ion-molecule reactions. The section of the flow tube

which houses the window is connected to the flow tube via mated flanges with 'O'-ring seals. This versatility allows new components for the flow tube to be added with minimal down time depending on individual experimental needs. A series of ports were welded onto the flow tube to allow for installation of the cold-cathode discharge and ion gun, introduction of substrate gases without disturbing the flow, and measurement of the flow tube pressure using a pressure transducer. The He flow was measured with a precalibrated tri-flat flowmeter (Fisher & Porter #449-306). A pressure of 0.5 torr (monitored with a calibrated Celesco 0-900 torr pressure transducer) was maintained by a partially throttled gate valve leading to a Stokes Roots blower/mecahnical pump system (model 1722-s). This corresponds to a flow velocity of 80 m s^{-1} when corrected for a parabolic flow profile. Opening or closing the valve gave faster and slower flows respectively.

C. Ion Sources

Two ionization sources were used in these experiments. The first was an electron gun which consists of a 2.0 mil. x 27 mil. x 1.25 in. long thorium oxide coated iridium filament (supplier: Electron Technology) and an accelerating grid made of fine mesh tungsten screen. Later, an uncoated rhenium filament, 0.5 mil. x 30 mil. x 1.24 in. long (supplier: H. Cross Inc.), was used to reduce costs. Both filaments have very low work functions for vaporization of electrons. The heater power supply for the filament was a Hewlett Packard series MPB-S model 6286 A DC power supply which delivers 0 to 24 volts and 0 to 12 amps. This power supply was operated at 2 V and 6 amps for the ThO_2-coated Ir filament, and 2 V and 2 amps for the Re filament. The accelerating voltage power supply used was a Heathkit high voltage regulated power supply capable of supplying up to 400 V and 150 ma. This power supply was set between -100 and -200 V

for both filaments. The current between the filament and grid was monitored with a Micronta multi-meter (supplier: Radio Shack), and varied between 5 and 50 ma. High background noise was a problem until the EAI console, DC power supply, high voltage power supply, multimeter, and lens potential meter were wired to a common ground.

The second ion source was a cold-cathode discharge which was introduced into the FA in order to produce metastable atoms of the rare gases. The rare gas (10 to 15% of the helium buffer gas flow) was introduced through the cold-cathode discharge producing a low concentration of metastable atoms (1×10^{10} atoms cm^{-3}) which are added to the buffer gas. The decay of the metastable atoms involve loss due to diffusion to and reaction with the walls of the flow tube, collision with the buffer gas or substrate gas, or slow radiative decay.[23] The neutral substrate gas was injected downstream of the metastable production region (d, Figure 1) where Penning ionization takes place by metastable/substrate collisions. The product ions flow with the He carrier gas through the reaction region, about 75 cm, before reaching the ion sampling nose cones.

The discharge tube (Figure 4) was inserted into the flow tube via an 'O'-ring slip-seal (Figure 5), so, it could be withdrawn from the main flow to allow operation of the electron gun (Figure 1). Some previously described cold-cathode discharge tubes were used as models.[23]

The discharge tube consisted of two 8 mm I.D. glass tubes (9.75 O.D.) connected by an 'O'-ring joint seal. Both electrodes are made of rolled tantalum foil, and are spot-welded to tungsten wire leads. The tungsten was then sealed into the bottom tube with a metal to glass seal. The electrodes must fit snugly in the walls of the glass tube to allow the maximum amount of rare gas to flow through the discharge. The cathode was placed downstream and the lead wire has a glass sleeve (3 mm glass

Figure 4. Cold-cathode discharge tube.

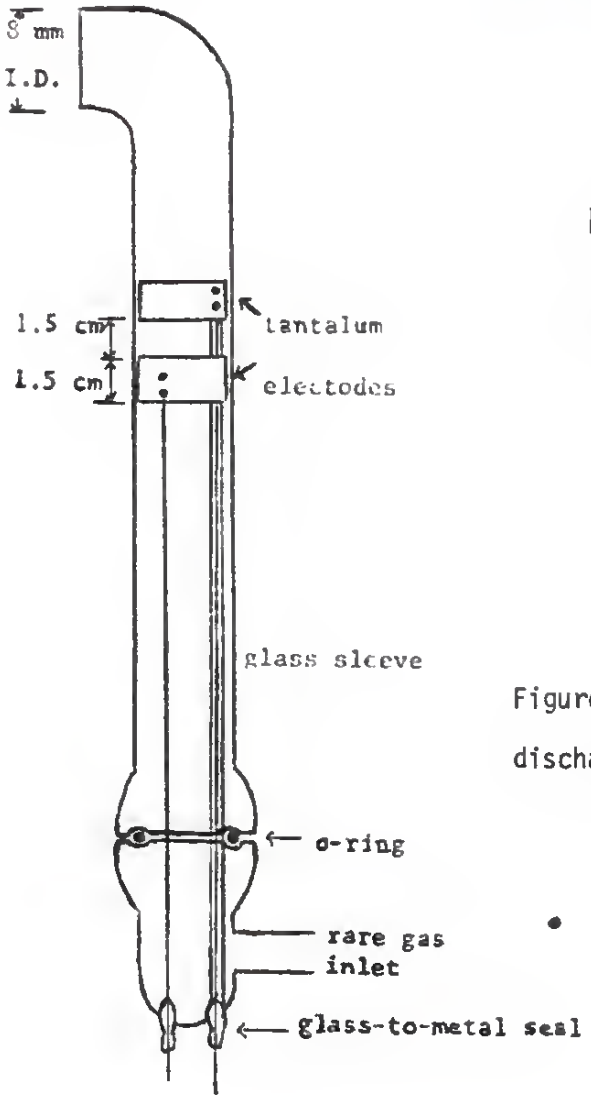

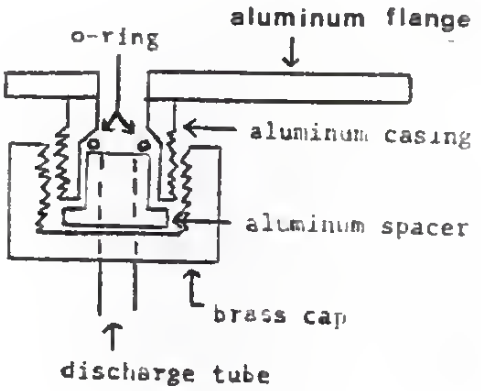

Figure 5. Slip seal for cold-cathode discharge tube.

tubing) to prevent arcing between it and the anode lead wire. A 250 to 300 V difference was applied to the electrodes with a 20 K resister to ground on the cathode. The best results occur for argon with flows of 12 m s^{-1} and a 260 V potential difference applied to the electrodes. For neon and helium, a flow of 10 m s^{-1} with differences of 280 V and 300 V potentials, respectively, applied to the electrodes. These flow rates were measured with a tri-flat flow meter #449-209-0018 from which the rare

gas flows through 3 meters of 6.35 mm copper tubing before passage through the discharge. The pressure in the discharge tube was not measured and is probably higher than the 0.5 torr measured in the flow tube.

The slip-seal (Figure 5) consisted of a threaded brass cap, an aluminum spacer, an 'O'-ring, and a female threaded aluminum casing. When the brass cap is tightened, the spacer squeezes the 'O'-ring against the inserted glass discharge tube and the lip of the casing giving a vacuum tight seal. The casing is welded off center to a flange which seals to the flange on a neck of the flow tube via an 'O'-ring which allows both the cold-cathode discharge tube and the electron gun to be present in the flow tube (Figure 1). The end of the discharge tube is bent at a 90° angle so that it is roughly centered in the main flow tube (Figure 1). This provides better mixing with the helium buffer gas and helps avoid photoionization of the reagent gas or photoactivation of the electron multiplier. The mixing geometry was tested by producing argon metastable atoms, and adding N_2 through port e (Figure 1) of the flow tube. The N_2 emission from the excitation transfer reaction between $Ar(^3P_{0,2})$ and N_2 can then be observed through the viewing port in the flow tube.

D. Differentially Pumped Analysis Section

The differentially pumped analysis section was designed by Dr. John Kolts and built by Mr. Al Nielson.[24] The ion containing helium flow is sampled through a 1.4 mm orifice in the first of two molybdenum nose cones (supplier: Amax Specialty Metals Corp.) into chamber 2, Figure 3, which is maintained at a pressure of 10^{-4} torr by a Varian 6" oil diffusion pump backed by a Welch #1397 mechanical pump. This portion of the flow is further sampled through a 1 mm orifice in the second molybdenum nose cone into the mass spectrometer-electron multiplier compartment (Chamber 3), which is pumped by a 4" oil diffusion pump backed by a Welch #1402 mechanical

pump, and operates between (2 to 6) x 10^{-7} torr. Chamber 3 is separated from the oil diffusion pump by a Varian cryotrap cooled by liquid nitrogen, while a Varian low profile water cooled baffle separates the 6" diffusion pump from chamber 2. The molybdenum nose cones are electrically isolated by Teflon spacers (e, Figure 2) from the stainless steel main housing. Electrical feedthroughs allow each molybdenum nose cone to be biased with a variable potential of $\pm$15 V relative to ground. The potentials are set by trial and error, the best results for positive ions were for settings between 0 and +1.0 V on the first nose cone and -15.0 V on the second nose cone.

The EAI quad #250 positive ion quadrupole mass spectrometer has an on-axis ionizer/ion lens system in front of the mass filter. This ion lens system can be controlled by bias potentials, with optimum potentials of -15 volts on all lenses with the exception of the extractor which should be adjusted for maximum peak height of the ions being studied. The quadrapole can also be operated as a conventional low pressure mass spectrometer (ionizer on) with the potentials set according to the operation manual. The nominal mass range of the quadrupole is 1 to 500 atomic mass units (AMU) with the best resolution observed in the 1 to 150 AMU range.

E. Calibration

In order to check the rate constants obtained with this FA system against accepted results obtained in other laboratories, the rate constant for the reaction of N_2 with He^+ was determined to be (1.2 $\pm$ 0.2) x 10^{-9} cm^3 $molecules^{-1}$ s^{-1}. This value was determined by averaging the results of eight different experiments and the error is the maximum deviation from the average. This value is in good agreement with the literature value of (1.2 $\pm$ 0.1) x 10^{-9} cm^3 $molecules^{-1}$ s^{-1}.[25] The rate constant and product ions for the reactions of He^+ with other reagents (CH_2CO,

$C_6H_5N_3$, $(CF_3)_2C{=}N_2$) are given in Appendix II.

The natural abundance and observed isotope ratios of Xe^+ produced from $He^+ + Xe$ are given in Table I. The spectrum obtained for the isotopes of Xe^+ produced from He^+ is shown in Figure 6. This illustrates the resolution capabilities of the instrument.

The throughput of the mass filter of the quadrupole mass spectrometer for ions of different masses was determined by observing the ions of a known mixture of argon, krypton, and xenon reacting with helium metastable atoms to form the respective rare gas ions. By inletting low concentrations of the rare gas mixture ((5 to 10) x 10^{10} molecules cm^{-3}) the relative ratios of each rare gas ion can be calculated using eq 5, where the ratio of the ion signal of the rare gas X to the total ion signal is sought, $[Ar^+]$, $[Kr^+]$, and $[Xe^+]$ are ion concentrations, k_I^{Ar}, k_I^{Kr}, and k_I^{Xe} are the Penning ionization rate constants which are known, [12,26] [Ar], [Kr], and [Xe] are the known concentrations of the rare gases introduced

Table I

Isotopes of Xe

AMU	Calculated values	Observed values*
128	1.92	1.9
129	26.23	27.6
130	4.05	4.6
131	21.24	21.1
132	26.93	25.7
134	10.52	9.5
136	8.93	7.6

*The values listed are those obtained from $He^+ + Xe \rightarrow He + Xe^+$.

Figure 6

Isotopic spectra of Xe

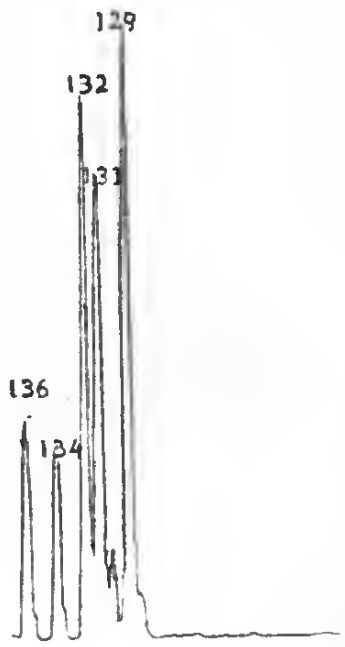

into the flow tube and [He*] is the concentration of the He* metastable atom which will be the same in each case and thus will cancel out of the equation (see model calculation section). The values obtained from eq (5)

$$\frac{[X^+]}{[Ar^+] + [Kr^+] + [Xe^+]} = \frac{k_I^X[X][He^*]t}{k_I^{Ar}[Ar][He^*]t + k_I^{Kr}[Kr][He^*]t + k_I^{Xe}[Xe][He^*]t} \quad (5)$$

are then compared to the ratios of the ion signals obtained from the experiment. The experimental ratios were then corrected to match those calculated.

For calibration of the mass range of 28 to 40 AMU, reactions 6 and 7 were monitored by varying the concentration of a 50/50 mixture of Ar and N_2 which was added to He* in the flow tube. At large concentrations of the Ar/N_2 mixture, reactions 8 and 9 will begin to occur. In order to reduce the possibility of reactions 8 and 9, the ion signals are monitored at low concentrations of the mixture. The reaction rates for the reactions 6-9 have been determined[27,28] and the mass discrimination between AMU 28

$$He^* + Ar \xrightarrow{k_1} Ar^+ + He + e^- \quad (6)$$

$$He^* + N_2 \xrightarrow{k_2} N_2^+ + He + e^- \quad (7)$$

$$N_2 + Ar^+ \xrightarrow{k_3} N_2^+ + Ar \quad (8)$$

$$Ar + N_2^+ \xrightarrow{k_4} Ar^+ + N_2 \quad (9)$$

and 40 can be calculated from the ion signals. The correction factors for each mass unit are shown in Figures 7 and 8. The resolution of the instrument plays a large part in the adjustment of mass discrimination as shown in both Figures 7 and 8. It must also be pointed out that larger mass discrimination increases as unit mass resolution is obtained. Since the

correction factors for mass discrimination at the resolution of the instrument employed have been determined (Figures 7 and 8), any of these settings may be used to obtain the corrected data. For resolution adjustments, see the owners manual. In each experiment the resolution was adjusted to one of the values shown in Figures 7 and 8, and the correction factor used for each mass encountered was taken directly from that line.

F. Materials

The helium buffer gas (Welder Products) was purified by passage through two traps filled with Oavison type 4A molecular sieves cooled with liquid nitrogen. The He was warmed to room temperature in a glass coil prior to introduction into the flow tube. Other gas and liquid substrates and their suppliers were nitrogen, argon, and oxygen (Welder Products), krypton and xenon (Cryogenic Rare Gas Labs), Ne(Union Carbide), CH_3Cl, NO, CO, C_2F_4, and $(CH_3)_3CH$ (Matheson), $(CH_3)_4C$ (Fluka), and C_6F_6 (Aldrich), PhN_3 (ref. 29), $\underline{c}$-$C_5H_4N_2$ (ref. 30), and $(CF_3)_2CN_2$ (ref. 31).

The CH_2Cl_2 was purified by shaking it with portions of concentrated H_2SO_4 until the acid layer remained colorless. The CH_2Cl_2 was washed with water, 5% aqueous Na_2CO_3, then again with water. It was then dried with $CaCl_2$ and distilled from $CaSO_4$, and a constant boiling fraction, bp 40°, was stored in the dark in a brown bottle containing Linde type 4A molecular sieves. $CHCl_3$ was purified by washing with water (to remove ethanol stabilizer), dried by refluxing with $CaCl_2$, distilled, and a constant boiling fraction, bp 61°, was stored in the dark in a brown bottle containing Linde type 4A molecular sieves. Other liquids used (CCl_4, $(C_2H_5)_2O$, C_6H_6, and C_6F_6) were fractionally distilled and the centercut, constant boiling fraction was used. All substrates were transferred to their gas storage bulbs after three freeze-pump-thaw degassing cycles.

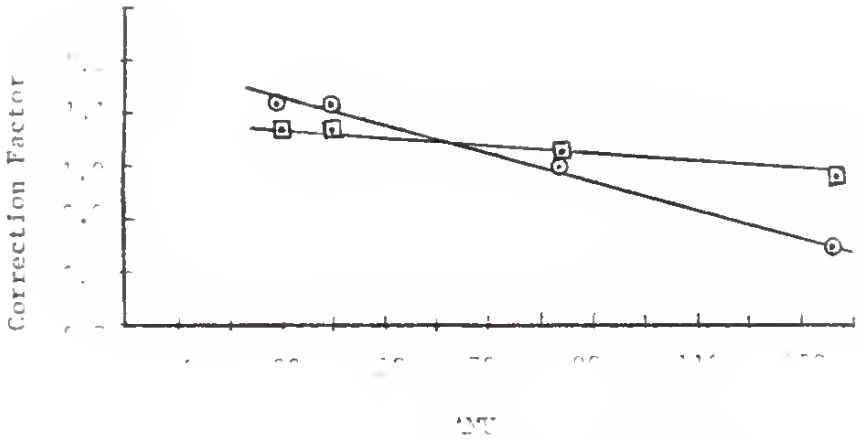

Figure 7. Plot of AMU vs correction factor for mass distribution of the medium mass range (AMU 1-150) for the quad #250, resolution = 5.00 ( ) and resolution = 5.14 ( ). The discharge was operated at 265 V with -1 V on the first nose cone, -15 V on the second nose cone and remaining lenses.

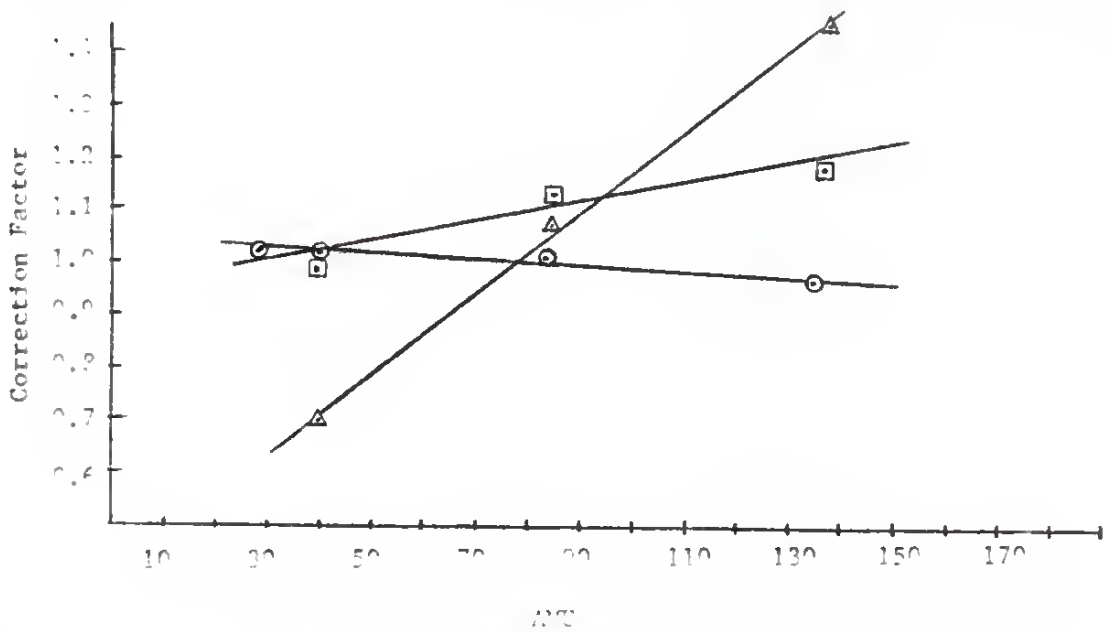

Figure 8. Plot of AMU vs correction factor for mass discrimination of the high mass range (AMU 1-500), resolution = 5.00 ( ), 4.92 ( ), and 5.14 ( ). The discharge was operated at 265 V with -1 V on the first nose cone, -15 V on the second nose cone and remaining lenses.

IV. Model Calculations

One of the goals in this study was to make relative measurements of the Penning ionization branching fractions for Ar*, Ne*, and He*. Before this could be accomplished with any certainty, we must establish the effect of diffusion and the subsequent quenching at the walls of the flow tube for the various metastable atoms and ions in helium carrier gas have on the measurements of the relative branching fractions. The concentrations of the neutral reagent which produce the best results must also be determined. Finally one must ask the question, can reagents with different quenching rates be compared in order to determine the relative branching fractions for Penning ionization?

In order to answer these questions, model calculations were used to evaluate the usefulness of the flowing afterglow/mass spectrometer in the measurement of ionization branching fractions for the metastable atoms from the variation of ion signals as a function of added substrate gas. Two general models will be discussed, then the model for each metastable atom will be examined. The first model ignores diffusion while the rest take diffusion into consideration.

A. Kinetic Model Without Diffusion

The slopes from plots of ion signals vs the concentration of the substrate at low flow rates and the constant (maximum) ion signals from high concentrations of the substrate gas can be related to the relative quenching rate constants and the Penning ionization rate constants using expressions (14) and (17). These expressions are developed from the reactions in equations (10) and (11), where A* represents the metastable atom, Q is the

$$A^* + Q \xrightarrow{k_I} B^+ + A \qquad (10)$$

$$\xrightarrow{k_i} X_i + A$$

substrate molecule, k_I is the Penning ionization rate constant, B^+ is the product ion from Penning ionization, and k_i is the rate constant for all other quenching processes forming neutral products, X_i. The total quenching rate constant, k_Q, is $k_I + \Sigma k_i$. The differential rate equations are;

$$-d[A^*]/dt = k_I[Q][A^*] + \Sigma k_i[Q][A^*] = (k_I + \Sigma k_i)[Q][A] = k_Q[Q][A] \quad (12)$$

$$d[B^+]/dt = k_I[Q][A^*] \quad (13)$$

where $[A^*]$ is the concentration of the metastable atom and $[Q]$ is the concentration of the substrate gas. If the initial concentration of A^* is $[A]_o$, integration of eq (12) gives,

$$[A^*] = [A^*]_o \exp(-k_Q[Q])t \quad (14)$$

Substituting eq (14) into eq (13) gives,

$$d[B^+]/dt = k_I[Q][A^*]_o \exp(-k_Q[Q])t \quad (15)$$

which can be integrated to give eq (16)

$$[B^+] = (k_I[A^*]_o/k_Q)(1 - \exp(-k_Q[Q]t)) \quad (16)$$

Expanding eq (16) for the case where Δt or $[Q]$ is small gives:

$$[B^+] = (k_I[A^*]_o/k_Q)(1 - (1 - k_Q[Q]t)) \quad (17\ a)$$

$$= (k_I[A^*]_o/k_Q)(k_Q[Q]t) \quad (17\ b)$$

$$= k_I[A^*]_o[Q]t. \quad (17\ c)$$

Thus, at sufficiently low concentrations of Q, a plot of $[B^+]$ vs $[Q]$ will produce a linear plot with a slope of $k_I[A^*]_o t$. When comparing the slopes from two substrate gases at low concentrations for the same value of $[A^*]$, the ratio corresponds to the ratio for the k_I's, as seen in eq (18):

$$\frac{[B^+]}{[C^+]} = \frac{(k_I^B[A^*]_o t)}{(k_I^B[A^*]_o t)} = \frac{k_I^B}{k_I^C} \quad (18)$$

If enough reagent Q is added to quench all of the metastable atoms, the ion signal reaches a plateau, which is proportional to the fraction of the metastable atoms converted to ions, i.e. the branching fraction for Penning ionization. This is shown in eq (19), which is obtained from eq (16) for large Q or long t. By multiplying the pleateau signal ratio by the quenching rate constant ratio, the ratio k_I^B/k_I^C can be obtained.

$$\frac{[B^+]}{[C^+]} = \frac{[A^*]_o(k_I/k_Q)^B}{[A^*]_o(k_I/k_Q)^C} = \frac{(k_I/k_Q)^B}{(k_I/k_Q)^C} \tag{19}$$

Thus, the high and low concentration data sets provide a check. Since many quenching rate constants have been determined for Ar*,[18,32,35] Ne*,[17,34] and He*,[33] the two experimental measurements plus the quenching rate constants can provide a good consistency check for k_I^B/k_I^C.

B. Kinetic Model with Diffusion

A different set of rate equations emerges when diffusion is included as a loss process for ions and metastable atoms. These processes are shown in eqs (20) and (21).

$$A^* \xrightarrow{k_w} \text{wall} \tag{20}$$

$$B^+ \xrightarrow{k_w'} \text{wall} \tag{21}$$

The differential rate equations are given by eqs (22) and (23)

$$-d[A^*]/dt = k_I[Q][A^*] + k_i[Q][A^*] = k_w[A^*] \tag{22}$$

$$d[B^+]/dt = k_I[Q][A^*] - k_w'[B^+] \tag{23}$$

where $k_i[Q][A^*]$ includes all quenching processes except for Penning ionization. The total quenching rate constant is defined as, $k_Q = (k_I + \Sigma k_i)$ so that $(k_I + \Sigma k_i)[Q][A^*] = k_Q[Q][A^*]$. The rate constants k_w and k_w' represent the rate constants for diffusion to the wall of the flow tube where unit

quenching probability is assumed to take place for the metastable atoms and ions. The rate constant for diffusion can be defined in terms of the pressure independent diffusion coefficient, D_o, is shown in eq (24).

$$k_w = D_o/\Lambda^2[M]\eta \tag{24}$$

where [M] is the concentration of the buffer gas (1.63×10^{16} molecules cm^{-3} at a pressure of 0.5 torr), η is the correction factor for parabolic flow (1.6), and Λ is the diffusion length, defined as $\Lambda^{-2} = (\pi/L^2) + (4.82/d^2)$; L is the length and d is the diameter of the flow tube.[B,23] For the tube used in the present experiments, d is 7.15 cm and L is 73 cm when the substrate gas is introduced at port f in Figure 1. The value for Λ^{-2} is 0.0945 cm^{-2}. Equation (22) can be integrated to give:

$$[A^*] = [A^*]_o \exp -(k_w + k_Q[Q])t \tag{25}$$

Substitution into eq (23) yields:

$$d[B^+]/dt = k_I[Q][A^*]_o \exp -(k_w + k_Q[Q])t - k_w'[B^+] \tag{26}$$

If there is no secondary reaction or decay involving the primary ion, eq (26) can be rewritten as:

$$d[B^+]/dt + k_w'[B^+] = k_I[A^*]_o[Q] \exp -(k_w + k_Q[Q])t \tag{27}$$

The integration factor is $\exp(k_w't)$[36] and eq(27) can be written as eq (28).

$$[B^+] = \frac{1}{\exp(k_w't)} \int \exp(k_w't) \cdot k_I[A^*]_o[Q] \exp[-(k_w + k_Q[Q])t] \cdot dt + \frac{C}{\exp(k_w't)}$$

$$= \frac{k_1[A^*]_o[Q]}{\exp(k_w't)} \int \exp[k_w' - (k_w + k_Q[Q])t] \cdot dt + \frac{C}{\exp(k_w't)}$$

$$= \frac{k_1[A^*]_o[Q]}{\exp(k_w't)} \left| \frac{\exp[k_w' - (k_w + k_Q[Q])t]}{k_w' - (k_w + k_Q[Q]} \right| + \frac{C}{\exp(k_w't)} \tag{28}$$

At t = 0, B = 0; so $C = k_1[A^*]_o[Q]/[k_w' - (k_w + k_Q[Q])]$ and

$$[B^+] = \frac{k_1[A^*]_o[Q]}{\exp(k_w't)\cdot(k_w' - k_w - k_Q[Q])}\,[\exp[k_w' - (k_w + k_Q[Q])t] - 1] \qquad (29)$$

this can be reduced to;

$$[B^+] = \frac{k_1[A^*]_o[Q]}{(k_w' - k_w - k_Q[Q])}\,[\exp(-k_w - k_Q[Q])t - \exp(-k_w't)] \qquad (30)$$

The quenching rate constant, k_Q, ranges from 1 to 10 x 10^{-10} for most molecules.[12,32,35] At low concentrations of Q (1 to 10) x 10^{10} molecules cm^{-3}, $k_Q[Q] < k_w$ and $\exp(-k_w - k_Q[Q])t = \exp(-k_w t)$. Using eq (30), a ratio of the ion signals for two substrate gases at low concentrations is;

$$\frac{[B^+]}{[C^+]} = \frac{\left[\frac{k_I[A^*]_o[Q]}{k_w' - k_w}\right]^B \left[\exp(-k_w t) - \exp(-k_w't)\right]^B}{\left[\frac{k_I[A^*]_o[Q]}{k_w' - k_w}\right]^C \left[\exp(-k_w t) - \exp(-k_w't)\right]^C} \qquad (31)$$

The rate constants for diffusion, k_w and k_w', are proportional to the diffusion coefficient, D_o (eq 24), which has been shown to be inversely proportional to the square root of the reduced mass, μ, of the ions considered.[37] For most ions in helium $(\mu)^{\frac{1}{2}}$ changes only slightly. For example, when comparing the square root of the reduced mass of argon (mol. wt. 40 AMU) in helium with that of CCl_4 (mol. wt. 152 AMU) in helium, $(\mu)^{\frac{1}{2}}$ is 1.90 for argon and 1.97 for CCl_4. Thus, the mass of the ion has little effect on the diffusion rate. This has been verified in a number of studies of ions in helium.[20,39,40] Table II lists some values of diffusion coefficients for various ions and metastable atoms in helium.

If it is assumed that the diffusion rate constants for B^+ and C^+ are equal, then eq (31) can be reduced to eq (32) which is the same result

$$\frac{[B^+]}{[C^+]} = \frac{k_I^B}{k_I^C} \tag{32}$$

obtained for low concentrations of the substrate when diffusion was ignored (eq 18).

In eq (31), the differences $(k_w - k_w')$ and $(\exp(-k_w t) - \exp(-k_w' t))$ appear. If these differences approach zero, the arguments presented here are no longer valid. However, for $He(2^3S)$ is similar to that for various ions in helium. In this case, both the exponential and the pre-exponential portions of eq (30) would be zero. The $He(2^3S)$ case will be discussed in the next section.

Next we wish to consider the high concentration regime with diffusion included as a loss mechanism. The general case for large values of Q, (1 to 10) x 10^{12} molecules cm^{-3}, such that $(k_Q[Q] + k_w) > 500\ s^{-1}$ gives $\exp(-k_w - k_Q[Q])t = 0$. Thus, eq (33) follows from eq (30) and a ratio of

$$[B^+] = \left[\frac{k_I[A^*]_o[Q]}{k_w' - (k_w + k_Q[Q])}\right]^B \left[\exp(-k_w' t)\right] \tag{33}$$

two ion signals can be represented by eq (34), where k_w and k_w' are assumed to be different. If $k_Q[Q] > k_w' - k_w$, eq (34) reduces to eq (35).

$$[B^+] = \left[\frac{k_I[A^*]_o}{k_Q}\right] \exp(-k_w' t) \tag{34}$$

and

$$\frac{[B^+]}{[C^+]} = \frac{(k_I/k_Q \exp(-k_w' t))^B}{(k_I/k_Q \exp(-k_w' t))^C} \tag{35}$$

C. Kinetic Model for the Penning Ionization by He*

Since He(2^3S) has a similar diffusion coefficient to most ions in helium (Table II), we must consider the case for which the diffusion rate constant of He*, k_w, is equal to the diffusion rate constant for the ions, k_w', in helium. A new rate constant of diffusion, k_w'', will be used to account for the diffusion of both the He* and the ions. Substituting k_w'' into eq (30) leaves eq (36). For low [Q]

$$[B^+] = \frac{k_I[A^*]_o}{-k_Q} \exp(-k_w''t)[\exp(-k_Q[Q]t) - 1] \tag{36}$$

eq (36) can be written as

$$[B^+] = -(k_I[A^*]_o/k_Q)\exp(-k_w''t)\ [(1 - k_Q[Q]) - 1] \tag{37}$$

$$= -(k_I[A^*]_o[Q]\exp(-k_w''t)). \tag{38}$$

This can be compared to eq (30) but now the problem of the terms approaching zero for $k_w = k_w'$ has been avoided. Since most ions have the same diffusion rate (Table II), a ratio of the product ions from the Penning ionization reaction of two substrate gases at low concentrations will yield a ratio of the Penning ionization rate constants. This is the same result we obtained in eq (32) and also when we ignored the diffusion terms as in eq (18). A check of these results can be made by varying the pressure in the flow tube. As the flow pressure was varied from 0.4 torr to 1.0 torr, no change in ion signal peak height was observed. Thus, we have demonstrated that diffusion is not a serious problem for k_I measurements providing $k_w'(B) = k_w'(C)$.

For large [Q], $k[Q] > 100\ s^{-1}$ and eq (36) reduces to eq (39).

Table II. (Free Ion Diffusion Coefficient x Gas Number Density) (DN) and Diffusion Rate Constants (k_w) in Helium.

Ionic species	DN (10^{19} cm^{-1} s^{-1})	k_w (s^{-1})[f]
He^* (2^3S)	1.44[a] 1.50[e]	139
Ar^* ($^3P_2$)	0.69[g]	70[g]
Ne^* ($^3P_2$)	2.00[e]	189
He^+	0.66[b]	62
O^+	1.43[b] 1.53[a]	140
O_2^+	1.42[c]	134
N_2^+	1.33[b]	126
Ar^+	1.42[d]	134
D^+	1.54[b]	145
OH^-	1.59[b]	150

[a]Ref. 38. [b]Ref. 39. [c]Ref. 41. [d]Ref. 42. [e]Ref. 43. [f]Calculated from eq (23). [g]Estimated value (see text).

$$[B^+] = \frac{k_I[A^*]_o}{k_Q} \exp(-k_w'' t) \tag{39}$$

Since $\exp(-k_w'' t) < 1.0$, the ion signal can never obtain a maximum value as large as in the case where diffusion was ignored. However, since $\exp(-k_w'' t)$ will be the same for most ions in helium, a ratio of the plateau obtained from the ion signal heights of two substrate gases at high concentrations is proportional to $(k_I/k_Q)/(k_I'/k_Q')$. This is the same conclusion we reached with eqs (34) and (35) and is the same result obtained when diffusion is ignored in eq (19).

In summary, when studying the Penning ionization by He*, the diffusion

rates have no effect on the relative branching fractions. Care must be taken in deciding if the assumptions made hold for the ion under investigation.

O. Kinetic Models for the Penning Ionization by Ar*

There have been no studies to date which report a value for the diffusion of argon metastable atoms in helium gas. DePuy, et al.,[44] reported their observations that the diffusion rate of Ar* in helium appeared to be slower then the diffusion of ions in helium. From their results at 0.5 torr, the diffusion rate of the ions were thought to be 2-3 times greater than the diffusion rate of the argon metastable atoms. The diffusion coefficient of Ar* in argon gas has been reported (1.8×10^{18} molecules cm^{-1} s^{-1})[45] and a rough estimate of the diffusion rate of the Ar* in helium can be made by comparing this value to that of another species which has been studied in both He and Ar. The diffusion coefficient of $N(^2O)$ has been determined in both He (25.5×10^{18} molecules cm^{-1} s^{-1}) and Ar (6.7×10^{18} molecules cm^{-1} s^{-1})[38]. From these values the diffusion coefficient for Ar* in helium can be estimated as 6.85×10^{18} molecules cm^{-1} s^{-1} which is about one-half the value for most ions (Table II) and is consistent with DePuy's observations.[44]

The diffusion rate of the argon metastable atoms and the ions in helium should have no effect on the product ion signals from Ar* for low concentrations of the substrate gas (eq 30-32). However, for high concentrations of the substrate gas, the rate of diffusion of both the ions and the metastable atoms will affect the observed ion signal peak heights (eq 34).

A series of model calculations were done using literature values of rate constants and diffusion coefficients in order to determine the effects that various diffusion rates have on the observed ion signals and the sub-

sequent calculations of the branching fractions, and as a guide on the best way to take experimental measurements. The concentration of ions produced was calculated for the Penning ionization of NO by Ar* by substituting the values of Table III into eqs (16) and (30). A semi-log plot for the calculated [Ar*] and [NO^+](molecules cm^{-3}) vs time (ms) was made

Table III. Quenching Rate Constants, Diffusion Rate Constants, and Penning Ionization Branching Fractions for NO and CH_3Cl.

Substrate Gas	$k_w(s^{-1})^d$	k_w' $(s^{-1})^d$	Quenching Rate Constants$(cm^3s^{-1})^a$	Branching Fractions[b]
NO		140	2.2×10^{-10}	0.28,0.20[c]
CH_3Cl		140	7.5×10^{-19}	0.42
Ar*	70			

[a]Ref. 46 [b]Ref. 18 [c]Ref. 32 [d]No values for k_w' were found for any of the species listed so the ions are assumed to have similar values to those listed in Table II and the Ar* is assumed to be one-half of this value.

to display the effects changes in substrate [Q] have on the ion signals (Figure 9). As Figure 9 shows, when time is increased the ion signal reaches a maximum and then decays. This process has been observed for our experimental conditions.[20,41,44] This decay in ion-signal peak height can be explained using eq (30), where [Q] is constant and t is changing. When t becomes larger, the second exponential term becomes dominant which decreases the value of the entire equation. Thus, a decay in the ion concentration should occur.

In our experiments, time is constant and the [Q] is varied. The time is given by eq (40) where z is the distance between the NO inlet and the

first sampling nose cone, $\bar{v}$ is the velocity of the buffer gas, and α is the correction factor (1.6)[23] for parabolic flow in helium buffer gas.[8]

$$dt = dz/(\bar{v}\alpha) \tag{40}$$

The time for our system is 5.7 ms which is fortuitously close to the maximum concentration of NO^+ in (f) of Figure 9 where the NO concentration is 1 x

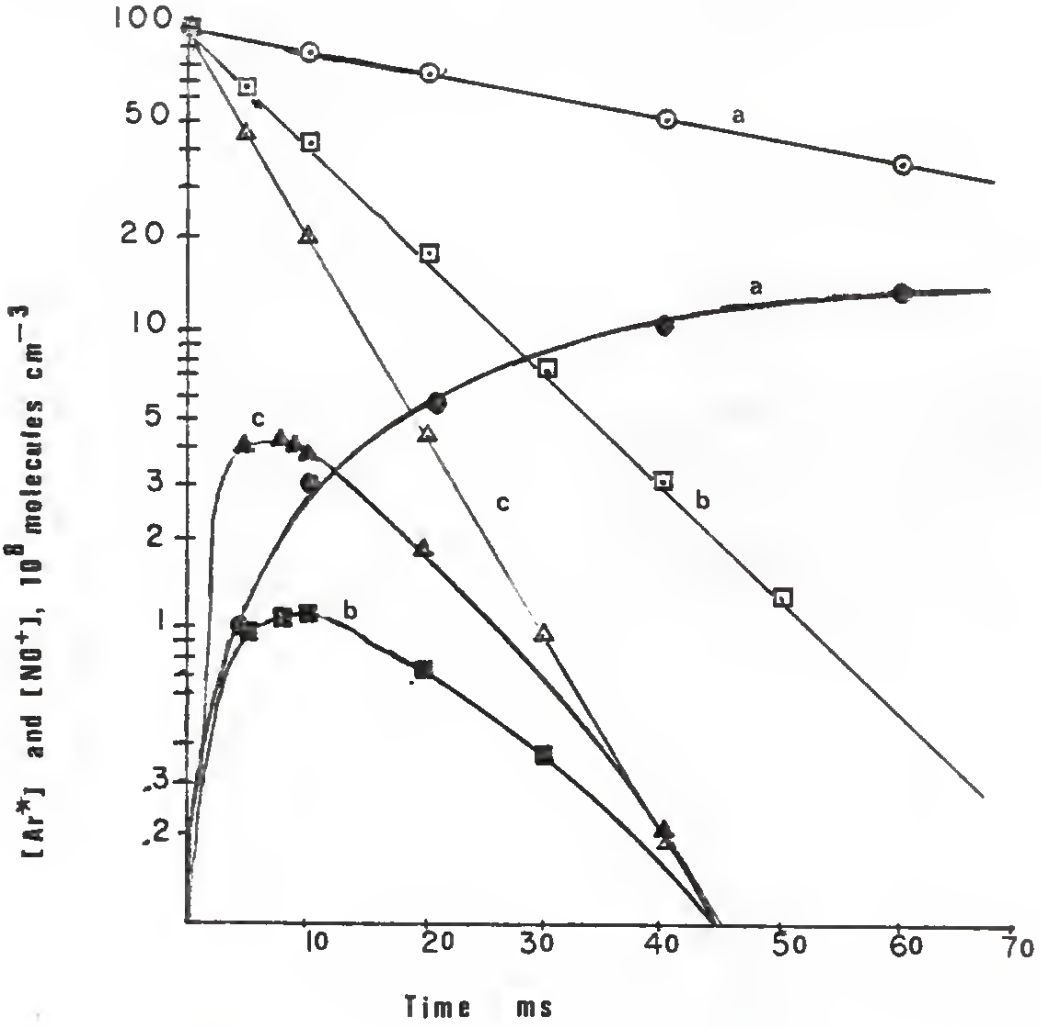

Figure 9. Calculated plot of log [Ar*] and $[NO^+]$ vs time in ms, P_{He} = 0.5 torr: (a) [Ar*] (○) and NO^+ (●) without diffusion, [NO] = 1 x 10^{11} molecules cm^{-3}; (b) [Ar*] (□) and $[NO^+]$ (■) with $k_w' = 2k_w = 140\ s^{-1}$, [NO] = 1 x 10^{11} molecules cm^{-3}; (c) [Ar*] (△) and $[NO^+]$ (▲) with $k_w' = 2k_w = 140\ s^{-1}$, [NO] = 5 x 10^{11} molecules cm^{-3}.

10^{11} molecules cm^{-3}. Figure 10 is a semi-log plot of [Ar*] and [NO^+] against [NO] for the Penning ionization of Ar* by NO for t = 5.7 ms. Several values for the diffusion coefficient of Ar* and NO^+ were used to graphically display the change in [Ar*] and [NO^+] as a function of the

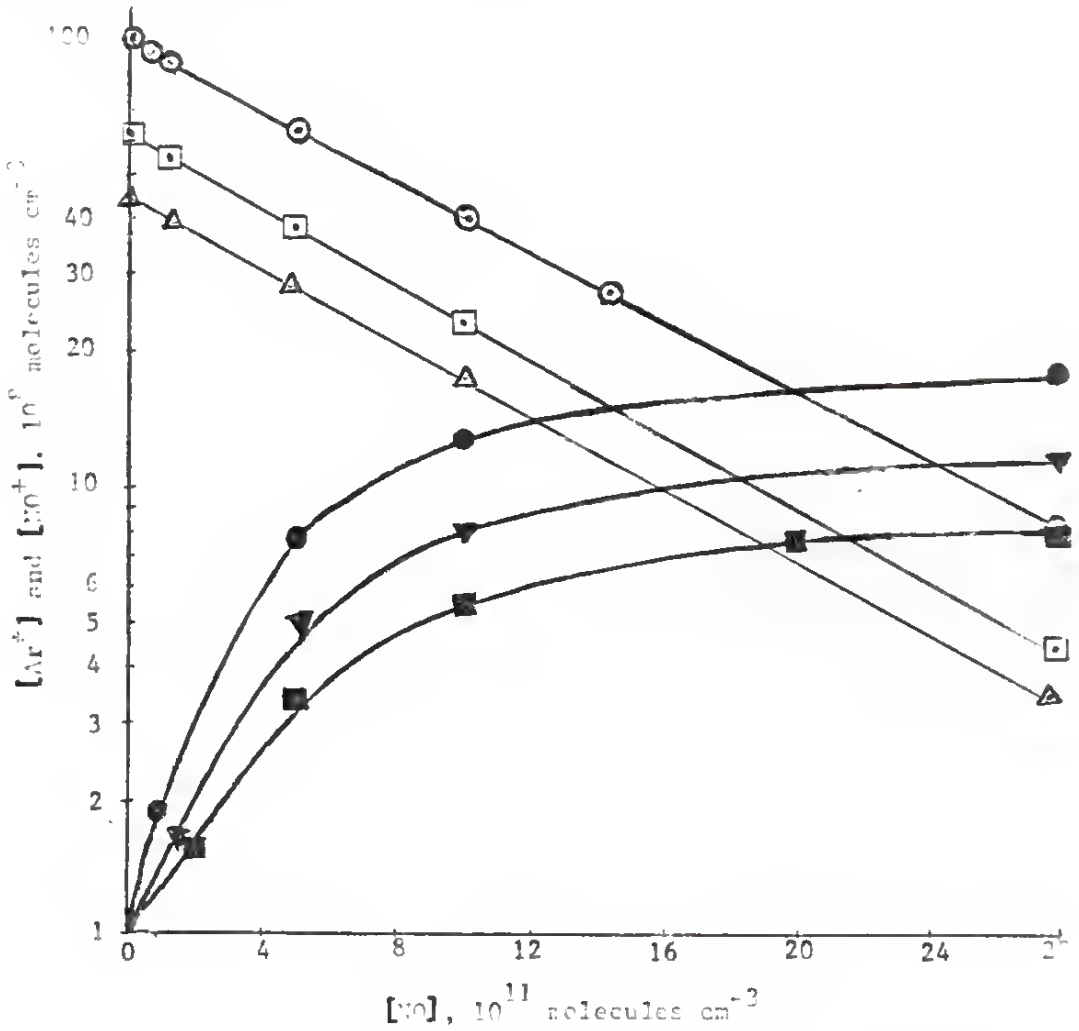

Figure 10. Calculated plot of log [Ar*] and [NO^+] vs added [NO] for t = 5.7 ms and P_{He} = 0.5 torr: (a) [Ar*] (○) and [NO^+] (●) without diffusion; (b) [Ar*] (□) and [NO^+] (▼) with $k_w' = 2k_w = 140\ s^{-1}$; (c) [Ar*] (△) and [$NO^+$] (□) with $k_w' = k_w = 140\ s^{-1}$

diffusion constant. As the diffusion coefficient is increased, the concentration of Ar* is reduced even at [NO] = 0, as is expected from eq (25) and Figure 9. The decay rate of [Ar*] vs [NO] however, is invariant with D_0. The $[NO^+]$ vs [NO] plot is affected by D_0 and D_1, but, the plot is linear at low concentrations of NO, as seen in the expanded plot Figure 11, as expected from eq (30-32). The curvature of the plot of $[NO^+]$ vs [NO]

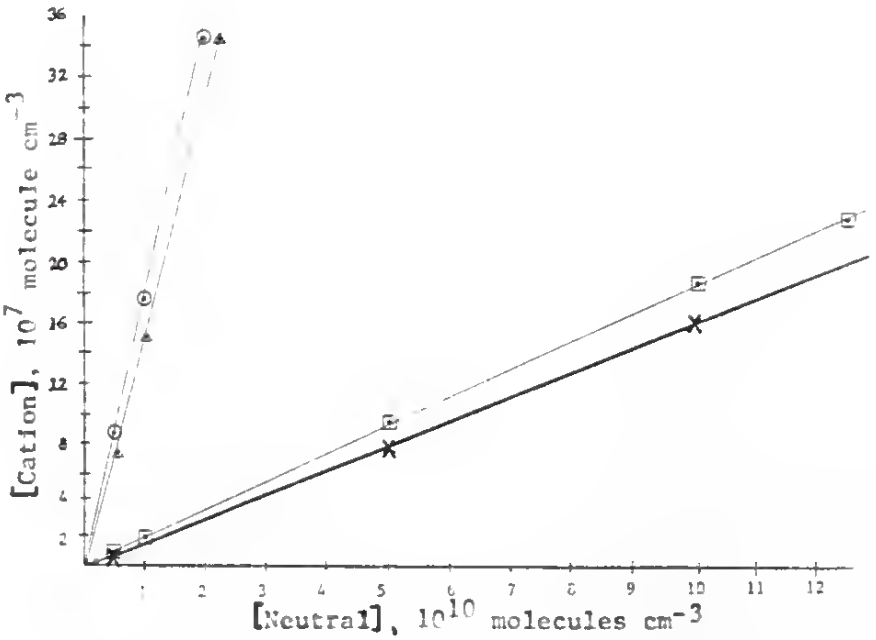

Figure 11. Calculated plot of $[NO^+]$ and $[CH_3Cl^+]$ vs added [NO] and $[CH_3Cl]$ at t = 5.7 ms and P_{He} = 0.5 torr: (a) $[NO^+]$ (□) and $[CH_3Cl^+]$ (○) without diffusion; (b) $[NO^+]$ (×) and $[CH_3Cl^+]$ (△) with $k_w' = 2k_w = 140\ s^{-1}$.

for large concentrations of NO is slight and points taken from > 2 to 7 x 10^{12} molecules cm^{-3} will have the same value within 5%. In this [NO] regime the plot is flat and this regime will be referred to as the plateau region of the graph. From eq (33) we see that if $k_w' > k_w$, the plot of $[B^+]$ vs [Q] at large concentrations of the substrate gas, will start to decay. The amount of the decay will depend on the value of k_w' and k_w.

When $k_w' = k_w$ a plateau will be obtained, as shown for the case of He*. If $k_w' < k_w$ then the same plot will reach a plateau only when $k_Q[Q] >> k_w' - k_w$. The value of $\exp(-k_w t)$ in eq (33) is 0.6 for most ions in helium at a helium pressure of 0.5 torr. The plateau decreases in value, as the diffusion rate increases, since an increase in the diffusion rate decreases the value of $\exp(-k_w' t)$ in eq (33). For the calculations of rate constants and product ratios of individual ions, this effect can be minimized using the normalization technique described by DePuy et al.[44] For the determination of relative branching fractions it still remains to be proven that eq (19) = eq (35). A comparison of two substrates with different k_Q's and k_I's, will enable us to determine what effect, if any, the diffusion rates will have on the determined branching fractions.

The comparison of $[NO^+]$ to $[CH_3Cl^+]$ using both eq (16) and (30) at high and low concentrations of the substrate gases will be used to determine the effect, if any, of diffusion on the relative measurements. The values for the rate constants and branching ratios are taken from Table II and substituted into eqs (16) and (30). Figure 12 is the calculated semi-log plots resulting from eqs (16) and (30).

The results obtained from a comparison of the branching fractions with and without the diffusion terms, are tabulated in Table IV. Since the differences in all values in Table IV are well within experimental error, there is no effect due to diffusion when comparing two ion signals to obtain the ratios. One must be careful, however, and check the assumptions for each substrate in order to verify that the assumptions are correct for that particular gas.

The concentration of Q that will provide the best results can now be determined. A plot of ion signal peak heights for low concentrations of Q (1 to 10 x 10^{10} molecules cm^{-3}) vs the concentration of Q will produce

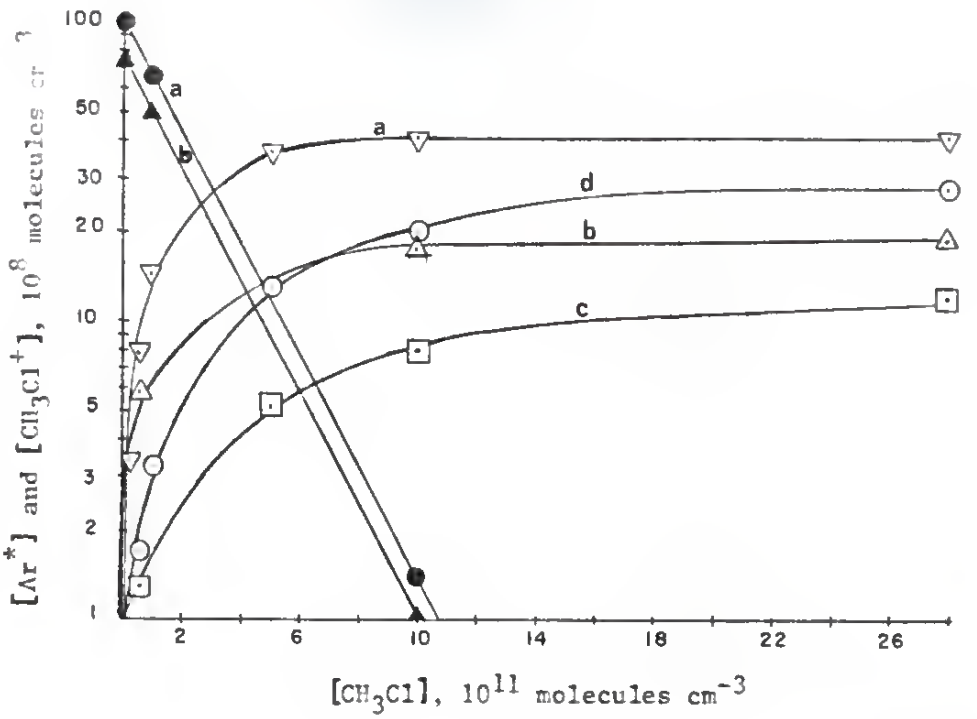

Figure 12. Calculated plot of log [Ar*] and $[CH_3Cl^+]$ vs added $[CH_3Cl]$ for t = 5.7 ms and P_{He} = 0.5 torr: (a) [Ar*] (●) and $[CH_3Cl^+]$ (▽) without diffusion; (b) [Ar*] (▲) and $[CH_3Cl^+]$ (△) with $k_w' = 2k_w = 140\ s^{-1}$; (c) $[CH_3Cl^+]$ (□) with $k_w' = k_w = 140\ s^{-1}$; (d) $[CH_3Cl^+]$ (○) with $k_w' = 140\ s^{-1}$ and $k_w = 190\ s^{-1}$.

a slope of $k_I[A^*]_o t$ as seen in eq (32) and Figure 11. A plot of the ion signal peak height for high concentrations of Q (1 to 10 x 10^{12} molecules cm^{-3}) will produce a plateau which is related to the branching fraction for Penning ionization as seen from eq (35), Figures 10 and 12, and Table IV. Care must be used when assessing the plateau region since the ion signal will start to decay at very large concentrations of Q (1 to 10 x 10^{13} molecules cm^{-3}).

As the inlet of [Q] was changed from f to e in Figure 1 the ion signal

Table IV. Ion Signal Ratios and Branching Fractions for NO^+ and CH_3Cl^+.

	Ratio of Ion Signals, NO^+/CH_3Cl^+		
	$k_w = k_w' = 0\ s^{-1}$	$k_w = 2k_w' = 140\ s^{-1}$	Literature Value[a]
	v		
Plateau Region			
$(k_I/k_Q)^{NO}/(k_I/k_Q)^{CH_3Cl}$	0.667	0.669	0.667
Slope Region			
$(k_I)^{NO}/(k_I)^{CH_3Cl}$	0.203	0.205	0.197
Branching Fraction for CH_3Cl[b]	0.420	0.419	0.420

[a]Ref. 18 and 32. [b]The branching fraction for CH_3Cl is given by $(k_I/k_Q)^{CH_3Cl} = (k_I/k_Q)^{NO}/0.667$; $(k_I/k_Q)^{NO} = 0.28$ in ref. 18.

observed decreased slightly (0 to 5%). When b in Figure 1 was used as the inlet for Q, a larger decrease in the ion signal was observed (15 to 35%) compared to addition via f. A possible explanation for this occurrence may involve obstruction of the flow of Q by the electron gun and the cold-cathode discharge tube creating an uneven distribution of Q in the flow tube leading to more collisions of Q^+ with the walls.

E. Kinetic Models for the Penning Ionization by Ne*.

The $Ne(^3P_2, 16.62\ eV)$ diffusion coefficient in helium has been reported to be 20×10^{18} molecules $cm^{-1}\ s^{-1}$ [43] compared to the diffusion rate of $He(2^3S)$ in helium of 15×10^{18} molecules $cm^{-1}\ s^{-1}$. This results in a faster rate of diffusion for $Ne(^3P_2)$ than most ions in helium. Using eq (30), a plot may be calculated similar to Figures 10 and 12 for Ar*, and a comparison of the ion signals at high and low concentrations for two

different substrate gases can be made. The ratios of the slopes, and the plateaus for NO^+ and CH_3Cl^+ again show that diffusion has no effect on the calculations of the relative branching fractions for Penning ionization.

In summary, if all assumptions made during this discussion hold true for the substrate gas in question, then the diffusion rate of the ion and the metastable will have no effect on the relative branching fractions obtained from the ion signals at high and low [Q].

F. Kinetics for Cases with Secondary Reactions of Primary Ions.

In some cases the ion formed from Penning ionization will react with its neutral precursor to form secondary ion products. When this occurs a question is raised as to whether the primary ion can be studied without interference from the secondary ions produced. To answer this question a series of rate equations are developed and solved at various concentrations of the substrate gas. The secondary ion production process can be represented by eq (41), where P^+ is the product ion of the secondary ion-molecule

$$Q + B^+ \xrightarrow{k_s} P^+ \tag{41}$$

reaction. Since this reaction does not affect the decay rate of the metastable atom, the equation for A* will be the same as eq (25). Ignoring diffusion, the rate equation for the primary ion, B^+ is:

$$d[B^+]/dt = k_I[Q][A^*]_o \exp(-k_Q[Q])t - k_s[B^+][Q] \tag{42}$$

Rearranging eq (42) gives,

$$d[B^+]/dt = k_s[B^+][Q] = k_I[Q][A^*]_o \exp(-k_Q[Q])t \tag{43}$$

which can be integrated using an integration factor $\exp(k_2[Q]t)$ into,

$$[B^+] = \left[\frac{k_I[Q][A^*]_o}{\exp(k_s[Q]t)(k_s[Q]-k_Q[Q])}\right]\left[\exp(k_s[Q] - k_Q[Q])t - 1\right] \tag{44}$$

$$= \left[\frac{k_I[Q][A^*]_o}{(k_s[Q] - k_Q[Q])} \right] [\exp(-k_Q[Q]t) - \exp(-k_s[Q]t)] \quad (45)$$

Adding the diffusion terms of eq (26) to eq (42), the rate equation for B^+ becomes,

$$d[B^+]/dt = k_I[Q][A^*]_o \exp(-k_w - k_Q[Q])t - k_w'[B^+] - k_s[Q][B^+] \quad (46)$$

Rearranging eq (46) gives,

$$d[B^+]/dt = (k_w' + k_s[Q])[B^+] = k_I[Q][A^*]_o \exp(-k_2 - k_Q[Q])t \quad (47)$$

Using the integrating factor, $\exp(k_w' + k_s[Q])t$, eq (47) is integrated to yield eq (4B)

$$[B^+] = \left[\frac{k_I[Q][A^*]_o}{\exp(k_w' + k_s[Q])t\,(k_w' + k_s[Q]) - (k_w + k_Q[Q])} \right] x \quad (4B)$$

$$[\exp((k_w' + k_s[Q])t - (k_w + k_Q[Q])t)] - 1$$

Rearranging eq (48) gives eq (49).

$$[B^+] = \left[\frac{k_I[Q][A^*]_o}{k_w' + k_s[Q]) - (k_w + k_Q[Q])} \right]$$

$$[\exp(-k_2 - k_Q[Q])t - \exp(-k_w' - k_s[Q])t] \quad (49)$$

For the product, P^+, formed in the secondary ion-molecule reaction, the rate expression is given in eq (45) where the diffusion term for P^+ has been omitted. If $[P^+]_o = 0$ at $t = 0$, than $[A^*] + [B^+] + [P^+] = [A^*]_o$ where $[A^*]_o$ is the initial concentration of the metastable atom at $t = 0$.[64] $[P^+]$ can be found using eq (46).

$$\frac{d[P^+]}{dt} = k_s[Q]\, B^+ \quad (50)$$

$$[P^+] = [A^*]_o \left[1 - \exp[-(k_w + k_Q[Q])t] - \left[\frac{k_I[Q]}{[\exp(k_w' + k_s[Q])t][(k_w' + k_s[Q]) - (k_w + k_Q[Q])]} \right] x \right.$$

$$\left. [\exp((k_w' + k_s[Q])t - (k_w + k_Q[Q])t) - 1] \right] \qquad (51)$$

If the assumption is made that steady state conditions exist for B^+ at large concentrations of Q, then eq (42) is equal to zero and

$$[B^+] = \frac{k_I[A^*]_o \exp(-k_Q[Q]t)}{k_s} \qquad (52)$$

so

$$[P^+] = [A^*]_o \left[1 - \exp -(k_w + k_Q[Q])t - \frac{k_I \exp(-k_Q[Q]t)}{k_s} \right] \qquad (53)$$

In the present system, if secondary ion-molecule reactions are observed between the primary ion and its neutral precurser, a study of the properties of the primary ion become very difficult at large concentrations of Q (Appendix II).

One way around this problem is to use low concentrations of the primary reagent where secondary ion-molecule reactions are at a minimum. The remaining metastable atoms may be quenched by the addition of N_2 or CO into the flow downstream of the primary inlet. The N_2 or CO will quench Ar* via energy transfer pathways that do not include ionization and will not interfere with reaction processes. The reactions of the primary ions may then be studied by inletting another reagent into the flow where hetero-ion-molecule reactions can take place.

V. Experimental Results.

A. Reference Reactions.

In order to measure the relative branching fractions for Penning ionization by metastable atoms of various substrate gases, a standard must be established which can then be compared to all other substrate gases. Both CO and N_2 quench the $He(2^3S)$ atoms entirely by Penning ionization.[42] Either molecule would make a suitable standard. However, the reaction with CO was used because unknown experimental problems seem to give less than unit Penning ionization upon quenching the He* by N_2 possibly due to impurities in the gas. The reaction with CO was assumed to be well behaved since comparisons of branching fractions determined using CO as a standard were in better agreement with literature values than those obtained using N_2 as the standard. CO quenches both He* and Ne* by Penning ionization somewhat better (10%) than N_2 in our system. Even though this difference is within experimental error, the problem is systematic which suggests that another factor may be involved. CO quenches Ne* entirely by Penning ionization[34] and was chosen as the standard when studying reactions using Ne*.

None of the reagents previously studied with Ar* are known to have unit branching for Penning ionization. Nitric oxide was chosen as the standard gas in the Penning ionization by Ar*, since its branching fraction (0.28 ± 0.10) was measured by Golde, et al.[18] We repeated his measurements to obtain an independent check of the branching fraction. The method used consisted of measuring ion signals and photon emission for the $N_2^+(B^2\Sigma_u^+) \rightarrow N_2^+(X^2\Pi_g^+)$ and $N_2(C^3\Pi_u) \rightarrow N_2(B^3\Pi_g)$ transitions formed in the reactions of N_2 with He* and Ar*. The reaction of N_2 with He* produces ions through three different channels (eqs 54-56) of which channel (54) accounts for 42% of the Penning ionization of N_2.[48,49] The reaction of

$$He^* + N_2 \rightarrow He + N_2^+(8^2\Sigma_u^+) + e^- \quad (54)$$

$$He^* + N_2 \rightarrow He + N_2^+(X^2\Pi_g^+) + e^- \quad (55)$$

$$He^* + N_2 \rightarrow He + N_2^+(A^2\Sigma_u^+) + e^- \quad (56)$$

N_2 with Ar* produces the excited states of N_2 shown in eqs (57) and (58).

$$Ar^* + N_2 \rightarrow Ar + N_2(C^3\Pi_u) \quad (57)$$

$$Ar^* + N_2 \rightarrow Ar + N_2(B^3\Pi_g) \quad (58)$$

The branching fraction for reaction 57 has been repeatedly studied and values ranging from 60 to 100% can be found in the literature.[50-55] A value of 0.80 ± 0.20 was used as the branching fraction of the quenching process described by eq (57).

In order to observe the emission spectra, a 0.3 m McPherson vacuum monochromater equipped with a RCA photomultiplier tube was used. The spectra obtained was interpreted and corrected for wavelength response (Appendix II). A comparison of the $N_2^+(B\text{-}X)$ and $N_2(C\text{-}B)$ relative emission intensities for the same N_2, yield the relative concentrations of He* and Ar* (eq 59), where $I_{N_2^+}^{He^*}$ and $I_{N_2}^{Ar^*}$ are the intensities of the emissions; $k_Q^{He^*}$ are the total quenching rate constants for the reaction of He* + N_2 (7×10^{-11} cm^3 molecules^{-1} s^{-1})[47] and Ar* + N_2(3.8×10^{-11} cm^3 molecules^{-1} s^{-1})[50] respectively. The results are shown in Figure 13.

$$\frac{[He^*]}{[Ar^*]} = \frac{I_{N_2^+}^{He^*}(0.80k_Q^{Ar^*})[N_2]}{I_{N_2}^{Ar^*}(0.42k_Q^{He^*})[N_2]} \quad (59)$$

The ion signal for N_2^+ produced from the Penning ionization of N_2 by He* was monitored for channels (54-56) at the same time the emission for reaction (54) was being recorded. At high concentrations of N_2, each He*

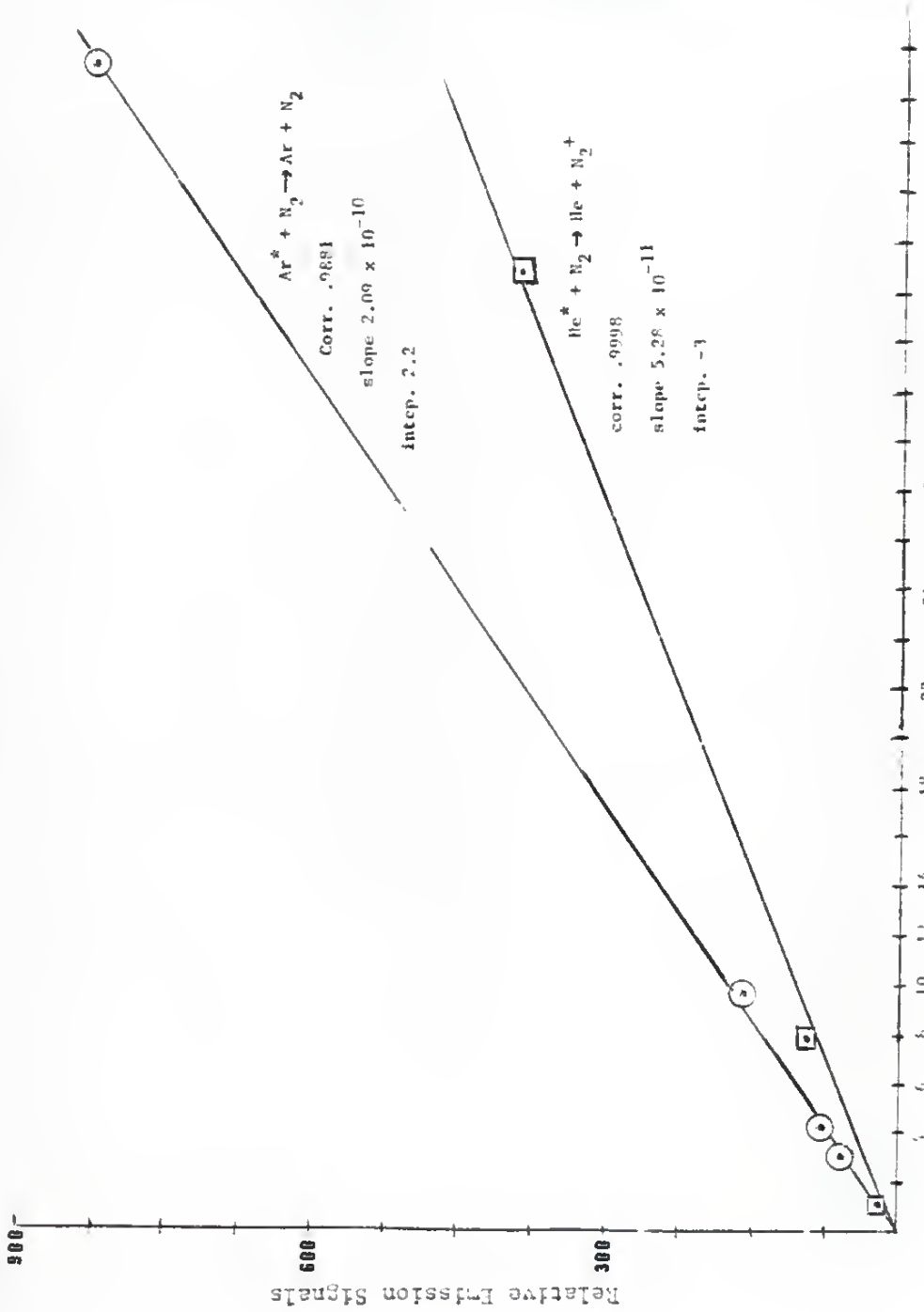

Figure 13. Plot of $N_2^+(B)$ and $N_2(C)$ vs $[N_2]$ from the emission spectra of He* + N_2 and Ar* + N_2.

atom has reacted with a N_2 molecule to produce N_2^+. Thus, the N_2^+ peak height, which corresponds to the total quenching of He* by N_2, is recorded.[47,56] A peak height can now be calculated which would represent the total quenching of Ar* using eq (59). Comparison with another substrate, in this case NO reacting with Ar*, to the hypothetical total quenching ion peak height will yield the branching fraction of Penning ionization by that substrate.

At low concentrations of the substrate, branching fractions for Penning ionization may also be inferred. From eq (17c) and (32) the Penning ionization rate constant for low concentrations of the substrate reacting with Ar* may be calculated as shown in eq (60), where the ion signals, $(Q^+)^{He^*,Ar^*}$, the concentration of Q, and the ratio [He*]/[Ar*] (from eq (59)) are known. The ion signal ratio is measured and hence k_1 is obtained, since the Penning ionization rate constants for many substrates with He* has been reported.[57]

$$k_I^{Ar^*} = \frac{k_I^{He^*}[He^*][Q](Q^+)^{Ar^*}}{[Ar^*][Q](Q^+)^{He^*}} \qquad (60)$$

If the total quenching rate constant for the substrate with Ar* has been reported than the branching fraction for Penning ionization can be determined.

The substrate used in these experiments was NO, for which the Penning ionization rate constant for the reaction with He* and the total quenching rate constant for the reaction with Ar* (2.2×10^{-10} cm^3 $molecules^{-1}$ s^{-1})[46] have been reported. The total quenching rate constant for NO with He* has been reported as 24.2×10^{-11} cm^3 $molecules^{-1}$ s^{-1}.[58] Chang and Setser[47] reported a quenching rate constant for NO with He* of 19.9×10^{-11} cm^3 $molecules^{-1}$ s^{-1} by measuring individual reaction channel rate constants and summing them for the total quenching rate. The Penning ionization rate constant would then be the sum of the reaction channels producing ions. In

a study which provided relative ratios of the ionization channels for the reaction of NO with He*, Hotop[56] reported two major quenching channels that were not seen in Chang and Setser's Study.[47] Addition of these channels to those observed by Chang and Setser gave a total quenching rate constant of 32.6×10^{-11} cm^3 $molecules^{-1}$ s^{-1} and a Penning ionization rate of 27.26×10^{-11} cm^{-3} $molecules^{-1}$ s^{-1} compared to the Penning ionization rate constant obtained from Chang and Setser[47] of 14.56×10^{-11} cm^3 $molecules^{-1}$ s^{-1}. The average of these two values results in a Penning ionization rate constant of $(20.91 \pm 6.35) \times 10^{-11}$ cm^3 $molecules^{-1}$ s^{-1}.

The NO was monitored over a range of concentrations of the parent molecule in reactions with both He* and Ar* in order to determine the best conditions for the experiment. The results of the emission study and the branching fraction determination for the Penning ionization of NO by Ar* are summarized in Table V. The individual peak heights with correction factors are listed in Appendix II along with the concentrations used. The branching fraction average of 0.43 ± 0.15 for the Penning ionization of NO by Ar* from Table V is in agreement with the branching fraction of 0.28 ± 0.10 reported by Golde et al.,[18] using the same technique. It must be pointed out at this time that for the calculation of [He*]/[Ar*] a branching fraction of 0.80 was used for reaction (57) while Golde used a value of 0.60. Therefore, the value of the branching fraction for the Penning ionization reaction of NO by Ar* obtained from our results using a value of 60% for reaction (57) is also listed in Table V. The approximate value of 0.20[32,33] has also been reported as the branching fraction due to Penning ionization of NO by Ar*.

The other major quenching pathway of Ar* with NO is thought to be the dissociation process shown in eq (61). The branching fraction for this process has recently been measured (0.69 ± 0.10)[59] which is in reasonable agreement with the average branching fraction of 0.43 ± 0.15

Table V. The Penning Ionization Rate Constants and Branching Fractions for $Ar^* + NO \rightarrow Ar + NO^+ + e^-$

Concentrations of NO (molecules cm^{-3})	$k_I^{Ar^*}(NO)$ (10^{11} cm^3 s^{-1})	Branching Fraction
0.8 to 3.0 x 10^{11}	9.8 ± 3.4	0.46 ± 0.17[a]
5.0 to 10.0 x 10^{12}	8.2 ± 1.1	0.41 ± 0.12[a]
		0.32 ± 0.10[b]
		0.28 ± 0.10[c]

[a]These values were obtained using 0.80 as the branching fraction for eq (57).

[b]Mean value obtained using 0.60 as the branching fraction for eq (57).

[c]Ref. 18.

obtained from our measurements of the Penning ionization reaction.

$$Ar^* + NO \rightarrow Ar + N + O \qquad (61)$$

The average of the two branching fraction values listed in Table V (0.43 ± 0.15) will be used as the standard value by which all other branching fractions for quenching of Ar* will be assigned.

8. Primary Ions from Penning Ionization of Ar*, Ne*, and He*.

In most cases, associative ionization is a very minor process[26] and it was never observed in the present system. The primary ions obtained are assumed to arise from simple Penning ionization and/or dissociative ionization. In many cases a single primary ion was produced in the Penning ionization reaction by Ar*, however, with both Ne* and He* it was not unusual to see several primary ions. For cases producing secondary ions, the relative yields of the primary ion products are determined at low

concentrations of the neutral where secondary processes will be at a minimum. The growth and decay of ion signals at higher concentrations of neutral are then used to confirm such secondary processes. For example, in the reaction of C_2F_4 with He*, several primary ions are produced along with the secondary ion m/z 131 (Figure 14). In order to calculate the percentage of the ion signal due to each primary ion, the values of the ion signals at low concentrations of C_2F_4 (between 5×10^{10} and 10×10^{10} molecules cm^{-3}, not shown in Figure 14) were measured. The throughput was corrected for mass discrimination in each case calibrating the instrument once a week to check reliability.

The parent ions produced from each reactant and Ar* are summarized in Table VI along with their ionization potentials and the difference in energy between these potentials and the energy of $Ar(^3P_2)$. In many cases, the reaction of a substrate with $Ar(^3P_2)$ yielded a single fragment ion (Table VII). A single ion (parent or fragment) is often the only product of the Penning ionization by Ar*, which provides a method of selectively producing positive ions in order to study their hetero-ion-molecule reaction processes.

Fragmentation into a series of daughter ions occurs more readily when He* and Ne* are used in the Penning ionization process. Table VIII summarizes the parent ions produced from Penning ionization by He* and Table X lists these values for the Penning ionization by Ne*. For the diatomic molecules studied, the parent ion was the sole ionic species and no secondary ion-molecule reactions between the parent ion and the diatomic precurser were observed. A summary of the fragment ions resulting from the Penning ionization by Ne* and He*, are listed in Tables IX and X, respectively. A comparison of Tables VII, IX, and X show the advantage that Ar* has over Ne* and He* in selectively producing one major ionic species.

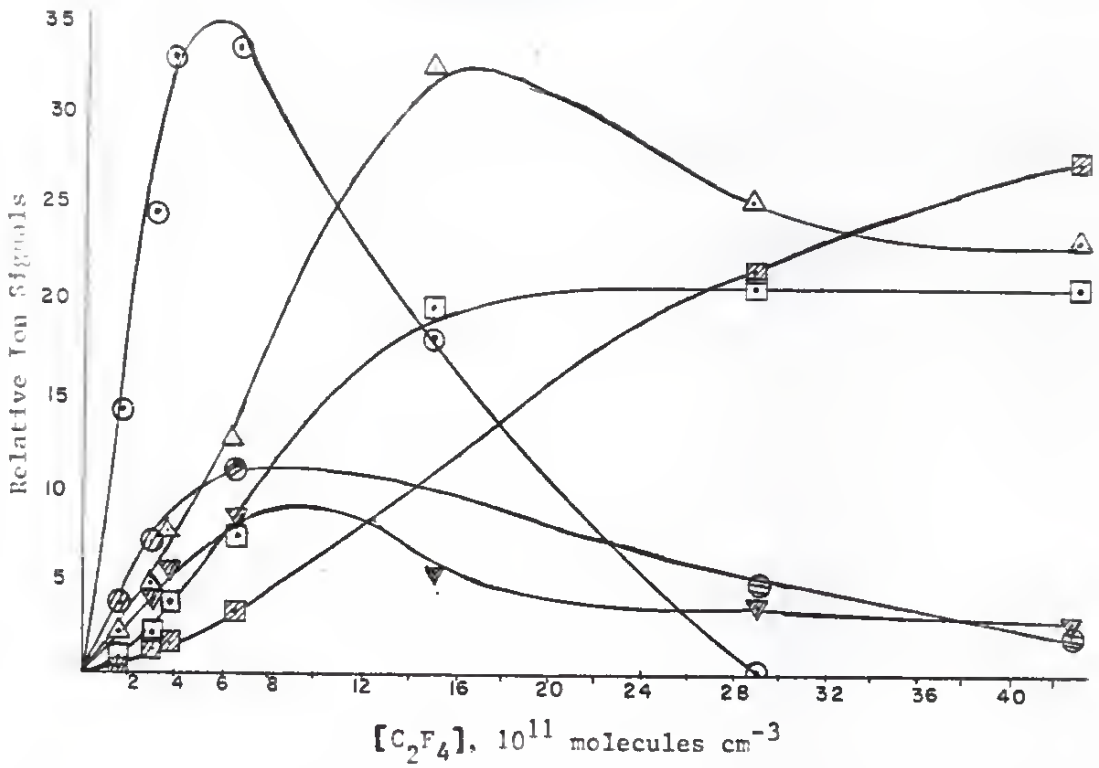

Figure 14. Plot of product ion signals m/z 31 (○), 50 (▽), 69 (□), 81 (△), 100 (○), and 131 (▨) for the Penning ionization of C_2F_4 by He* vs added C_2F_4. Signals are corrected for mass discrimination.

C. Secondary Ions from Ion-molecule Reactions with the Neutral Precursor.

In some cases, secondary ion-molecule reactions were observed between the primary ion from Penning ionization and its neutral precursor. The secondary ion-molecule processes with C_2H_2, CH_3Cl, and CH_2Cl_2 by Ar* are plotted against concentration of substrate in Figures 15, 16, and 17, respectively. The reaction of Ar* with C_2H_2 exclusively yielded $C_2H_2^{+\cdot}$ which formed higher oligomers with C_2H_2 (Figure 15). The parent ion $CH_3Cl^{+\cdot}$, which is the sole product from Ar* with CH_3Cl, undergoes ion-molecule reactions to give secondary product ions m/z 65 and 99. The reaction

Ar* with CH_2Cl_2 produces the parent ion $CH_2Cl_2^{+\cdot}$ as the only product, which then reacted to produce ions m/z 97 and 133 (see Discussion). The other reactions which produced secondary ionic products involved PhN_3, C_6H_6, C_6F_6,

Table VI. Parent Ions Produced by Ar* Penning Ionization

Parent	%P^{+a}	IP (eV)[b]	E (kcal mol^{-1})[c]
NO	100	9.26	53
CCl_4	0	11.47	2
$CHCl_3$	0	11.42	3
CH_2Cl_2	100	11.35	5
CH_3Cl	100	11.28	6
C_2F_4	100	10.12	31
C_2H_2	100	11.40	3.5
$(CH_3CH_2)_2O$	31	11.42	3
$(CH_3)_3CH$	18	10.57	23
$(CH_3)_4C$	0	10.35	28
C_6H_6	100	9.25	53
C_6F_6	100	9.75	36
$(CF_3)_2CO$	33	11.68	-3
PhN_3	10[d]		
$(CF_3)_2C{=}N_2$	77[d]		
c-$C_5H_4N_2$	75[d]		
CS_2	100	10.10	32

[a]At flows low enough to minimize secondary ion-molecule reactions; P^+ is the parent ion. [b]Ref. 60. [c]$E = E(Ar(^3P_2)) - IP(P)$. [d]Limited study at low flows; secondary ion-molecule reactions were taking place.

CS_2, C_2F_4, and $(CF_3)_2CO$. The mechanisms involved in each of these cases will be considered in the discussion section.

The secondary ion-molecule products for various ions are listed in Table XI. The same secondary ion-molecule products were observed in most cases when the substrates reacted with He*, Ne*, and Ar*. The few exceptions, i.e. C_6H_6 and C_2F_4, are explained since fragment ions produced upon collisions with He* are not formed by collision with Ar*. The fragment ions undergo ion-molecule reactions with the neutral precursor. For C_6F_6, small signals of the (dimer - F)$^+$ ion were observed with He* and Ne* at large concentrations of C_6F_6 (1×10^{13} molecules cm^{-3}) (Table XI). This secondary ion product may be due to excited vibrational states when reacting

Table VII. Primary Fragment Ions Produced by Ar* Penning Ionization

Parent	Fragment Ion	AP[a]	% of Total Ion Signal
CCl_4	CCl_3^+	11.65	100
$CHCl_3$	$CHCl_2^+$	11.64	100
$(CH_3)_4C$	$(CH_3)_3C^+$	10.56	100
PhN_3	PhN^+		90
$(CF_3)_2CO$	$(CF_3)CO^+$	12.04	67
$(CH_3)_3CH$	$C_3H_6^+$	10.93	29
	$C_3H_7^+$	11.23	31
	$C_4H_9^+$	11.60	15
$(CH_3CH_2)_2O$	$(C_2H_5)OCH_2^+$	10.30	54
	$(C_2H_5)OCH_2CH_2^+$		

[a]Ref. 60

Table VIII. Parent Ions Produced by He* Penning Ionization

Parent	%P^{+a}	IP (eV)[b]	E (kcal mol^{-1})[c]
NO	100	9.26	243.5
CO	100	14.10	131.6
N_2	100	15.58	97.5
O_2	100	12.06	178.8
CCl_4	0	11.47	192.4
$CHCl_3$	0	11.42	193.6
CH_2Cl_2	21	11.35	195.2
CH_3Cl	90	11.28	196.8
C_2F_4	20	10.12	223.6
CHF_3	15	13.80	138.6
C_6H_6	68	9.25	243.5
C_6F_6	26	9.97	227.1
CS_2	85	10.10	224.0
PhN_3	10[d]		
$(CF_3)_2CO$	20[d]	11.68	

[a]At flows low enough to minimize secondary ion-molecule reactions.

[b]Ref. 60. [c]$E = E(He(2^3S)) - IP(P)$. [d]Limited study at low flows.

with He* and Ne* that are not energetically accessible in reactions with Ar*.

D. Penning Ionization Branching Fractions.

A series of tests were performed for reactions of the metastable atoms with a substrate gas in helium carrier gas to establish: 1) that a constant ion signal could be maintained, 2) that under the same conditions the ion signal could be reproduced, 3) that the concentrations needed to produce accurate results could be obtained, and 4) what effect mass discrimination

Table IX. Primary Fragment Ions Produced by He* Penning Ionization

Parent	Fragment Ions	AP[a] (eV)	% of Total Ion Signal
CCl_4	CCl_3^+	11.65	45
	CCl_2^+	15.40	43
	CCl^+	19.40	12
$CHCl_3$	$CHCl_2^+$	11.64	81
	$CHCl^+$	17.5	18
CH_2Cl_2	CH_2Cl^+	12.81	79
CH_3Cl	CH_3^+	13.87	07
C_2F_4	CF^+	13.76	30
	CF_2^+	14.63	10
	CF_3^+	13.70	10
	$C_2F_3^+$	15.84	30
CHF_3	CHF_2^+	15.75	68
C_6H_6	$C_5H_3^{+\cdot}$	15.70	05
	$C_4H_4^+$	14.50	15
	$C_3H_3^{+\cdot}$	14.70	10
C_6F_6	$C_6F_5^+$	16.9	18
	$C_5F_5^{+\cdot}$	17.20	16
	$C_5F_4^+$	16.10	10
	$C_5F_3^{+\cdot}$	15.80	25
	$C_3F_3^{+\cdot}$	16.80	05
CS_2	S_2^+	14.9 - 18.2	10
	CS^+	9.6	05

[a]Ref. 60

Table X. Primary Ions Produced by Ne* Penning Ionization

Parent	Ions Produced	% of Total Ion Signal	AP (eV)[a]	E(kcal/mol)[b]
CO	$CO^{+\cdot}$	100	14.10	57.9
N_2	$N_2^{+\cdot}$	100	15.58	23.8
O_2	$O_2^{+\cdot}$	100	12.06	104.9
NO	NO^+	100	9.26	169.5
CCl_4	CCl_3^+	85	11.65	114.4
	$CCl_2^{+\cdot}$	15	15.40	27.9
$CHCl_3$	$CHCl_2^+$	100	11.64	114.6
CH_2Cl_2	$CH_2CL_2^{+\cdot}$	20	11.35	121.3
	CH_2Cl^+	80	12.81	87.6
CH_3Cl	$CH_3Cl^{+\cdot}$	90	11.28	26.0
	CH_3^+	10	13.87	63.2
C_6H_6	$C_6H_6^{+\cdot}$	78	9.25	169.8
	$C_5H_3^{+\cdot}$	7	15.70	21.6
	$C_4H_4^+$	2	14.50	48.7
	$C_3H_3^{+\cdot}$	13	14.70	44.1
C_6F_6	$C_6F_6^{+\cdot}$	90	9.75	58.2
	$C_5F_3^{+\cdot}$	10	15.80	18.7

[a]Ref. 44. [b]$E = E(Ne(^3P_2)) - IP(P)$. [c]Determined at high concentrations of neutral, considered to be less accurate.

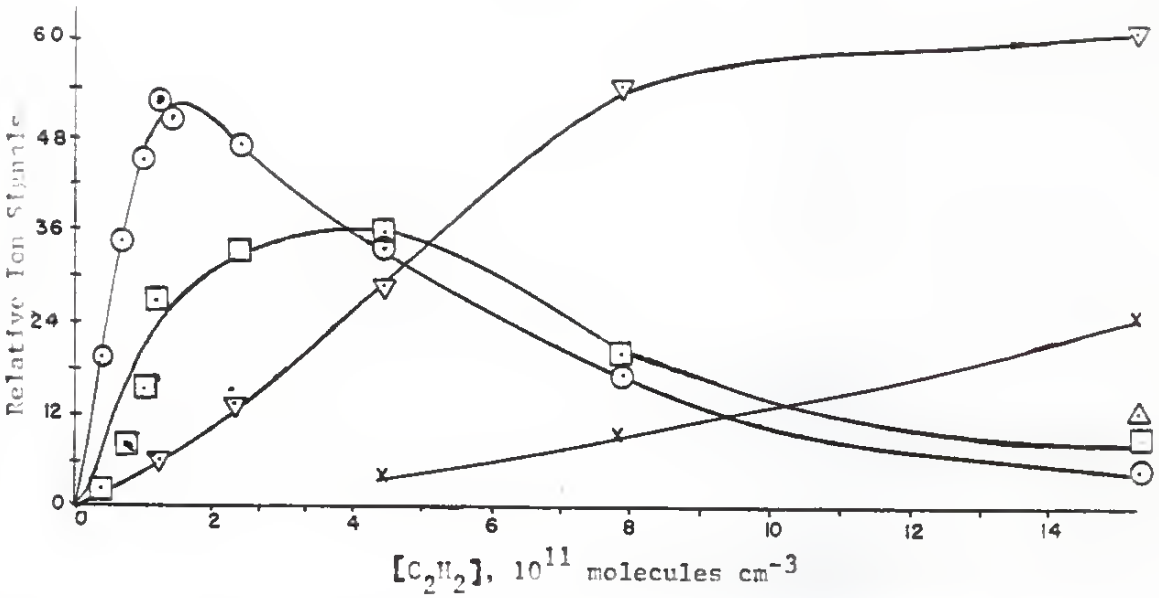

Figure 15. Plot of product ion signals $C_2H_2^+$ (○), $C_4H_3^+$ and $C_4H_4^+$ (□), $C_6H_4^+$, $C_6H_5^+$, and $C_6H_6^+$ (△), $C_8H_6^+$, $C_8H_7^+$, and $C_8H_8^+$ (×), and $C_{11}H_{10}^+$ (▼) for the Penning ionization of C_2H_2 by Ar* vs added C_2H_2.

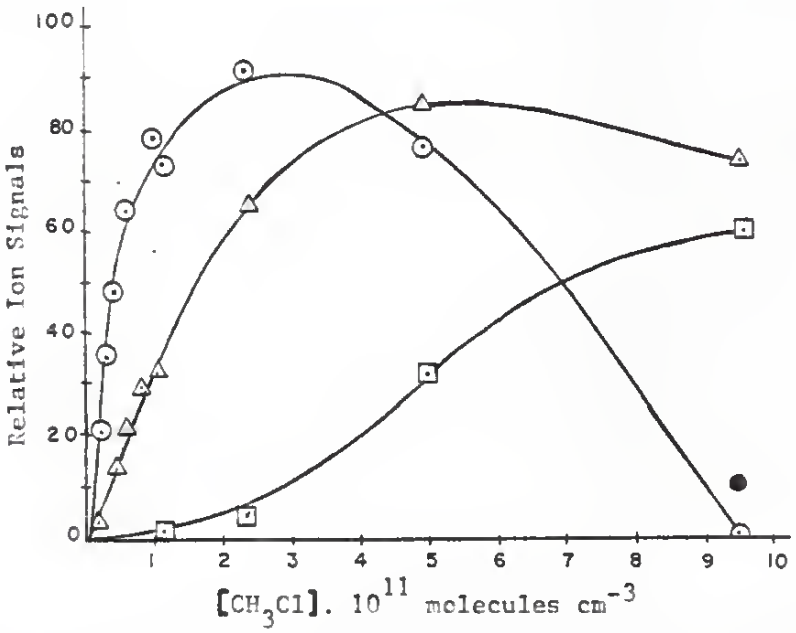

Figure 16. Plot of product ion signals CH_3Cl^+ (○), CH_3ClH^+ (△), $C_2H_6Cl^+$, (□), $C_2H_5Cl_2^+$ (▽) for the Penning ionization of CH_3Cl by Ar* vs added CH_3Cl.

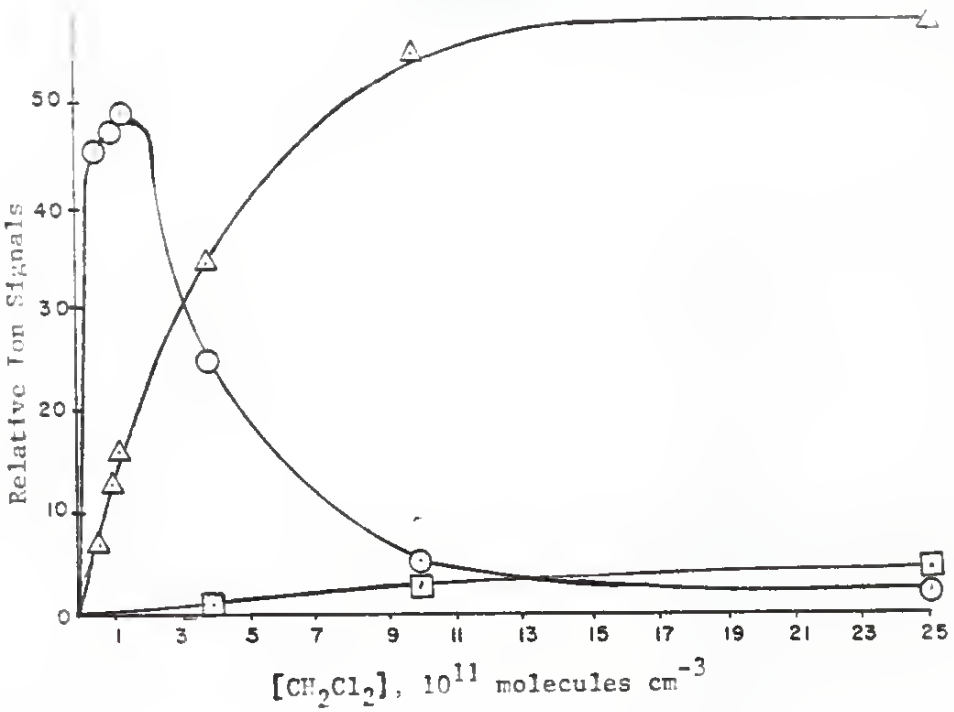

Figure 17. Plot of product ion signals CH_2Cl^+ (○), $C_2H_3Cl_2^+$ (△), $C_2H_2Cl_3^+$ (□) for the Penning ionization of CH_2Cl_2 by Ar* vs added CH_2Cl_2.

Table XI. Secondary Ion-molecule Products Produced in the Penning Ionization Reactions of Ar*, Ne*, and He*.

Substrate	Secondary-ion Product Using Ar*	Secondary-ion Product Using Ne*	Secondary-ion Product Using He*
CH_2Cl_2	$C_2H_3Cl_2^+$; $C_2H_2Cl_3^+$	$C_2H_3Cl_2^+$; $C_2H_2Cl_3^+$	$C_2H_3Cl_2^+$; $C_2H_2Cl_3^+$
CH_3Cl	CH_4Cl^+; $C_2H_6Cl^+$; $C_2H_5Cl_2^+$	a	a
C_2H_2	$C_4H_2^+$;$C_4H_3^+$;$C_6H_6^+$;$C_6H_7^+$;$C_8H_7^+$ $C_8H_5^+$;$C_8H_6^+$;$C_{10}H_{10}^+$;$C_{11}H_{10}^+$	b	b
C_6H_6	$C_{12}H_{11}$	$C_9H_8^+$; $C_{12}H_{11}^+$	$C_9H_8^+$; $C_{12}H_{11}^+$
C_6F_6	--------	$C_{12}F_{11}^+$	$C_{12}F_{11}^+$
CS_2	CS_4^+	b	CS_4^+

Table XI. cont.

Substrate	Secondary-ion Product Using Ar*	Secondary-ion Product Using Ne*	Secondary-ion Product Using He*
PhN_3	$C_6H_5N_2^+$	b	$C_6H_5N_2^+$
C_2F_4	--------	b	$C_3H_5^+$
$(CF_3)_2CO$	--------	b	$C_4F_{11}CO^+$

[a]The same secondary-ion products are seen for Ne* and He* as for Ar*.

[b]These substrates were not studied.

has on the ion signal. Mass discrimination was accounted for using the technique described in the experimental section. A stable ion signal in our system is defined as being reproducible (± 5%) under the same conditions. Since the branching fractions reported here are relative to a standard gas, the concentrations that will provide the best results should be the same for both reagents. For most substrates a plot of three points taken between a concentration range of 5 to 10 x 10^{10} molecules cm^{-3} will produce a slop with a correlation > 0.99. Using eq (31) the ratio of the Penning ionization rate constants can be determined. Addition of (1 to 10) x 10^{12} molecules cm^{-3} of substrate will totally quench the metastable atoms, and comparison of their ion signal peak heights will yield a ratio of the branching fractions (eq 35). In the case of Penning ionization by Ar*, there exists a region of [Q] of about 5 x 10^{12} molecules cm^{-3} where the ion signal peak height remains constant before decaying. It is at this point the ion signals of the standard and the substrate gases must be compared. Figures 18 to 22 are plots of the ion signal vs. substrate concentration for a number of substrates with Ar*, He*, and Ne*. These measurements with the standard and each of the neutral substrate molecules

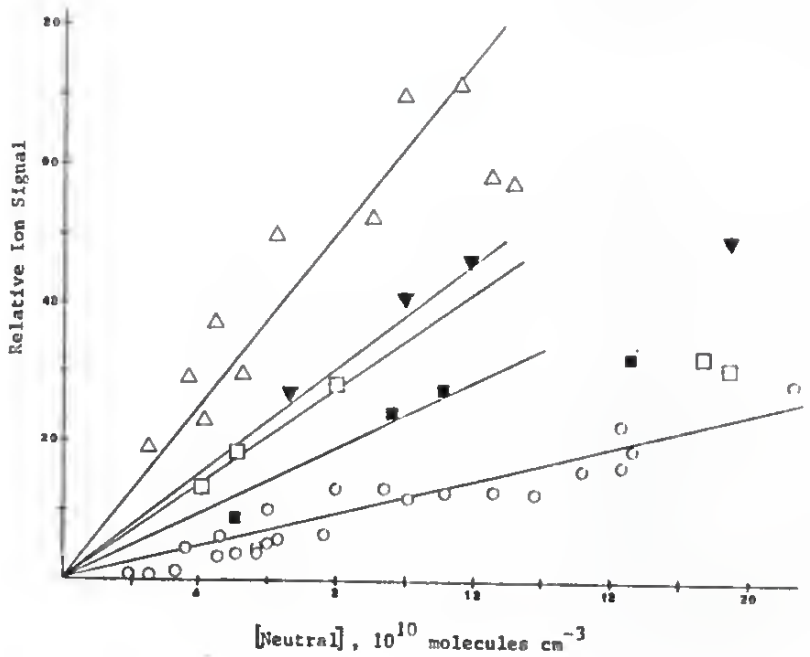

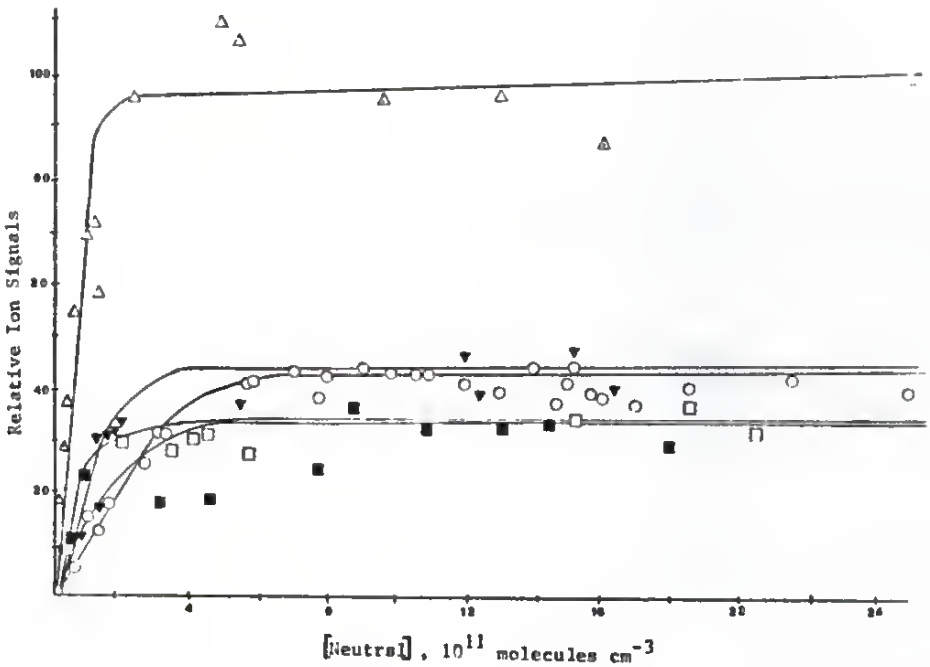

Figures 18a and b. Plot of total ion signals for NO (○), CCl_4 (□), $CHCl_3$ (▼), CH_2Cl_2 (■), and CH_3Cl (△) for the Penning ionization reactions with Ar*. The signals are corrected for mass discrimination.

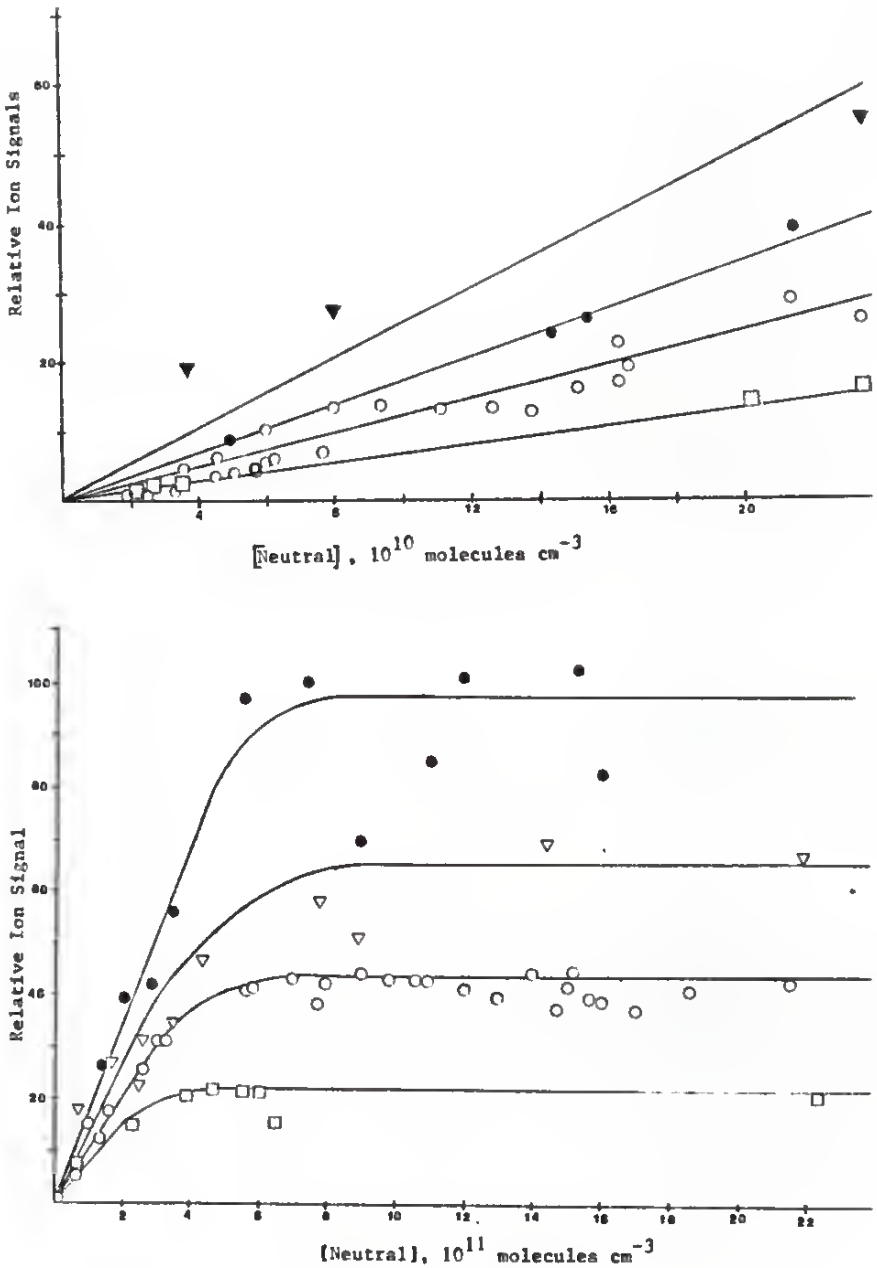

Figures 19a and b. Plot of total ion signals for NO (○), C_6F_6 (●), C_2F_4 (□), C_2H_2 (▽), and C_6H_6 (▼) for the Penning ionization reactions with Ar*. The signals were corrected for mass discrimination.

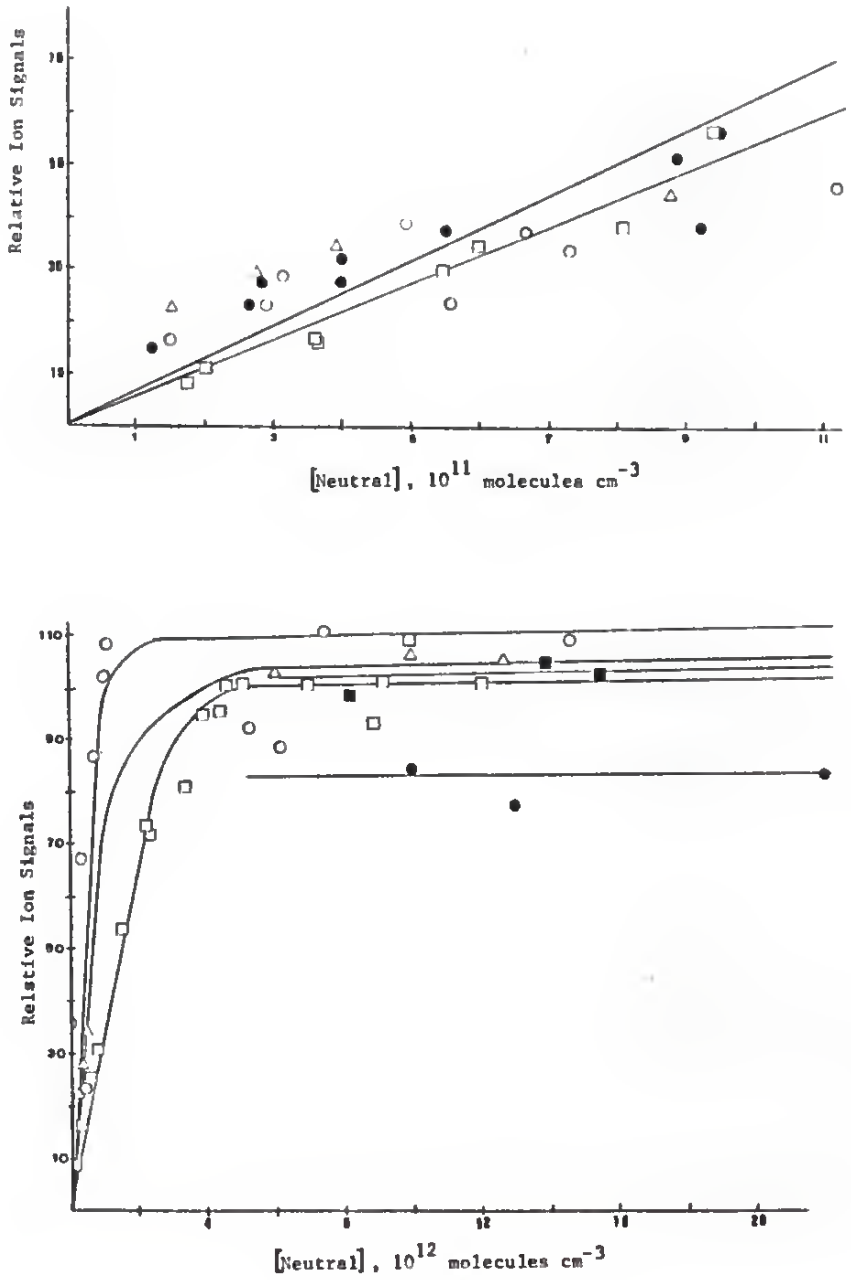

Figures 20a and b. Plot of total ion signals for CO (□), CCl_4 (△), $CHCl_3$ (■), CH_2Cl_2 (○), and CH_3Cl (●) for the Penning ionization reactions with He*. The signals were corrected for mass discrimination.

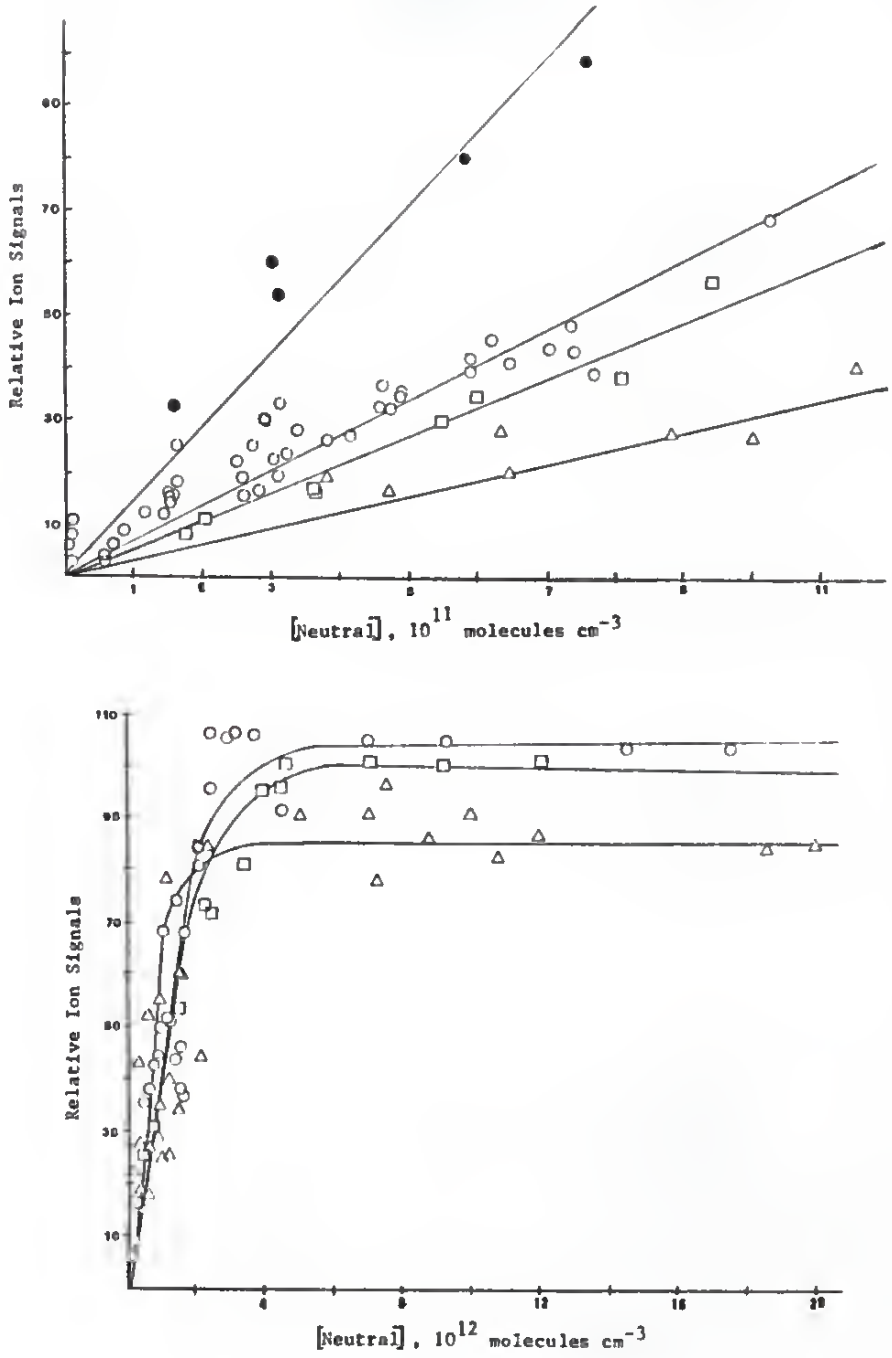

Figures 21a and b. Plot of total ion signals for CO (□), NO (○), N_2 (△), and C_2F_4 (●) for the Penning ionization reactions with He*. The signals were corrected for mass discrimination.

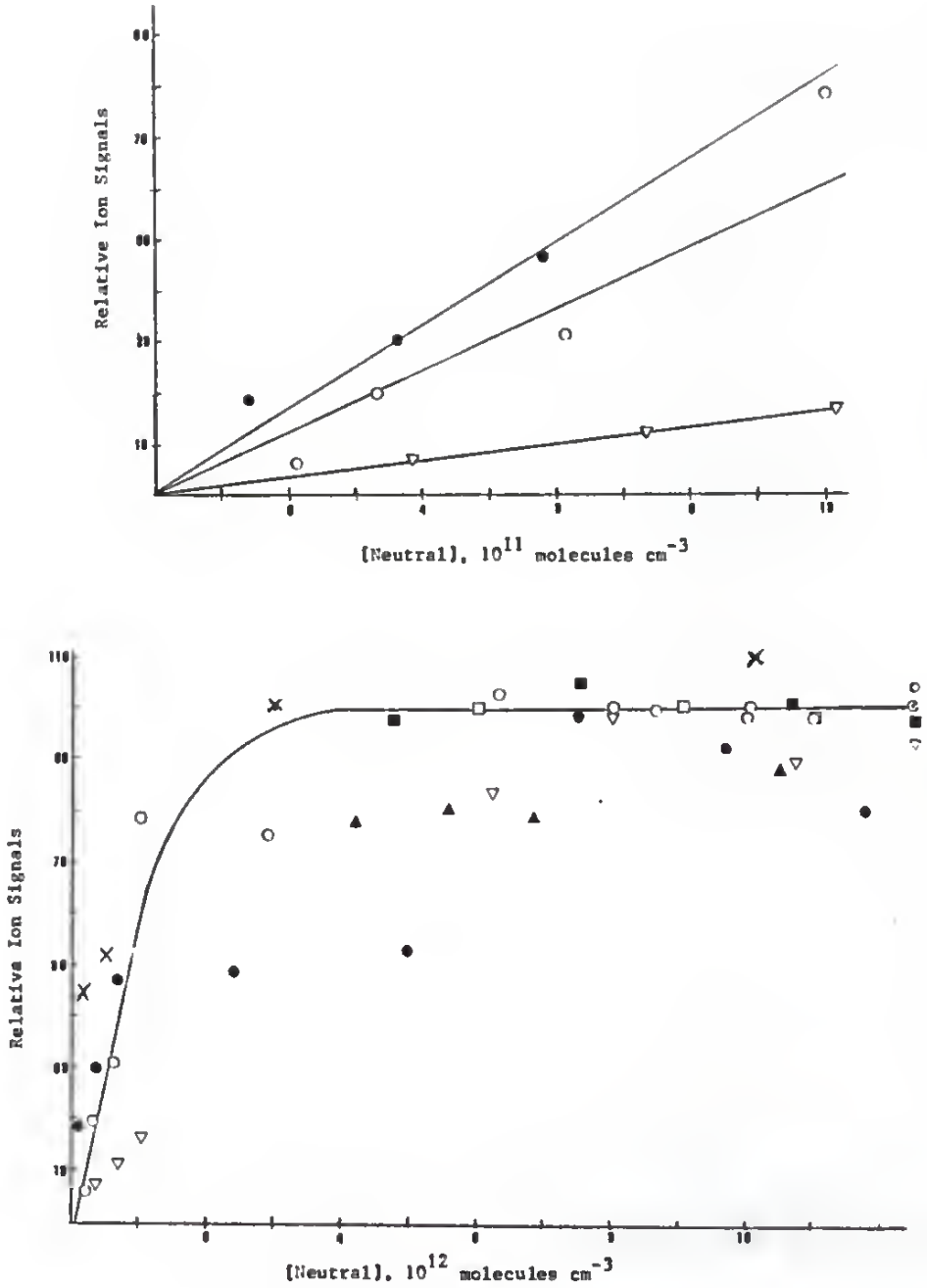

Figures 22a and b. Plot of total ion signals for CO (□), NO (○), N_2 (▽), C_6H_6 (x), CCl_4 (■), CH_2Cl_2 (▲), and CH_3Cl (●) for the Penning ionization reactions with Ne*. The signals were corrected for mass discrimination.

Table XII. Branching Fractions for Ar* Penning Ionization.

Substrate[a]	$\frac{k_I(NO)}{k_I(X)}$[b]	$\frac{k_Q(X)}{k_Q(NO)}$[c]	$\frac{k_1(NO)k_Q(X)}{k_I(X)k_Q(NO)}$[d]	$\frac{k_1(NO)k_Q(X)}{k_I(X)k_Q(NO)}$[e]	$\frac{k_I(X)}{k_Q(X)}$[f]	$\frac{k_I(X)}{k_Q(X)}$[g]	$\frac{k_1(X)}{k_Q(X)}$[h]
NO	1.00	1.00	1.00	1.00	0.43	0.43	0.43
CCl_4	0.28	4.4	1.23	1.31	0.33	0.35	0.18
$CHCl_3$	0.29	5.0	1.15	0.97	0.44	0.37	0.23
CH_2Cl_2	0.23	4.2	0.97	1.25	0.34	0.43	0.40
CH_3Cl	0.18	3.7	0.67	0.36	0.96	0.64	0.65
C_2H_2	0.24	2.4	0.58	0.62	0.69	0.74	0.63[i]
C_2F_4	1.75			1.76	0.25		
$(CH_3)_4C$	0.56			1.00	0.43		
$(CF_3)_2C=N_2$				0.72	0.60		
$(CF_3)_2C=O$	----			2.71	< 0.01		
C_6H_6	0.47	4.2	1.97	0.71	0.60	0.23	0.39[i]
C_6F_6	0.72			0.47	0.92		
CS_2		4.5		0.51	0.84		

[a]NO is used as the standard. [b]These values are taken from the ratio of the slopes. [c]Ref. 35. [d]Multiplication of columns 2 and 3. [e]These values are taken from the ratio of the plateaus. [f]Calculated from column 5 by dividing by 0.28 and then taking the reciprocal; from the plateau region. [g]Same as f only for the slope region. [h]Ref. 18. [i]Ref. 61.

were carried out under the same conditions (e.g. P_{He}, $\bar{v}_{He}$, F_{A^*}, lens potentials, and potential difference across the electrodes of the cold-cathode sischarge), and the results of 3 to 5 experiments for each neutral were averaged to obtain these plots. The average error in the data from separate experiments was ± 6%.

The observed branching fractions for the quenching of Ar* via Penning ionization are summarized in Table XII, using the average branching fraction for Ar* with NO yielding NO^+ of 0.43. Table XII lists the neutral substrates along with the ratios of the slopes of ion signals at low concentrations of the standard and the substrate gas. The third column lists the ratio of the total quenching rate constants from the literature[32,35] which can be multiplied with the second column to obtain the ratio of the branching fractions. These branching fraction ratios can be compared to the plateau values of the ion signal measured in the high Q region. The individual branching fractions can be calculated by dividing each number in column 5 by the branching fraction of the reference (0.43), and then taking the reciprocal of that number. The branching fractions from the plateau and slope regions are compared in Tables XII and XIII while only those from the plateau region were used in Table XIV due to limited amounts of neon gas. In most cases, reasonable agreement between the slope and plateau branching fractions were obtained.

For CH_3Cl the slope value is considered to be in error. This is attributed to the fact that in order to obtain the slope region of CH_3Cl^+ vs CH_3Cl a very low concentration of CH_3Cl was needed (Figure 18); at the same concentration the ion signal of the standard, NO^+ was barely visible. Therefore, a small error in the determination of the peak height for NO^+ would produce a large error in the slope ratios. In cases where two or more ions were formed the total ion signal was used, after corrections for

mass discrimination, to determine the slope and the pleateau values. The final column of Table XII lists the branching fractions obtained from other laboratories.[18,61] The values from ref. 18 have been placed on a scale relative to a branching fraction of 0.43 for NO yielding NO^+.

Table XIII. Branching Fractions for He* Penning Ionization.

Substrate[a] X	$\frac{k_I(X)}{k_I(CO)}$[b]	$\frac{k_Q(CO)}{k_Q(X)}$[c]	$\frac{k_I(X)k_Q(CO)}{k_I(CO)k_Q(X)}$[d]	$\frac{k_I(X)k_Q(CO)}{k_I(CO)k_Q(X)}$[e]	$\frac{k_I(X)}{k_Q(X)}$[f]
CO	1.00	1.00	1.00	1.00	1.00
N_2	0.34	2.87	0.98	0.86	1.00
NO	1.02	0.83	0.85	1.05	0.78
O_2	1.04	0.83	0.86	1.07	0.71
CCl_4	0.90			1.05	
$CHCl_3$	0.90			1.03	
CH_2Cl_2	0.90			1.10	
CH_3Cl	1.04			0.81	
CHF_3	0.69			0.88	
C_2F_4	2.33			2.57	
C_6F_6	0.68			1.07	
CS_2		5.26		1.05	
C_6H_6	0.77			0.80	

[a]CO is used as the reference. [b]These values are the ratio of the slopes. [c]Ref. 12. [d]Product of columns 2 and 3, and are equal to the branching fraction. [e]These values are the ratio of the plateaus, and are equal to the branching ratios. [f]Ref. 42 and 60.

The values obtained for the Penning ionization reaction of He* with various substrates are summarized in Table XIII and those for Ne* are listed in Table XIV. These values were calculated using CO as the standard and are listed in a similar manner as those for Ar* in Table XII. In Table XIII the branching fraction for C_2F_4 is well above 100%. This result may be due to the fact that many primary ions and a secondary ion are produced from the reaction of C_2F_4 with He* and the error in measuring the signal peak heights, coupled with the error in the mass discrimination corrections, could produce a gross exaggeration of the branching fraction. All other branching fractions obtained by both He* and Ne* reactions are mainly unity.

Table XIV. Branching Fractions for Ne* Penning Ionization.

Substrate X	$\frac{k_I(X)k_Q(CO)}{k_I(CO)k_Q(X)}$ [b]	Ionization Yields[c]
CO	1.00	
N_2	0.89	0.84
NO	1.00	
O_2	0.8	
CCl_4	1.11	
$CHCl_3$	1.00	
CH_2Cl_2	0.77	
CH_3Cl	0.78	
C_6H_6	1.08	0.72
C_6F_6	0.98	

[a] CO is the reference gas. [b] These values are the ratios of the plateaus and are equal to the branching fractions. The slope and plateau ratios for NO and N_2 were compared and the same branching fraction was obtained in each case. [c] Ref. 61.

VI. Discussion.

A. Penning Ionization.

Penning ionization provides a method of reducing fragmentation accompanying ionization so that the chemistry of these molecular ions produced may be individually studied.[44,62,63] Penning ionization is very similar to the collisional autoionization of a two-particle system A*-B where excitation transfer is followed by autoionization of the target molecule.[64] For Penning ionization to occur, the energy E(A*) of the excited particle, A*, must exceed the ionization potential IP(B) of the collision particle B. Penning ionization, thus, can be viewed as an ionization process, which may occur even in the limit of zero relative collision energy E_k.[65] Eqs (62) and (63) show the simple Penning ionization (62) process along with

$$A^* + B \xrightarrow{E_k} \begin{cases} \xrightarrow{PI} A + B^+ + e^-(E_{el}) & (62) \\ \xrightarrow{AI} AB^+ + e^-(E_{el}) & (63) \end{cases}$$

the associative ionization process (63) which occurs when the electron carries away enough energy such that;

$$E_{el} > E(A^*) - IP(B) + E_K \qquad (64)$$

where the AB^+ system now has energy below the AB^+ dissociation energy and is truly bound.[65] In order to gather a better understanding of the Penning ionization process, a schematic potential energy diagram is provided in Figure 19 with NO as the molecule to be ionized. The inlet channels have an additional small amount of energy over the excitation energy of the metastable atom due to collisional energy of the A*-B system, which is governed by the Maxwell-Boltzmann distributions. The exit channels are also of the Born-Oppenheimer type, i.e. the motion of the nuclei is separated from the motion of the electrons so we can sketch the potential

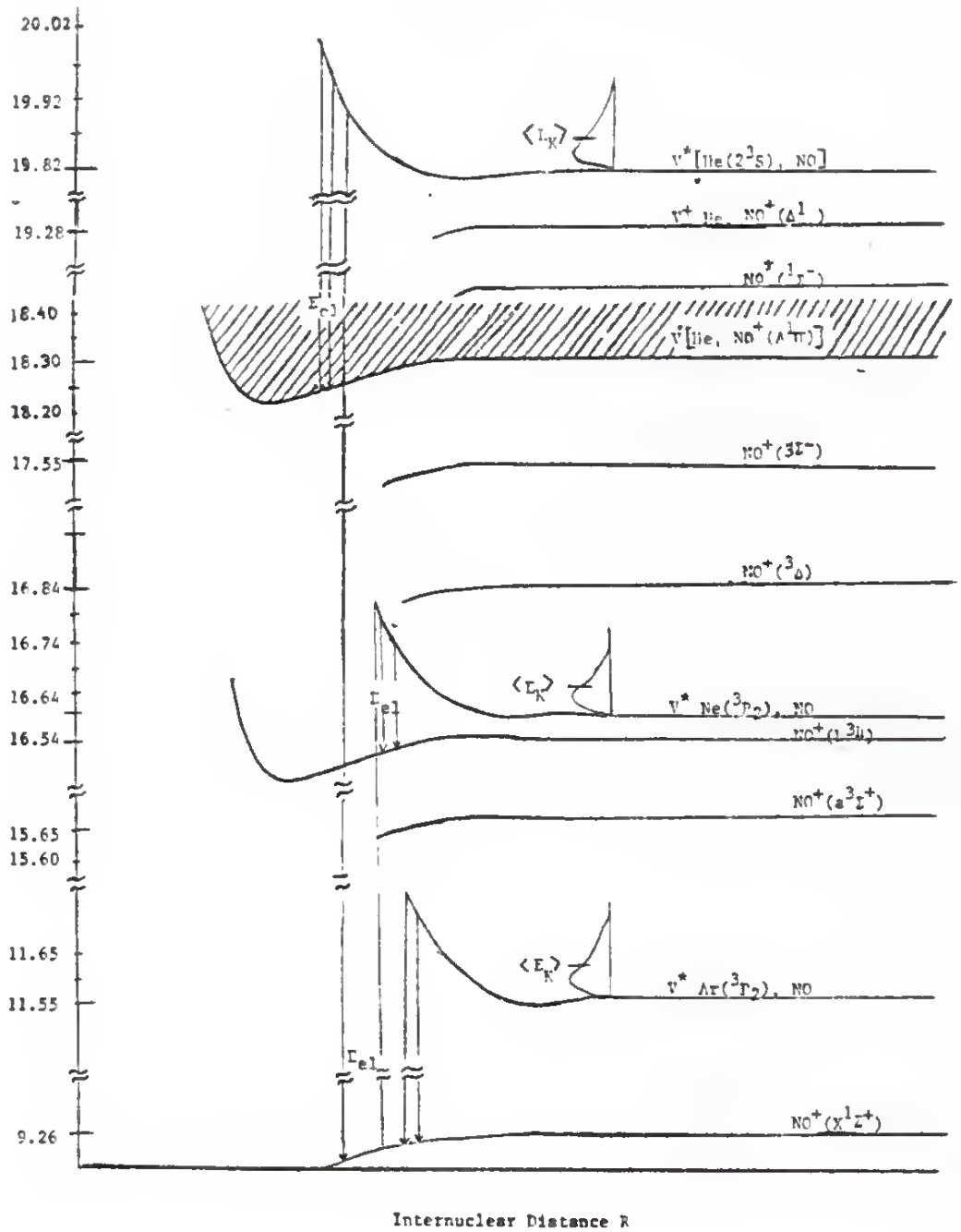

Figure 23. Schematic representation of the model for Penning ionization. The scale has been expanded to show the weakly attractive features of $V^*(R)$ and $V^+(R)$ which are repulsive-type channels governed by van der Waals potentials (see text).

energy vs internuclear distance of the colliding pairs. The transition from the inlet channel to an exit channel occurs with conservation of nuclear position and velocity with the electron carrying off the energy difference between the A*-NO and A^*-NO^+ states. Consequently, the ionization can be viewed as a vertical Frank-Condon type transition between V* and V^+ with simultaneous ejection of the electron energy (E_{el}) which is the difference between the two potential curves at the internuclear separation (R) for which the transition occurs (eq 65).[66]

$$E_{el}(R) = V^*(R) - V^+(R) \tag{65}$$

This means that the Penning process in most cases lead to vibrational state distributions of the ion in accord with the Frank-Condon transition probabilities. This is important because it means the vibrational excitation generally will be small.

Ionization of NO by $He(2^3S)$ gives the state distributions shown in Table XV in which the $NO^+(b^3\Pi)$ is the most populated. This state is also energetically accessible to Ne*. However, photoionelectron spectroscopy indicates that the $NO^+(X^1\Sigma^+)$ state is the highest populated using Ne(I) (16.85 eV)[67,68] which is the only ionization state available to Ar* (see Figure 23).

Associative ionization corresponds to transitions with insufficient relative kinetic energy to carry the bound states out of the potential wells.

The Penning ionization process using NO as the model compound is discussed since it is the simplest system (diatomic) which has been extensively studied, and NO has an ionization potential below the excitation energy of Ar*. The potential energy diagram (Figure 23) has been simplified, however, since the $NO(X^2\Pi)$ molecule has a single outer antibonding π-elec-

Table XV. Relative Populations of NO Ionic States in 584.3 Å Photoionization and in $He(2^3S)$ Penning Ionization.

NO^+ Ionic State	PES 584.3 Å	PIES $He(2^3S)$	
	Ref. 56	Ref. 56	Ref. 47
$X^1\Sigma^+$	40	26	34
$a^3\Sigma^+$	19	28	
$b^3\Pi$	100	100	100
$w^3\Delta$	65	115	
$A^1\Pi$	50	42	46

tron which combines with the unpaired electron of the metastable atoms to give two types of entrance channels with different total spin. There is a doublet surface which, based on the spin-conservation rule,[69] will yield, NO^+ ions in both the singlet and triplet states, and there is a quartet surface which will selectively feed the triplet ionic states. Hotop has assumed repulsive-type quartet channels and relatively more attractive doublet surfaces.[70] Other exit channels besides Penning ionization may also be available to the two-particle system, A*-B, such as dissociation into excited state atoms, which is the case with NO,[47,59] or into fragment ions, which may occur for larger molecules. Data from photoelectron spectroscopy[79] shows eight states of NO^+ with energies less than 19.8 eV above the ground state, $NO(X^2\Pi, v=0)$. They can become product channels for the Penning ionization reaction as shown in Figure 19 and Table XV.

Penning ionization resembles photoionization in the fact that one electron carries away the excess energy of the process. For this reason comparisons of the vertical and adiabatic ionization potentials for the

different electronic states of molecules studied by photoelectron spectroscopy (PES) will be compared to the excitation energies of the metastable rare gas atoms used in these experiments. Also, the fragmentation from each entrance channel V*(A*-BC) will be explored.

B. Branching Fractions.

The recent results of Golde, et al.,[18] are the only reported branching fractions for chemi-ionization by metastable Ar($^3P_2$, $^3P_0$) are placed on an absolute scale. Approximate values for the reaction of Ar* with NO are the only other available data.[32,33]

The accuracy of the present branching fractions was tested by comparisons with previous data.[18] The branching fraction of Ar* with NO which produces chemi-ionization has been reported as 0.20[32,33] and 0.28 ± 0.10.[18] This compares favorably with the value of 0.43 ± 0.15 obtained in this study (Table V). Golde, et al.,[18] also reported a lower limit of 0.70 ± 0.10 for the branching fraction for reaction (66) while emitting channels are absent. This result supports the ionization branching fraction for NO

$$Ar^* + NO \rightarrow Ar + N + O \qquad (66)$$

reported here. The branching fractions for the Penning ionization of the substrate gases by Ne($^3P_{0,2}$) (Table XIV) are compared to the literature values of ionization yields calculated by Person.[61] The values for the branching fractions of substrate gases reacting with He(2^3S) (Table XIII) are compared to the results obtained by Chang and Setser[47] and by Hotop.[56] The slopes of the ion signals plotted against the substrate concentrations were obtained for concentrations of the substrate below 1×10^{11} molecules cm^{-3}. The plateau values were obtained by monitoring the ion signal for the substrate concentrations between 1×10^{12} and 1×10^{13} molecules cm^{-3}. The ion signal should remain constant in this area as all of the metastable

atoms should be quenched. In the case of Ne($^3P_{0,2}$) the ion signal peak heights were monitored over a range of concentrations ((1 to 50) x 10^{12} molecules cm^{-3}). While only a few concentrations were actually determined the ion signal over this range remained constant (Figure 22). Although chemi-ionization is an important channel with Ar*, the data in Table XII indicate that it is not usually the dominant channel for the reagents studied. These results contrast sharply with the results obtained for chemi-ionization with He* and Ne* (Tables XIII and XIV) where this is the dominate channel in each case. This could be due to increased competition between Penning ionization and atom transfer of molecular dissociation channels in the case of Ar*. These channels are closer in energy to the excitation energy of Ar* then those of Ne* and He* where Penning ionization dominates.[18] Molecular dissociation and atom transfer by reaction of Ar* with a substrate has been shown to compete with the Penning ionization exit channel via curve crossing.[18,19,59]

The uncertainty in the absolute branching fractions for chemi-ionization of NO with Ar* is subject to uncertainties in the yields of $N_2^+(B^2\Sigma_u^+)$ in the reaction of He* with N_2, and of $N_2(C^3\Pi_u)$ in the reaction of Ar* with N_2, as well as the uncertainty in the He* + N_2 ion signal peak height and the peak height of the NO standard which is estimated at ± 35%. The overall uncertainty in the relative branching fractions of the substrate molecules are subject only to the uncertainty in the peak height of the ion signals obtained from the standard and the substrate. This will result in uncertainties of less than ± 20%.

The literature values of the branching fractions for Penning ionization by Ar*[18] (Table XII) with those obtained in the present study, agree within experimental error. CH_3Cl and C_6F_6 have the largest branching frac-

tions which suggests that they quench Ar* entirely by Penning ionization. While CH_3Cl reacts to produce secondary ions as well as the parent ion, C_6F_6 gave only the parent ion when reacting with Ar*. This would suggest that in future studies, C_6F_6 would be useful as the standard substrate.

The lowest branching fraction for Penning ionization by Ar* was observed to occur when $(CF_3)_2CO$ was used as the substrate gas. This is because the ionization potential of the ketone (IP = 11.68 eV)[60] is greater than the excitation energy of the $Ar(^3P_2)$ (E = 11.55 eV)[60] the major metastable species in the flow, while reacting only with the small amount of $Ar(^1P_0)$ (E = 11.73 eV)[60] that is present.

The branching fractions for most of the substrates studied with He* and Ne* are close to unity. N_2 and CO have both been reported to totally quench He* by Penning ionization,[47] while the exit channels for the quenching of He* with NO and O_2 include dissociation to the excited atomic states.[47] The slope values used for the determination of the branching fraction for Penning ionization of these diatomic molecules are in better agreement with the reported values than those obtained from the plateau region. However, both are the same within experimental error.

Penning ionization branching fraction values obtained from Ne* are compared (Table XIV) to ionization yields obtained from studies of the Jesse effect,[61] i.e. the increase in ionization produced in a gas by ionizing radiation (α, β, γ) when a small concentration of gas with lower ionization potential is present.[61]

A brief summary of the ionic states and the ionization potentials of some of the substrates studied here are listed in Table XV1. These values can be compared to the excitation energy of each metastable atom ($Ar(^3P_2)$ E = 11.55 eV, $Ar(^3P_0)$ E = 11.65 eV, $Ne(^3P_2)$ E = 16.61 eV, $Ne(^3P_0)$ E = 16.71 eV, and $He(2^3S)$ E = 19.81 eV)[23] in order to compare the possible

Table XV1. Ionic States of Parent Ions and Their Ionization Potentials.[a]

Parent Ion	Ionic State	Adiabatic IP(eV)	Parent Ion	Ionic State	Vertical IP(eV)		
N_2	$X^2\Sigma_g^+$	15.60[b]	CH_3Cl[c]	(X)	11.29		
	$A^2\Pi_u$	16.98[b]		others	11.31	14.4	15.4
	$8^2\Sigma_u$	18.78[b]			16.0	21.7	24.1
CO	$X^2\Sigma_g^+$	14.01[b]	CH_2Cl_2[c]	(X)	11.40		
	$A^2\Pi_u$	16.91[b]		(A)	12.2		
	$8^2\Sigma_u$	19.72[b]		others	15.3	15.9	16.8
O_2	$X^2\Pi_g$	12.07			21.0	21.5	
	$A^4\Pi_u$	16.12			(23-26.5)		
	$b^4\Sigma_g$	18.70	$CHCl_3$[c]	(X)	11.5		
	$^4\Sigma_u$ or $^2\Sigma_g^-$	20.29		(A)	12.0		
NO	$X^1\Sigma^+$	9.26		(8)	12.9		
	$^3\Sigma^+$	15.65		others	16.0	17.0	20.8
	$^3\Pi$	16.54			25		
	$^3\Delta$	16.84	CCl_4[c]	(X)	11.69		
	$^3\Sigma^-$	17.55		(A)	12.44		
	$^1\Pi$	18.30		others	13.37	13.50	16.6
	$^1\Sigma^-$	18.39			19.9	20.4	25.5
	$^1\Delta$	19.28	C_6H_6	(X)	9.25		
				(A)	11.49		
				others	12.1	13.8	14.7
					15.4	16.9	19.2
					22.5	25.9	

[a]Ref. 71. [b] These values are vertical IPs. [c] Ref. 72.

exit channels available to each complex, A*-B. As stated before, Ar* does not have enough energy to ionizize most diatomic molecules, while for many larger molecules, only the first ionic state can be produced.[72-78] In cases where ionization is not available as an exit channel because of energy restrictions, the quenching cross sections are as large or larger than when ionization is an available product channel.[79] Therefore, ionization does not need to be the dominant reaction channel for quenching of metastable argon atoms.

From the present results, we can conclude that for He* and Ne*, Penning ionization represents the major quenching channel. However, with Ar*, other product channels seem to be in competition with Penning ionization.

C. Fragmentation and Secondary Ion-molecule Reactions.

1) Diatomic Molecules. In the case of diatomic molecules, the parent ion was the only ionic species produced with no evidence of ion-molecule reactions occurring between the primary ion and its neutral precursor. Reactions of He* and Ne* can be distinguished from the reactions of He^+ with these diatomic molecules. Where the reaction of the metastable atom produced only the parent diatomic cation, chemi-ionization with He^+ produced mainly the ion fratments (Table A.2 in Appendix II). These results demonstrate the advantage He* has over He^+ in selectively ionizing a single species.

2) Chlorinated Methanes. The chlorinated methanes undergo Penning ionization with Ar*, Ne*, and He*. For the ions containing Cl, only those of ^{35}Cl were listed. With Ar*, CCl_4 and $CHCl_3$ gave only one fragment ionic species each (Table VII) while the reactions with He* and Ne* produced several fragment ions (Tables IX and X). This demonstrates the utility of Ar* over He* and Ne* in producing predominantly a single ionic species. No secondary ion-molecule reactions were observed for either

$CHCl_3$ or CCl_4.

CH_3Cl has been studied extensively by various techniques,[80] electron impact mass spectrometry, charge exchange mass spectrometry, photoionization, photoelectron spectroscopy, threshold electron coincidence mass spectrometry, ion photodissociation, and Penning ionization.[44] In each case fragmentation occurs to some extent and two or more ions are produced except for the case of the Penning ionization by Ar*. The ionic species produced is the parent ion m/z 50. The Penning reactions of CH_3Cl with He* and Ne* yield both $CH_3Cl^{+\cdot}$ and a small concentration of CH_3^+ (Tables IX and X). In each case, the $CH_3Cl^{+\cdot}$ reacts with CH_3Cl to produce secondary ions m/z 51, 65, and 99. The m/z 51 and 65 ions have been previously reported from a study in another FA system[44] and in an ICR;[81] however, formation of the ion m/z 99 was not reported. The formation of these ions is explained in Scheme I.

Scheme I

$$Ar^* + CH_3Cl \rightarrow CH_3Cl^{+\cdot} + Ar$$

m/z 50, 52

$$CH_3Cl^{+\cdot} + CH_2Cl \rightarrow CH_3ClH^+ + \cdot CH_2Cl$$

m/z 51,53

$$CH_3\text{-}\ddot{Cl}: + CH_3\text{-}\ddot{Cl}^{+\cdot}\text{-}H \rightarrow CH_3\ddot{Cl}^{+\cdot}CH_3 + HCl$$

m/z 65, 67

$$CH_3\ddot{Cl}: \rightarrow [CH_2{=}\ddot{Cl}]^+ \leftarrow CH_3\ddot{Cl}^{+\cdot}$$

$$\downarrow CH_3\ddot{Cl}:$$

$$CH_3ClCH_2Cl^+$$

m/z 99, 101, 103

The primary ion produced from the reaction of CH_2Cl_2 with Ar* is m/z 84 and is assigned the formula $CH_2Cl_2^+$ based on the isotope peaks at m/z 86 and 88. Secondary ion-molecule reactions also take place with the neutral precursor producing ions m/z 97 and 133. A possible mechanism for these reactions is shown in Scheme II.

Scheme II

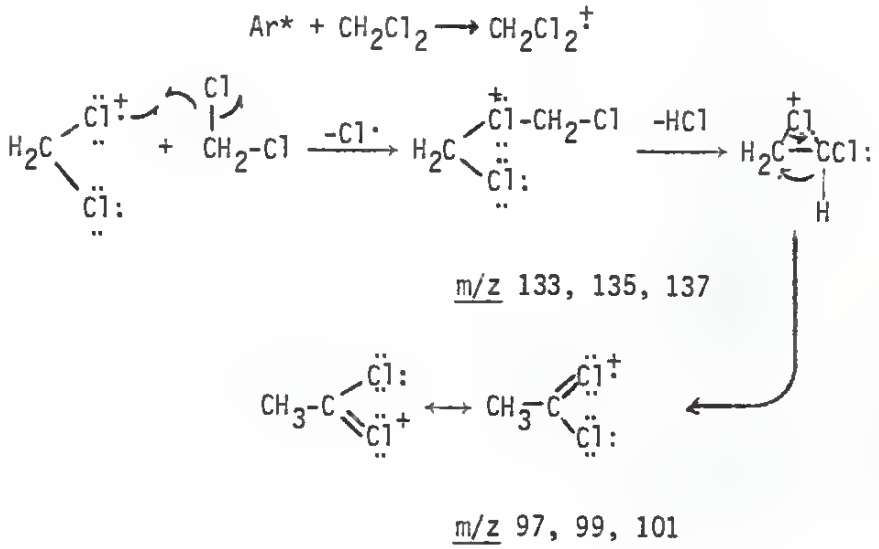

In reactions with He* and Ne*, CH_2Cl_2 fragments to form the ion m/z 49 (CH_2Cl^+). as well as producing the parent ion and the secondary ions in Scheme II. The number of chlorines in each case was determined by the isotope peaks and for M^+ 133 the $M^+ + 2$ (135) was about 98% of the M^+ so 3 chlorines are concluded to be in this formula.

CHF_3 was also observed to undergo Penning ionization with He* producing mainly ion m/z 51 (CHF_2^+) along with some m/z (CHF_3^+) (Tables VII and IX). The ionization potential of CHF_3 is 13.80 eV[60] which is too large to be ionized by Ar*. Indeed no reaction was observed when CHF_3 was added to the flow containing Ar*.

3) Acetylene. Acetylene has been studied in great detail using

various ionization techniques[32,35,82-89] and oligomerization of $C_2H_2^+$ has been well documented.[86-89] In most cases, however, it is reported that the primary ions from ionization consist of $C_2H_2^{+\cdot}$, C_2H^+, and $C_2^{+\cdot}$. In the present study, the exclusive reaction of Ar* with C_2H_2 formed exclusively the parent ionic species, $C_2H_2^{+\cdot}$, followed by oligomerization with C_2H_2 (Figure 15). The two major secondary ions, $C_4H_2^{+\cdot}$ and $C_4H_3^+$, are formed in a ratio of 0.49/1.00 which is in agreement with other reported ratios of 0.55/1.00,[55] 0.44/1.00,[89] and 0.40/1.00[90] found using trapped-ion and mass spectrotrometric techniques under conditions where $C_2H_2^{+\cdot}$ was the only primary ion. The major tertiary ions observed were $C_6H_5^+$ and $C_6H_6^{+\cdot}$. It has been suggested that two different reaction pathways are involved in the formation of $C_6H_6^{+\cdot}$.[83] One process involves the formation of benzene which does not react further and the other process forms the linear trimer which polymerizes further to form large ionic species. While $C_{11}H_{10}^+$ was the largest ionic product detected, oligomerization reactions producing products as large as $C_{14}H_{14}^+$ have been reported.[86]

4) Other Organic Substrates. While the Penning ionization reaction of C_2F_4, C_6H_6, C_6F_6 and CS_2 by Ar* produced only the parent ions, reactions of each with He* resulted in multiple fragmentations producing a number of ionic species. This further illustrates the increased selectivity of Ar* to produce ionic species relative to He*. Even the Penning ionization reaction of C_6H_6 by Ne* produced many fragment ion species (Table XIV). The reaction of Ar* with $(CH_3)_4C$ exclusively produced the tert-butyl cation,[44] while the reaction of $(CH_3)_4C$ with He* formed several fragment ions.

The reaction of Ar* with $(C_2H_5)_2O$ produced the ions $C_4H_{10}O^{+\cdot}$, $C_4H_9O^+$, and $C_3H_7O^+$. Formation of these ions is explained mechanistically by radical

fragmentation from the parent ion as shown in eqs (67-69).

$$Ar^* + (C_2H_5)_2O \rightarrow (C_2H_5)_2O^{+\cdot} \quad (67)$$

$$CH_3\text{-}CH_2\text{-}\overset{+\cdot}{O}\text{-}C_2H_5 \rightarrow CH_2{=}\overset{+}{O}\text{-}C_2H_5 + \cdot CH_3 \quad (68)$$

$$CH_3\text{-}CH_2\text{-}\overset{+\cdot}{O}\text{-}C_2H_5 \rightarrow CH_3CH{=}\overset{+}{O}\text{-}C_2H_5 + \cdot H \quad (69)$$

The reaction of Ar* with $(CH_3)_3CH$ is a bit more enigmatic. The product ions are $C_4H_{10}^{+\cdot}$, $C_4H_9^+$, $C_3H_7^+$, and $C_3H_6^{+\cdot}$. While ionization of $(CH_3)_3CH$ will produce $C_4H_{10}^{+\cdot}$, and intramolecular decomposition of the parent ion will produce $C_4H_9^+$ and $C_3H_7^+$ (eqs 70 and 71). Since formation of $C_3H_6^{+\cdot}$ from $C_4H_{10}^{+\cdot}$ requires the loss of CH_4 from the parent ion, generation of $C_3H_6^{+\cdot}$ in this Penning process is considered to arise by H-atom transfer

$$(CH_3)_3CH^{+\cdot} \rightarrow (CH_3)_3C^+ + \cdot H \quad (70)$$

$$(CH_3)_3CH^{+\cdot} \rightarrow (CH_3)_2CH^+ + \cdot CH_3 \quad (71)$$

in the ion-radical complex shown in eq (72).

$$CH_3\text{-}\overset{+}{C}H\text{-}CH_2\text{-}H/\cdot CH_3 \rightarrow CH_3CH{=}CH_2^{+\cdot} + CH_4 \quad (72)$$

One other very interesting reaction was the Penning ionization of PhN_3 by Ar*. The dominate ion in this case was m/z 91 which was assigned the structure $PhN^{+\cdot}$. Secondary ion-molecule reactions were also observed to take place which included the formation of ion m/z 115 assigned the structure PhN_2^+. Scheme III suggests the mechanism which describes these processes.

Scheme III

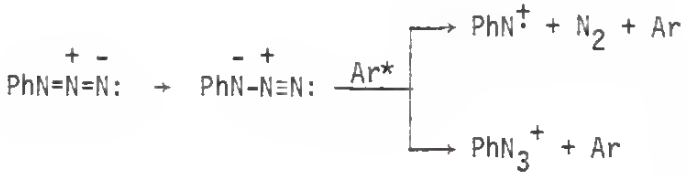

$$PhN^{\cdot} + PhN_3 \rightarrow [PhN_4Ph^{\cdot}] \rightarrow PhN_2^{+} + PhN_2\cdot$$

VII. Conclusions.

We have developed a cold-cathode discharge tube capable of producing rare gas metastable atoms which are used to study Penning ionization in a flowing afterglow apparatus. The effects of diffusion were modeled and found to be minimal.

Penning ionization is an efficient soft ionization technique which usually simplifies the mass spectra of compounds or mixtures compared to conventional high energy electron impact. The availability of a variety of metastable atoms permits the controlled fragmentation of compounds and allows the identification of structural isomers.[58]

The excitation energies of the dominant rare gas metastable atoms produced in the cold-cathode discharge are $He(2^3S)$ (19.81 eV), $Ne(^3P_2)$ (16.61 eV), $Ar(^3P_2)$ (11.55 eV), $Kr(^3P_2)$ (9.92 eV), and $Xe(^3P_2)$ (8.32 eV). Since the neutral molecules used in this study had ionization potentials around 9-12 eV, it was not surprising that chem-ionization with $Ne(^3P_2)$ and especially $He(2^3S)$ caused considerable fragmentation with the neutrals compared to the results using the less energetic $Ar(^3P_2)$ rare gas metastable atoms. Generally, the ionic fragmentation observed using $He(2^3S)$ was similar to that found using He^+ (ΔH_f° = 24.6 eV).

A major difference was observed in the contribution that Penning ionization makes to the total decay processes of $He(2^3S)$, $Ne(^3P_2)$, and

$Ar(^3P_2)$ in their interactions with the neutral substrates studied. While most (90%) of the $He(2^3S)$ and $Ne(^3P_2)$ decayed via Penning ionization, a smaller fraction (43%) of $Ar(^3P_0)$ was quenched by this process. However, the C_6F_6 and CH_3Cl quench $Ar(^3P_2)$ almost entirely by Penning ionization.

Appendix I.

Operating Instructions.

The operating procedures are outlined in a step-by-step method starting under the assumption that everything is turned off or closed.

1. Turn on forepumps to 4" and 6" diffusion pumps and open Vecco valves between forepumps and diffusion pumps. Open bypass valve between chamber 1 and 2. After about 10 minutes open gate valves and monitor pressure using thermocouple gauge tubes (caution: do not operate thermocouple gauge if system is at atmospheric pressure). When the pressure has reached 1 torr or less, carefully fill the liquid nitrogen cyrotrap for the 4" diffusion pump and turn water on in the water baffle for the 6" diffusion pump.
2. When the system reaches 0.01 torr (if it does not obtain this pressure the system should be checked for leaks) turn on water pumps for both 4" and 6" diffusion pump heat exchangers, making sure the distilled water level in the heat exchangers covers the water pumps. Turn on main water inlets for cooling heat exchangers. Be sure water is flowing through entire system and is not clogged.
3. Turn on heaters of both 4" and 6" diffusion pumps. Let diffusion pumps run for about 30 minutes then turn on the ion gauge and monitor pressure. Do not let the cyrotrap run out of liquid nitrogen when the diffusion pump is hot.
4. Turn on AC power switch on the EAI mass spectrometer. Leave on one hour before using electronics/ionizer.
5. Check pressure in the mass spectrometer chamber 3 (below 1×10^{-6} torr). Turn on oscilliscope, recorder, preamp, lens potentials and H.V. switch (the preamp must warm up for 30 minutes).
6. Close the air-inlet to the Stokes Roots blower/mechanical pump system

on the other FA system.

7. Close Vecco valve between the first and second chambers.
8. Operation of Roots blower
   a) Check 4 oil levels at windows. Once a week, check 5th level on blower with oil dipstick.
   b) Turn on water.
   c) Turn the switch to automatic (on).
   d) Push in green button.
9. After the Roots blower has pumped down, open upper gate valve (exhaust of chamber 1) all the way (counterclockwise).
10. Operation of transducer
   a) Make certain the switch on the operating box is turned toward the proper color since the transducers are color coded (in this case green).
   b) Check to see the span is set properly (911.0).
   c) Turn on the transducer with operating switch at +100 and adjust zero.
   d) Turn operating switch to +10 and readjust zero.
11. Open valve to allow the buffer gas (He) into the flow tube and adjust flow rate (220 cm^3 s^{-1} when triflat flow meter is reading 14).
12. Close the gate valve to the Roots blower until the pressure in the flow tube is 0.5 torr (about 90 transducer reading).
13. Put liquid nitrogen in the molecular sieve (Davison 4A) traps.
14. Turn on electron gun (if using cathode discharge see #15).
   a) Turn D.C. power supply to 2 amp.
   b) Turn H.V. power supply to 150 V.
   c) Adjust emission to about 250 amp or good ion signal.
15. Alternative: Turn on cold-cathode discharge.

a) Turn on H.V. power supply to 250 V.

b) Use tesla coil to initiate discharge.

16. The ions produced in the flow tube can now be monitored by switching the lens potentials of the quadrupole to bias conditions. Caution: Under no circumstance is the ionizer to be on when potential switches are in bias mode. Feedback can occur that could cause serious damage to the electronics. Adjust first nose cone to +0.5 volts, second nose cone, Faraday cage, and accelerator grid to -1.5 volts and the extractor to -8 volts.

17. At this point an ion signal should be detected if using the FA electron gun. If the cathode discharge is used addition of a neutral to the reaction region is required to produce an ion signal. The resolution should be set at 5.000.

18. When the ion signal has been obtained all potentials should be maximized as well as the ion source to produce the optimum signal.

19. The system is now ready for operation. Resolution and bias potentials can be adjusted for the spectrum of interest.

Shut Down Procedure

1. Turn off all power supplies to FA electron gun or cathode discharge. Turn off bias potential on lens and follow shut down procedure for quadrupole. Turn off ionization gauge tube.

2. Turn off carrier gas flow and any other gas flow inlets. Shut off Stokes Roots blower/mechanical pump system by pusing red button in and then turning switch to off position. Then open air-inlet on other FA system.

3. Turn off 4" and 6" diffusion pumps. Open Vecco valve between chambers 1 and 2.

4. Turn off heaters for 4" and 6" diffusion pumps and close gate valves

isolating the pumps from the rest of the system. Remove Dewar flasks with liquid nitrogen from the molecular sieve traps and pump them out.

5. After 4" and 6" diffusion pumps are cool to the touch (about 60 minutes) shut off main water supply to heat exchangers and water pumps.
6. If the system is to be left under vacuum, leave both forepumps operating with Vecco and gate valves open. If the system is to be entirely shut down, close gate valves to 4" and 6" diffusion pumps. Bring system pressure up to atmosphere with He using the transducer to measure pressure. Close both Vecco valves to forepumps, shut off forepumps, and bleed to atmosphere.

The operation and shut down procedures are meant as guidelines to be followed as one learns to use the system. After the operator is familiar with the system some steps may be changed.

Appendix II.

Calculations used in Data Work Up on the FA System.

A. Calculation of the concentration of reagents used.

The concentration of the reagents is represented by eq (A.1),

$$[Q] = \frac{F_Q \times P_{He} \times N}{F_{He} \times P \times V} \qquad (A.1)$$

where F_Q is the flow rate of the neutral species, P_{He} is the pressure of the He buffer gas (measured with a Celsco transducer), F_{He} is the buffer gas flow rate (measured with a tri-flat flow meter), N is avogadro's number (6.023×10^{23}), P is atmospheric pressure in torr (760 torr/atm), and V is the standard volume (22.4×10^3 cm^3) at 273° k.

$$[Q] = \frac{F_Q \times P_{He}}{F_{He}} \times 3.26 \times 10^{16} (\text{molecules torr}^{-1}\ \text{cm}^{-3}) \qquad (A.2)$$

F_Q is measured by inletting the substrate gas at a constant rate into an evacuated container of known volume, and monitoring the change in pressure with respect to time. This is accomplished by using a Celesco transducer indicator (model C025A). From the ideal gas law;

$$F_Q = \frac{dp\ (\text{torr})}{dt\ (\text{sec})} \times \frac{V(1)}{R \times T \times 760\ (\text{torr/atm.})} \qquad (A.3)$$

$$= \frac{dp}{dt} \times \frac{2.130(1) \times 24.5 \times 10^3 (cm^3)}{0.082(1 \cdot \text{atm/K}) \times 298(K) \times 760(\text{torr/atm})} \qquad (A.4)$$

$$= \frac{dp}{dt} \times 2.810\ (cm^3/\text{torr}) \qquad (A.5)$$

where 2.130 liters is the volume used to measure the neutral concentration, and 24.5×10^3 cm^3 is the standard volume at one atmosphere and 298 K which contains 6.023×10^{23} molecules, eq (A.6) is derived

$$F_N = \frac{T_r \times T_s \times 2.810\ cm^3/\text{torr}}{t\ \text{sec}} \qquad (A.6)$$

here T_r is the difference in the transducer reading between zero-time and time t, which is related to pressure by a constant T_s. Substituting eq. (A.5) into eq. (A.2) gives eq. (A.7).

$$[Q](\text{molecules cm}^3) = \frac{T_r \times T_s \times P_{He}}{F_{He} \times t}(\text{torr}^2\ \text{cm}^3) \times 1.5268 \times 10^{15}\ \frac{\text{molecules}}{\text{torr}^2} \quad \text{(A.7)}$$

The program in Table A.1 is used to calculate the [Q] on the Texas Instruments SR-55 programmable calculator.

The rate constant for the reaction is calculated by monitoring the rate of decay of the primary species vs the concentration of added neutral [Q]. A mass spectrum is recorded before and after each addition of the variable amounts of [Q] in order to normalize the peak heights of the ions formed from the reaction. After accumulating five or more data points at varying concentrations of [Q], a plot of log [Ion] intensity vs concentration of [Q], is drawn. The slope of the line that is produced is a function of the pseudo-first order rate constant given in eq. (A.4). The rate constant is calculated using eq. (A.8).

$$k = \frac{\text{slope} \times 1.086 \times F_{He}}{P_{He}} \quad \text{(A.8)}$$

the relationship comes from the derivations put forth by DePuy[91] where;

$$k = \frac{-d(\log[A^+])(2.303)(1.59)\bar{v}}{dz\ [Q]} \quad \text{(A.9)}$$

and the average buffer gas velocity $\bar{v}$, may be expressed as;

$$\bar{v} = \frac{F_{He} \times 760\ \text{torr/atm}}{P_{He} \times \text{area}\ (\text{cm}^2)} \quad \text{(A.10)}$$

Table A.1. Program for the T.I. SR-55 programmable calculator to calculate the concentration of reactants.

The program is entered in the following sequence:

OFF-ON LRN x RCL 0 RCL 1 x RCL 2 x RCL 3 RCL 4 x RCL 5 =
R/S RST LRN RST

In order to verify that the program has been entered correctly the following series of numbers should be entered into the program:

enter the 5 torr transducer plot slope (5.483×10^{-3}) STO 0,

enter the time in min. (0.245), STO 1,

enter (1.52×10^{-3}) from equation A.7 STO 2,

enter the flow tube pressure (0.49347), STO 3,

enter the flow rate of helium (210), STO 4,

enter the % of neutral reagents in decimal form (1.00), STO 5,

and enter the transducer reading (100) and press R/S,

The calculator should read 7.9935042×10^{12} (molecules cm^{-3}). If an error occurs first make sure all values were entered into the correct memory. If there is still a problem, the program should be reentered.

The program is now entered and checked and the data obtained from the experiment can be entered into the program in order to determine the concentration of the reagent.

B. Reactions of He^+.

The calculation of rate constants from reactions in the flowing afterglow has been discussed by Fehensefeld, et al,[8] for ion-molecule reactions. M. J. Shaw and H. M. P. Stock have demonstrated that the total rate constant and the ambipolar diffusion coefficients can be obtained from Penning ionization reactions in the flowing afterglow.[20]

The rate constants for the reactions of He^+ with substrate gases are given in Table A.2 along with the literature values for these rate constants.

Table A.2. Reactions of He^+ with Neutral Substrate Gases.

Reaction	Products	Rate Constants ($cm^3\ s^{-1}$)	Literature[a] Rate constants($cm^3 s^{-1}$)
$He^+ + N_2$	N^+; N_2^+	$(1.20\pm0.2) \times 10^{-9}$	$(1.20\pm0.1) \times 10^{-g}$
$He^+ + CO$	C^+; CO^+	$(1.60\pm0.1) \times 10^{-9}$	$(1.55\pm0.15) \times 10^{-9}$
$He^+ + CH_2CO$[b]	CH_2^+; CO^+; CH_2CO	$(1.70\pm0.1) \times 10^{-g}$	
$He^+ + C_6H_5N_3$[c]	$C_3H_2^+$; $C_3H_3^+$;		
	$C_3H_4^+$; $X_3H_5^+$;		
	$C_4H_3^+$; $C_4H_4^+$;		
	$C_5H_3^+$; $C_5H_5^+$;		
	$C_6H_5^+$; $C_6H_5N^+$;		
	$C_6H_5N_2^+$; $C_6H_5N_3^+$		
$He^+ + (CF_3)_2C{=}N$[cd]	$(CF_3)_2C^+$; CF_3^+		
	$(CF_3)_2C^+$; CF_2^+; N_2^+		
	CN^+; CN_2^+; CF^+		

[a]Ref. 17 [b]No literature value was found for this reaction. [c]The rate constants were not developed for these reactions. [d]A group of ion signal peaks was observed at m/a 190-200 and m/z 210.

The reaction of He^+ with ketene produced $CH_2^{\cdot+}$ (40%), CO^+ (40%) and the parent ion $C_2H_2O^{\cdot+}$ (20%); $CH_2^{\cdot+}$ undergoes secondary ion-molecule reactions with the neutral precursor to produce the ion m/z 56 ($C_3H_4O^{\cdot+}$). The reaction of ketene with Ar* was also studied and similar results to those obtained with He* were found.

C. Calculation of Rate Constants Needed to Observe Hetero-Ion-Molecule Reactions in the Presence of Homo-Molecule Reactions.

In order to observe hetero-ion-molecule reactions in the FA the metastable atom must be totally quenched so no ionic species could result from its reaction with the hetero-molecule, therefore, large concentrations of the primary substrate must be added to the flow to assure total quenching. In some cases the primary ion produced during this quenching reaction will react with its neutral precursor forming secondary ion products. Since the primary substrate will travel a distance down the flow tube before encountering the neutral substrate the amount of homo-ion-molecule reaction needs to be determined before reaching an understanding of the hetero-ion-molecule reactions taking place. To calculate the relative value that the rate constant for the hetero-ion-molecule reaction must have in order to be observed eq (A.15)-(A.17) were used; A* is the metastable species, B is

$$A^* + B \xrightarrow{k_1} B^+ + e^- \qquad \text{(A.15)}$$

$$B^+ + B \xrightarrow{k_2} B_2^+ \qquad \text{(A.16)}$$

$$B^+ + C \xrightarrow{k_3} BC^+ \qquad \text{(A.17)}$$

the primary substrate which produces the primary ion B^+ upon reaction with A*, B_2^+ is the secondary homo-ion produced from reaction of the primary ion with its neutral precursor, C is the hetero-molecule introduced downstream of the inlet for the primary substrate, BC^+ is the product of the hetero-ion-molecule reaction, k_1 is the quenching rate constant (the assumption is made that the quenching process occurs entirely by Penning ionization and is assigned a value of 1×10^{-10} cm^{-3} s^{-1}, k_2 is the homo-ion-molecule rate constant and is also assigned a value of 1×10^{-10} cm^3 s^{-1} (this assumes that a reaction occurs on one out of every ten collisions), and k_3 is the hetero-ion-molecule reaction rate constant which is to be determined. Setting up the rate equations for each species yields:

$$d[A^*]/dt = -k_1[A^*][B] \text{ or } [A^*] = [A^*]_0 \exp(-k_1[B]t) \qquad (A.1B)$$

where $[Ar^*]_0$ is the initial concentration of A*,

$$d[B^+]/dt = k_1[B][A^*]_0 \exp(-k_1[B]t) - [B^+](k_2[B] + k_3[Cl]) \qquad (A.19)$$

$$d[B_2^+]/dt = k_2[B^+][B] \qquad (A.20)$$

and

$$d[C^+]/dt = k_3[B^+][C] \qquad (A.21)$$

The substrate, B, is inlet at port e in Figure 1, while C is inlet at port f. Thus, from port e to port f (equivalent to 1.95 ms at P_{He} = 0.5 torr and a $\bar{v}$ = 80 m s^{-1}), B is the only substrate in the tube. The amount of A* and B^+ present at port f before any C is added, is calculated using eqs (A.1B) and (A.22) with t = 1.95 ms. The values of A*, B^+, and

$$[B^+] = \frac{k_1[B][A^*]_0}{k_2[B] - (k_1 + k_2)[B]} \exp-(k_1 + k_2)[B]t) - \exp(-k_2[B]t)] \qquad (A.22)$$

8_2^+ present under these conditions are listed in Table A.3. The initial amount of A* is considered to be 1×10^{10} molecules cm^{-3} and the concentration of 8 is varied from 5×10^{11} to 5×10^{13} molecules cm^{-3}.

At the point A* is quenched, 8^+ is absent having been converted to B_2^+. Thus at the point of introduction of C into the flow tube there is virtually no B^+ left to undergo the hetero-ion-molecule reaction. This limits the number of reagents useful for the study of hetero-ion-molecule reactions to those that either do not undergo secondary ion-molecule reactions or only slowly undergo such reactions with their parent precursors.

Table A.3. Calculated Concentrations of the Metastable Atom, Neutral Substrate, Primary and Secondary Ions at Inlet Port f.

8 molecules cm^{-3}	A* molecules cm^{-3}	8^+ molecules cm^{-3}	B_2^+ molecules cm^{-3}
5×10^{11}	9.1×10^9	8.43×10^8	5.7×10^7
1×10^{12}	8.2×10^9	1.46×10^9	3.1×10^8
5×10^{12}	3.8×10^9	2.35×10^9	3.8×10^9
1×10^{13}	1.4×10^9	1.22×10^9	7.4×10^9
2×10^{13}	2.0×10^8	1.98×10^8	9.6×10^9
5×10^{13}	5.8×10^5	5.83×10^5	9.9×10^9

However, if k_1 and k_2 are large and B_2^+ does not react further with substrate 8, the chemistry of B_2^+ can be investigated. A sufficient concentration of B must be added in the upstream end of the flow tube to convert all A* and B^+ into B_2^+ and still allow for theralization of the

B_2^+ ions in $\leq$ 20 cm of the tube before reaching the inlet port for addition of C. This appears to be the situation in the Penning ionization of PhN_3 with Ar* where 90% of this process is dissociative yielding PhN^+ and the secondary reaction of PhN_3^+ with PhN_3 yielding predominately PhN_2^+. If k_2 is determined to be large, the chemistry of PhN_2^+ can be investigated.

The primary ions may also be studied for this case. Low concentrations of reagent yielding primary ions can be used along with an inert gas such as N_2 or CO to quench all excess metastables. The hetero-ion-molecule reactions may then be studied by addition of a new reagent downstream of the primary ion production region.

O. Emission Data.

The data from the emission study in section Va, used to determine the absolute branching fractions for the Penning ionization reactions by Ar* are summarized in Table A.4. the wavelength of the emission bands are

Table A.4. Wavelength λ_{max}, Band Areas and Correction Factors for the Reactions $Ar^* + N_2 \rightarrow N_2(C^3\Pi_u) + Ar$ and $He^* + N_2 \rightarrow N_2^+(B^2\Sigma^+_u) + He + e^-$

λ_{max} (nm)	Area	Correction Factor of PM Tube at λ_{max}	Corrected Area
$Ar^* + N_2$; Concentration of N_2 = 4.7×10^{12} molecules cm^{-3}			
316.0	53.3	0.96	55.5
337.1	451.7	1.00	451.7
357.7	319.0	1.00	319.0
380.5	159.0	0.94	169.0
405.9	46.0	0.88	51.5

Table A.4. (Continued)

λ_{max} (nm)	Area	Correction Factor of RM Tube at λ_{max}	Corrected Area
426.9	15.5	0.81	18.5
			Total Area = 1065.2
$Ar^* + N_2$; Concentration of N_2 = 9.9 x 10^{11} molecules cm^{-3}			
316.0	30.0	0.96	31.3
337.1	93.0	1.00	93.0
357.7	72.0	1.00	72.0
380.5	30.0	0.94	32.0
405.9	8.0	0.88	9.0
426.9	2.1	0.81	2.7
			Total Area = 239.0
$Ar^* + N_2$; Concentration of N_2 = 4.3 x 10^{11} molecules cm^{-3}			
316.0	22.5	0.96	23.4
337.1	40.5	1.00	40.5
357.7	30.0	1.00	30.0
380.5	15.3	0.94	16.3
405.9	4.8	0.88	5.5
426.9	2.0	0.81	2.4
			Total Area = 118.1
$Ar^* + N_2$; Concentration of N_2 = 3.2 x 10^{11} molecules cm^{-3}			
316.0	17.3	0.96	18.0
337.1	33.0	1.00	33.0
357.7	20.1	1.00	20.1
380.5	9.6	0.94	10.6

Table A.4. (Continued)

λ_{max} (nm)	Area	Correction Factor of PM Tube at λ_{max}	Corrected Area
405.9	3.5	0.88	4.0
426.9	0.9	0.81	1.2
		Total Area =	86.8
$He^* + N_2$; Concentration of $N_2 = 3.9 \times 10^{12}$ molecules cm^{-3}			
358.2	30.1	1.00	30.1
391.4	345	0.92	375.0
427.8	131.5	0.82	160.0
459.9	39.8	0.70	57.0
		Total Area =	622.1
$He^* + N_2$; Concentration of $N_2 = 7.8 \times 10^{11}$ molecules cm^{-3}			
358.2	5.5	1.00	5.5
391.4	80.7	0.92	85.7
427.8	36.5	0.82	44.5
459.9	3.5	0.70	4.9
		Total Area =	140.6
$He^* + N_2$; Concentration of $N_2 = 1.1 \times 10^{11}$ molecules cm^{-3}			
358.2	0.6	1.00	0.6
391.4	13.2	0.92	14.3
427.8	5.6	0.82	6.8
459.9	1.0	0.70	1.4
		Total Area =	23.1

listed for each concentration of N_2 used, and the area under each band is tabulated. The area was corrected using a correction factor for each wavelength and then totaled. The monochromator slit was set at a constant width for both the He* and Ar* measurements.

In order to establish the absolute branching fraction, the emission of N_2 with He* and Ar* was used to evaluate the relative concentrations of metastable atoms using eq (A.23), where $I_{N_2^+}$ and I_{N_2} are the total

$$\frac{[He^*]_o}{[Ar^*]_o} = \frac{I_{N_2^+}(k_{N_2} 0.80[N_2])}{I_{N_2}(k_{N_2^+} 0.42[N_2])} \qquad (A.23)$$

emission intensities for the reactions He* and Ar* with N_2, respectively, $k_{N_2^+}$ is the total quenching rate constant for the reaction with He* (7×10^{-3} cm^3 molecules^{-1} s^{-1})[47], k_{N_2} is the total quenching rate constant for the reaction with Ar* (3.6×10^{-11} cm^3 molecules^{-1} s^{-1})[50] and $[N_2]$ was measured. These values along with the values for the rate constants and branching fractions for the Penning ionization of NO by Ar* are listed in Tables A.4 and A.5. The Penning ionization rate constants were calculated using eq (A.24), where the [He*]/[Ar*] is known from eq (A.23), the [NO]

$$k_I^{Ar^*} = \frac{(k_I^{He^*}[He^*][NO])NO^+_{Ar^*}}{([Ar^*][NO])\ NO^+_{He^*}} \qquad (A.24)$$

is calculated from the experiment, and the $NO^+_{He^*}$ and $NO^+_{Ar^*}$ are the measured ion signals from the reactions He* + NO and Ar* + NO, respectively, $k_I^{He^*}$ is the Penning ionization rate constant for NO with He* ($20.91 \pm 6.35 \times 10^{-11}$ cm^3 s^{-1})[50,55], and $k_I^{Ar^*}$ is the Penning ionization rate constnat for NO with Ar*. The value of the total quenching rate constant, k_Q, for Ar* by NO has been reported as $1.95 \pm 0.25 \times 10^{-10}$ cm^{-3} s^{-1}).[32,33] The

branching fraction for the Penning ionization reaction of Ar* and NO can now be determined (Table A.5.).

Table A.4. The Ratio of the Relative Concentrations of Ar* to He*[a]

N_2 with He* (molecule cm^{-3})	Relative Concentration of He*	N_2 with Ar* (molecules cm^{-3})	Relative Concentration of Ar*[b]
1.1×10^{11}	7.1	3.2×10^{11}	9.4
7.9×10^{11}	6.1	4.4×10^{11}	9.1
3.9×10^{12}	5.3	9.9×10^{11}	8.3
		4.7×10^{12}	7.9
Average	6.2 ± 0.9		8.9 ± 0.7

[a]The ratio was obtained using eq A.23. [b]Calculated using a branching fraction of 80% for reaction 53.

Table A.5. Branching Fraction of NO^+ by Ar*.[a]

NO with He* molecules cm^{-3}	NO with Ar* molecules cm^{-3}	k_I^{He*}	Branching Fraction
1.59×10^{11}	1.66×10^{11}	$6.5 \pm 1.8 \times 10^{-11}$	0.33 ± 0.11
2.89×10^{11}	4.83×10^{11}	$1.1 \pm 0.3 \times 10^{-11}$	0.52 ± 0.22
2.89×10^{11}	3.09×10^{11}	$1.2 \pm 0.3 \times 10^{-11}$	0.53 ± 0.21
		Average Branching Fraction = 0.46 ± 0.18[b]	
		Average Branching Fraction = 0.32 ± 0.10[c]	

[a]The rate constants were obtained using eq A.24 and the branching fractions were determined using a value of $1.95 \pm 0.25 \times 10^{-3}$ cm^{-3} s^{-1}.[32,33] [b]The branching fractions were obtained using an 80% branching fraction for eq 53. [c]This value was obtained using a 60% branching fraction for eq 53.

At the saturation region for N_2, all He^* is assumed to be totally quenched. Since the ion peak height for N_2 at concentrations 1 to 5 x 10^{13} molecules cm^{-3} is close to 115 mm on an arbitrary scale, total quenching of Ar* should give a peak of 115 mm x Ar*/He* or 167 ± 63 mm. At the plateau region of NO with Ar*, the signal height was 68 mm which corresponds to a branching fraction of 0.41 ± 0.12.

In order to check the total quenching signal of N_2, which was used to base the branching fraction of NO with Ar*, the ion signal from the reaction of CO with He* was monitored for concentrations of 1 to 5 x 10^{13} molecules cm^{-3}. Since Co has also been found to quench He* totally by Penning ionization this provides a check of the ion signal height obtained for N_2. At these concentrations, the CO^+ signal was found to be 14% larger than the N_2 signal. However, this is within the experimental error of the branching fraction.

References

1. DePuy, C.H.; Bierbaum, V.M. Acct. Chem. Res., 1981, 14, 146.
2. Oempster, A. J. Phil. May., 1916, 31, 438.
3. Tel'roze, V. L.; Lyubimoua, A. K. Doklady Akad. Nauk S.S.S.R., 1952, 86, 909.
4. Lane, F. W.; Field, F. H.; Franklin, J. L. J. Am. Chem. Soc., 1957, 79, 2419, 2665.
5. Stevenson, D. P.; Schissler, D. D. J. Chem. Phys., 1955, 23, 1353.
6. Hamill, W. H.; Meisels, G. G.; Williams, R. R. J. Phys. Chem., 1957, 61, 1456.
7. Fehsenfeld, F. C.; Ferguson, E. E.; Schmeltkoff, A. L. J. Chem. Phys., 1966, 44, 3022.
8. Fehsenfeld, F. C.; Ferguson, E. E.; Schmeltkoff, A. L. Adv. At. Mol. Phys., 1969, 5, 1.
9. Fehsenfeld, F. C.; Ferguson, E. E.; Schmeltkoff, A. L. Planet. Space Sci., 1964, 12, 1169.
10. Smith, M. A.; Barkley, R. M.; Ellison, G. 8. J. Am. Chem. Soc., 1980, 102, 6851.
11. Fehsenfeld, F. C.; Ferguson, E. E.; Schmeltkoff, A. L.; Schiff, H. I. Adv. Chem. Ser., 1969, 80, 1.
12. Golde, M. F., In "Gas Kinetics and Energy Transfer"; The Chemical Society, Ed., Burlington House, London, vol. 2, 1977.
13. West, W. P.; Cook, T. B.; Dunning, F. B.; Rundel, R. D.; Stebbings, R. F. J. Chem. Phys., 1975, 63, 1237.
14. Sholette, W. P.; Muschitz, E. E. J. Chem. Phys., 1962, 36, 3368.
15. Riola, J. P.; Howard, J. S.; Rundel, R. O.; Stebbings, R. F. J. Phys. B., 1974, 7, 376.
16. Lindinger, W.; Schmeltekoff, A. L.; Fehsenfeld, F. C. J. Chem. Phys.,

1974, 61, 2890.

17. Brom, J. M.; Kolts, J. H.; Setser, D. W. Chem. Phys. Lett., 1978, 55, 44.
18. Golde, M. F.; Ho, Y-S.; Ogura, H. J. Chem. Phys., 1982, 76, 3535.
19. Gundel, L. A.; Setser, D. W.; Clyne, M. A. A.; Coxon, J. A.; Nip, W. J. Chem. Phys. 1976, 64, 4390.
20. Shaw, M. J.; Stock, H. M. P. J. Phys. B, 1975, 8, 2752.
21. Klapstein, D.; Maier, J. P.; Misev, L.; Thommen, F.; Zambach, W. J. Chem. Soc. Faraday Trans. 2, 1982, 78, 1765.
22. Endoh, M.; Tsuji, M.; Nishimura, Y. J. Chem. Phys., 1982, 77, 4027.
23. Kolts, J. M.; Setser, D. W. In "Reactive Intermediates in the Gas Phase"; D. W. Setser, Ed., Academic Press, New York, 1979, chap. 3.
24. Kolts, J. M. Thesis, Kansas State University, 1979.
25. Albritton, D. L. At. Data. Nuci. Data Tables, 1978, 22, 1.
26. West, W. P.; Cook, T. B.; Dunning, F. B.; Rundel, R. D.; Stebbings, R. F.; J. Chem. Phys., 1975, 63, 1237.
27. Lindinger, W.; Howorka, F.; Lukac, P.; Kuhn, S.; Villinger, H.; Alge, E.; Ranler, H. Phys. Rev. A, 1981, 23, 2319.
28. Smith, D.; Adams, N. G. Phys. Rev. A, 1981, 23, 2327.
29. lindsay, R. O.; Allen, C. F. H. Org. Synthes. Coll. V. 3, 1955, 710.
30. Weil, T.; Cais, M. J. Org. Chem., 1964, 28, 2472.
31. Weil, S., Thesis, Carleton College, 1981.
32. Piper, L. G.; Velazco, J. E.; Setser, D. W. J. Chem. Phys., 1973, 59, 3323.
33. Holcombe, N. T.; Lampe, F. W. J. Chem. Phys., 1972, 56, 1127.
34. Yokoyama, A.; Hatano, Y. Chem. Phys., 1973, 58, 1452.
35. Bourene, M.; Lecalve, J. J. Chem. Phys., 1973, 58, 1452.
36. Eyring, H.; Lin, S. H., Lin, S. M. "Basic Chemical Kinetics",

Wiley, New York, 1980, 1.

37. Hirschfelder, J. O.; Curtiss, C. F.; Bird, R. B. "Molecular Theory of Gases and Liquids", Wiley, New York, 1965.

38. Fitzsimmons, W. A.; Lane, N. F. Phys. Rev., 1968, 174, 193.

39. McFarland, M.; Albritton, D. L.; Fehsenfeld, F. C.; Ferguson, E. E.; Schmeltekopf, A. L. J. Chem. Phys., 1973, 59, 6610.

40. Patterson, P. L. J. Chem. Phys., 1972, 56, 3943.

41. Stock, H. M. P. J. Phys. B, 1973, 6, LB6.

42. McDaniel, E. W., Mason, E. A., "The Mobility and Diffusion of Ions in Gas", Wiley, New York, 1973.

43. Phelps, A. V. Phys. Rev., 1955, 99, 1307.

44. Anderson, D. R.; Bierbaum, V. M.; DePuy, C. H.; Grabowski, J. J. Int. J. Mass Spectrom. Ion Phys., 1983, __, 0000.

45. Lin, C. L.; Kaufman, F. J. Chem. Phys., 1971, 55, 3760.

46. Velazco, J. E.; Kolts, J. H.; Setser, D. W. J. Chem. Phys., 1978, 69, 4357.

47. Chang, R. S. F.; Setser, D. W. Chem. Phys., 1978, 25, 201.

48. Hotop, H.; Niehaus, A. Int. J. Mass Spectrom. Ion Phys., 1970, 5, 415.

49. Yee, D. S. C.; Steward, W. B.; McDowell, C. A.; Brion, C. E. J. Elec. Spec. Rel. Phenom., 1975, 7, 93.

50. Kolts, J. H.; Brashears, H. C.; Setser, D. W.; J. Chem. Phys., 1977, 67, 2931.

51. Setser, D. W.; Stedman, D. H.; Coxon, J. A. J. Chem. Phys., 1970, 53, 1004.

52. Piper, L. G.; Richardson, W. C.; Taylor, G. W.; Setser, D. W. Disc. Faraday Soc., 1972, 53, 100.

53. Krenos, J.; Bruno, J. B. J. Chem. Phys., 1976, 65 5017.

54. Setser, D. W.; Sadeghi, N. J. Phys. (Paris) Lett., 1977, 3B, 283.

55. Sadeghi, N.; Setser, D. W. Chem. Phys. Lett., 1982, 82, 44.

56. Hotop, H.; Kolb, E.; Lorenzen, J. J. Elec. Spec. Rel. Phenom., 1979, 16, 213.

57. Lindinger, W.; Schmeltekopf, A. L.; Fehsenfeld, F. C. J. Chem. Phys., 1974, 61, 2890.

58. Schmeltekopf, A. L.; Fehsenfeld, F. C. J. Chem. Phys., 197D, 53, 3173.

59. Balamuta, J.; Golde, M. F., J. Chem. Phys., 1982, 76, 243D.

60. Rosenstock, H. M.; Draxl, K.; Steiner, B. W.; Herron, J. T. J. Phys. Chem. Ref. Data, 1977, 6, 1.

61. Person, J. C. Rad. Res., 1974, 59, 408.

62. Laudenslager, J. B.; Theard, L. P. Adv. Mass. Spectrom., 1978, 78, 1388.

63. Jones, E. G.; Harrison, A. G. Int. J. Mass Spectrom. Ion. Phys., 1970, 5, 137.

64. Niehaus, A. Ber. Bunsenges. Phys. Chem., 1973, 77, 632.

65. Hotop, H. Rad. Res., 1974, 59, 379.

66. Richardson, W. C.; Setser, D. W. J. Chem. Phys., 1973, 58, 1809.

67. Natalis, P.; Oelwiche, J.; Collin, J. E.; Caprace,; Praet, M-T. Chem. Phys. Lett., 1977, 49, 177.

68. Natalis, P.; Collin, J. E.; Delwiche, J.; Caprace, G.; Hubin, M.-J. J. Elec. Spec. Rel. Phenom., 1979, 17, 421.

69. Keliher, P. J.; Ounning, F. B.; O'Neill, M. R.; Rundel, R. O.; Walters, G. K. Phys. Rev. A, 1975, 11, 1271.

70. Hotop, H.; Kolbe, E.; Lorenzen, J. J. Elec. Spec. Rel. Phenom., 1979, 16, 213.

71. Turner, D. W.; Baker, C.; Baker, A. D.; Brundle, C. R. "Molecular Photoelectron Spectroscopy", Wiley, N. Y., 1970.

72. Niessen, W. V.; Asbrink, L.; Bieri, G. J. Elec. Spec. Rel. Phenom., 1982, 26, 173.

73. Bieri, G; Åsbrink, L. J. Elec. Spec. Rel. Phenom., 1980, 20, 149.

74. Åsbrink, L.; Niessen, W. V.; Bieri, G. J. Elec. Spec. Rel. Phenom., 1980, 21, 93.

75. Niessen, W. V.; Bieri, G.; Åsbrink, L. J. Elec. Spec. Rel. Phenom., 1980, 21, 175.

76. Bieri, G.; Åsbrink, L.; Niessen, W. V. J. Elec. Spec. Rel. Phenom., 1981, 23, 281.

77. Åsbrink, L.; Svensson, A.; Niessen, W. V.; Bieri, G. J. Elec. Spec. Rel. Phenom., 1981, 24, 293.

78. Bieri, G.; Åsbrink, L.; Niessen, W. V. J. Elec. Spec. Rel. Phenom., 1982, 27, 129.

79. Setser, D. W.; Piper, L. G.; Velazco, J. E. Rad. Res., 1974, 59, 441.

80. For a summary of these reactions see: Eland, J. H. D.; Frey, R.; Kuestler, A.; Schulte, H.; Brehm, B. Int. J. Mass. Spectrom. Ion Phys., 1976, 22, 155.

81. Beauchamp, J. L.; Holtz, D. Woodgate, S. D.; Patt, S. L. J. Am. Chem. Soc., 1972, 94, 2798.

82. Barker, R.; Hammill, W. H.; Williams, R. R. J. Phys. Chem., 1959, 63, 828.

83. Dorfman, M. L.; Shipko, F. J. J. Am. Chem. Soc., 1955, 77, 4726.

84. Field, F. H.; Franklin, J. L.; Lampe, F. W. J. Am. Chem. Soc., 1957, 79, 2665.

85. Buttrill, S. E. J. Chem. Phys., 1975, 62, 1834.

86. Wexler, S.; Lifshitz, A.; Quattroch, A. Adv. Chem. Ser., 1966, 58, 193.

87. Harrison, A. G.; Herod, A. A. Int. J. Mass Spectrom. Ion Phys., 1970, 4, 415.

88. Miasek, P. G.; Beauchamp, J. L. Int. J. Mass Spectrom. Ion Phys.,

1974, 15, 49.

89. Munson, M. S. B. J. Phys. Chem., 1965, 69, 572.

90. Futrell, J. H.; Tierman, T. O. J. Phys. Chem., 1968, 72, 158.

91. Bierbaum, V. M.; DePuy, C. H.; Shapiro, R. H.; Stewart, J. H. J. Am. Chem. Soc., 1976, 98, 4229.

92. Weston, R.; Schwarz, H. A. "Chemical Kinetics", Prentice-Hall, Englewood Cliffs, N. J., 1972, 1.

Acknowledgments

I would first like to express my appreciation and gratitude to my research advisor Dr. Richard N. McDonald for his guidance, encouragement, and support in this research. I would also like to thank Dr. D. W. Setser whose helpful suggestions and assistance provided vindication for the results of this research. Thanks also goes to Dr. A. K. Chowdhury for his ubiquitous assistance during the course of this research, and for the preparation of PhN_3, to Bill McGhee for the preparation of $\underline{c}$-$C_5H_4N_2$ and $(CF_3)_2CN_2$, to Fu Min Zhang for his assistance in obtaining the emission data, and to my other laboratory colleagues for their insights and enlightenment.

Many thanks must also be given to Mr. Albert Weyerts and Mr. Richard Bachamp for their suggestions during the construction, and help with the trouble-shooting of the system. Also Mr. M. Ohno receives my sincere thanks for the glass blowing necessary to become operational.

I would also like to thank my wife, Marsha, and my family for their continued support and confidence during the course of my graduate studies.

Appreciation is expressed to the U. S. Army Research Office and the National Science Foundation for support of this research, and to the Department of Chemistry, Kansas State University, for financial support in the form of a teaching assistantship in the early stages of my studies.

PENNING IONIZATION REACTIONS OF METASTABLE $Ar(^3P_{0,2})$, $Ne(^3P_{0,2})$ AND $He(2^3S)$ WITH ORGANIC MOLECULES IN A FLOWING AFTERGLOW APPARATUS

by

MICHAEL THOMAS JONES

B. S., Nebraska Wesleyan University, 1980

AN ABSTRACT OF A MASTER'S THESIS

submitted in partial fulfillment of the

requirements for the degree

MASTER OF SCIENCE

Department of Chemistry

KANSAS STATE UNIVERSITY

Manhattan, Kansas

1983

Abstract

The Penning ionization reactions of $Ar(^3P_{0,2})$, $Ne(^3P_{0,2})$, and $He(2^3S)$ metastable atoms with various substrate gases were investigated using a cold-cathode discharge source that was designed for a flowing afterglow apparatus. The metastable atoms produced in the cold-cathode discharge tube provide a method for ionization that minimize the fragmentation of the parent ions. The reactions of $Ar(^3P_{0,2})$ with NO, CCl_4, $CHCl_3$, CH_2Cl_2, CH_3Cl, C_2H_2, C_2F_4, C_6H_6, C_6F_6, $(CH_3)_4C$, $(CH_3)_3CH$, PhN_3, $C_5H_4N_2$, $(CF_3)_2C{=}N_2$, $(CF_3)_2CO$, and CS_2, were investigated. The same reactions were studied with $He(2^3S)$ except for $(CH_3)_4C$, $(CH_3)_3CH$, $C_5H_4N_2$, $(CF_3)_2C{=}N_2$, and $(CF_3)_2CO$. The reactions of $He(2^3S)$ with N_2, O_2, and CO were also studied. The reactions of $Ne(^3P_{0,2})$ with NO, N_2, CCl_4, $CHCl_3$, CH_2Cl_2, CH_3Cl, C_6H_6, and C_6F_6 are also reported. The product ions from the quenching process were mass characterized and the relative branching fractions were calculated by comparison to the results of a standard reaction. For He* and Ne*, Penning ionization accounts for the majority of the quenching process, while Penning ionization accounts for only a fraction of the quenching process with Ar*. A brief account is given for the reactions of He^+ with N_2, CO, CH_2CO, PhN_3, and $(CF_3)_2C{=}N_2$, and the pseudo-first order rate constants are discussed. A summary of the products formed from the reaction with He^+ with various neutrals is also presented.